

11/3/94
13755
P. 137

Final Technical Report

NAG-1-1147

High Power Diode Laser Master Oscillator - Power Amplifier (MOPA)

Principal Investigators:

Dr. John R. Andrews
Xerox Corporation

Professor P. Mouroulis
Rochester Institute of Technology

Professor G. Wicks
University of Rochester

NASA Technical Officer:

Mr. G. Schuster

June 15, 1994

N94-35488

Unclas

G3/36 0013755

(NASA-CR-196095) HIGH POWER DIODE
LASER MASTER OSCILLATOR-POWER
AMPLIFIER (MOPA) Final Technical
Report (Rochester Inst. of Tech.)
137 p

Final Technical Report

NAG-1-1147

High Power Diode Laser Master Oscillator - Power Amplifier (MOPA)

Principal Investigators:

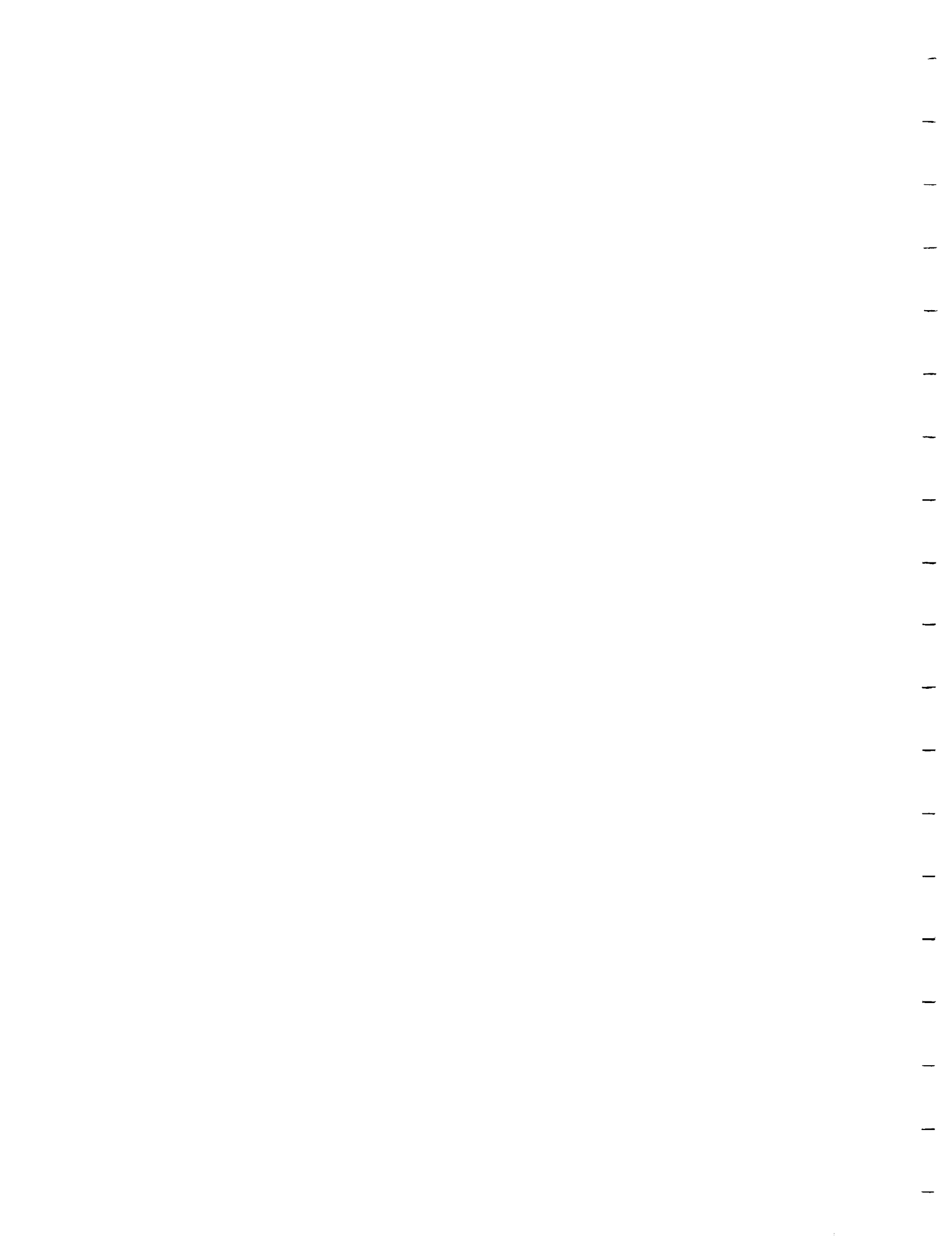
Dr. John R. Andrews, Xerox Corporation
Professor P. Mouroulis, Rochester Institute of Technology
Professor G. Wicks, University of Rochester

NASA Technical Officer:

Mr. G. Schuster

Summary:

High power multiple quantum well AlGaAs diode laser master oscillator - power amplifier (MOPA) systems were examined both experimentally and theoretically. For two pass operation, it was found that powers in excess of 0.3 W per 100 μm of facet length were achievable while maintaining diffraction-limited beam quality. Internal electrical-to-optical conversion efficiencies as high as 25% were observed at an internal amplifier gain of 9 dB. Theoretical modeling of multiple quantum well amplifiers was done using appropriate rate equations and a heuristic model of the carrier density dependent gain. The model gave a qualitative agreement with the experimental results. In addition, the model allowed exploration of a wider design space for the amplifiers. The model predicted that internal electrical-to-optical conversion efficiencies in excess of 50% should be achievable with careful system design. The model predicted that no global optimum design exists, but gain, efficiency, and optical confinement (coupling efficiency) can be mutually adjusted to meet a specific system requirement. A three quantum well, low optical confinement amplifier was fabricated using molecular beam epitaxial growth. Coherent beam combining of two high power amplifiers injected from a common master oscillator was also examined. Coherent beam combining with an efficiency of 93% resulted in a single beam having diffraction-limited characteristics. This beam combining efficiency is a world record result for such a system. Interferometric observations of the output of the amplifier indicated that spatial mode matching was a significant factor in the less than perfect beam combining. Finally, the system issues of arrays of amplifiers in a coherent beam combining system were investigated. Based upon experimentally observed parameters coherent beam combining could result in a megawatt-scale coherent beam with a 10% electrical-to-optical conversion efficiency.



Final Technical Report

NAG-1-1147

High Power Diode Laser Master Oscillator - Power Amplifier (MOPA)

Principal Investigators:

Dr. John R. Andrews, Xerox Corporation
Professor P. Mouroulis, Rochester Institute of Technology
Professor G. Wicks, University of Rochester

NASA Technical Officer:

Mr. G. Schuster

Table of Contents

1. Semiconductor Laser Power Amplifiers and Amplifier Arrays: Milliwatts to Megawatts, J. Andrews Colloquium Presentation at Institute of Optics, University of Rochester, April 27, 1994
2. High Power and high spatial coherence broad area power amplifier, J. R. Andrews and G. L. Schuster, Optics Letters, vol. 16, 1991, pp. 913-915
3. Coherent summation of saturated AlGaAs amplifiers, G. L. Schuster and J. R. Andrews, Optics Letters, vol. 18, 1993, pp. 619-621
4. Modeling and Optimization of Quantum Well Laser Amplifiers, Sinan Batman, draft of a Masters Thesis to be submitted to the Department of Electrical Engineering, Rochester Institute of Technology



1. Semiconductor Laser Power Amplifiers and Amplifier
Arrays: Milliwatts to Megawatts, J. Andrews
Colloquium Presentation at Institute of Optics,
University of Rochester, April 27, 1994

Webster Research Center

XEROX



***Semiconductor Laser Power Amplifiers
and Amplifier Arrays:
Milliwatts to Megawatts***

John R. Andrews



Acknowledgements

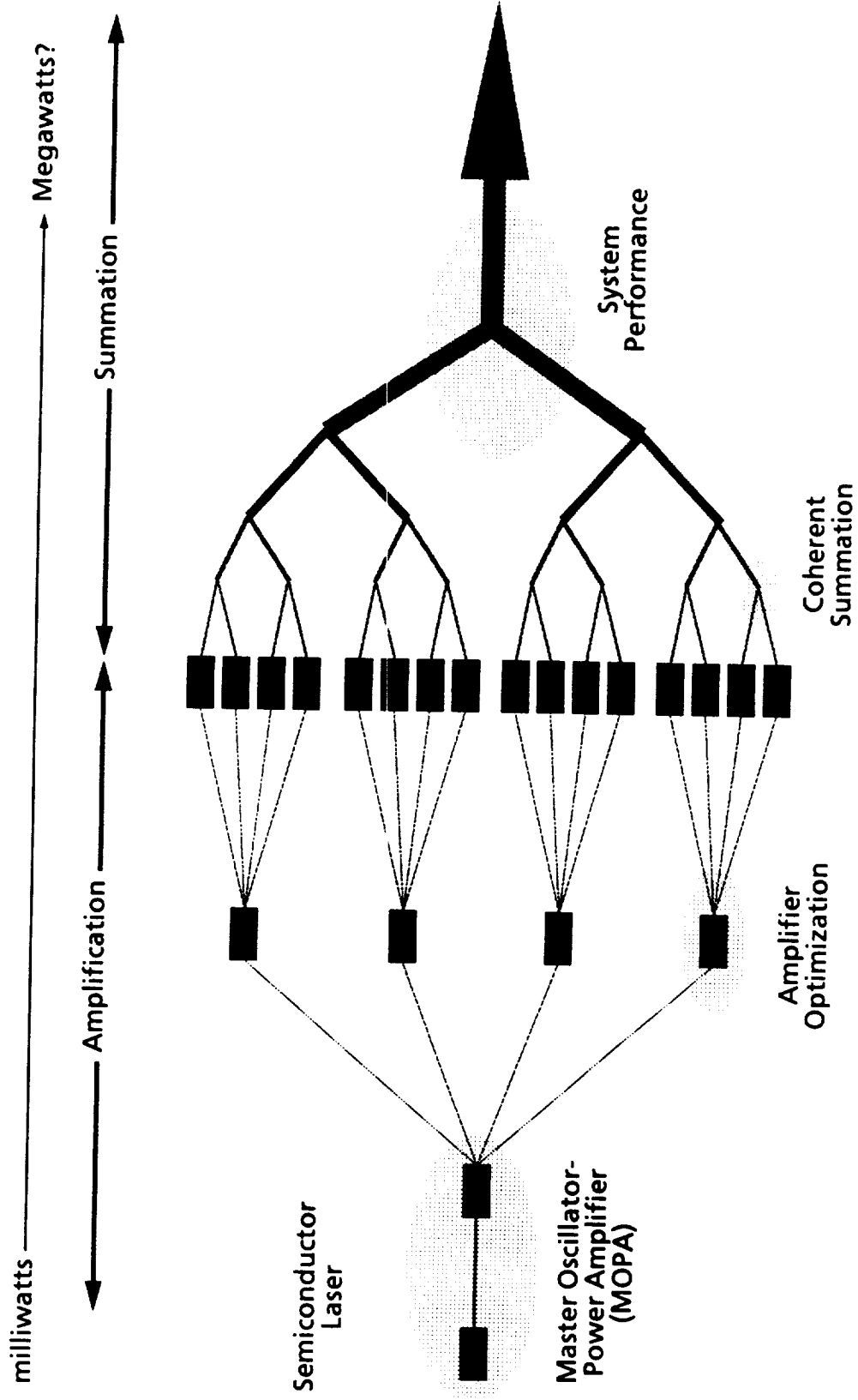
- *Greg Schuster--NASA Langley Research Center*
- *Sinan Batman--Masters/Ph.D. Student RIT, EE*
- *Grant co-investigators*

*Professor Zakos Mouroulis, RIT Center for
Imaging Science*

Professor Gary Wicks, UR Institute of Optics

- *Early work Robert Burnham, Tom Paoli*

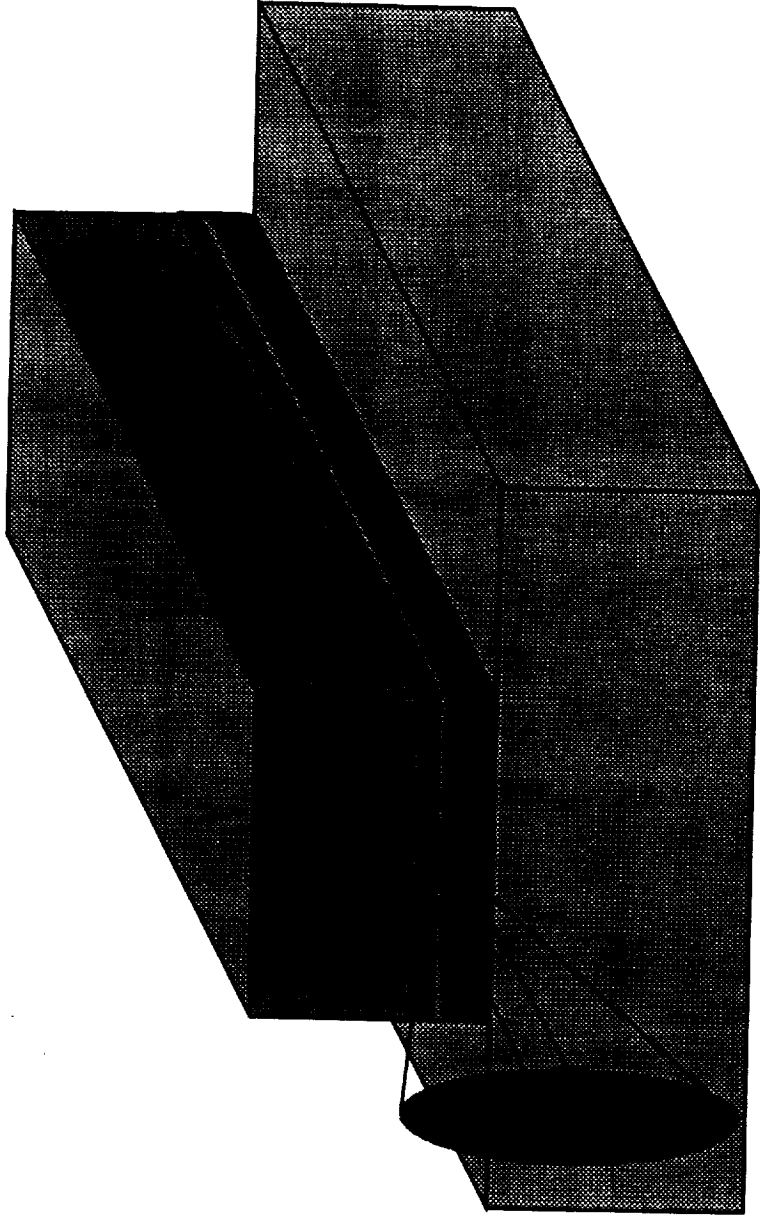
Outline



Motivation

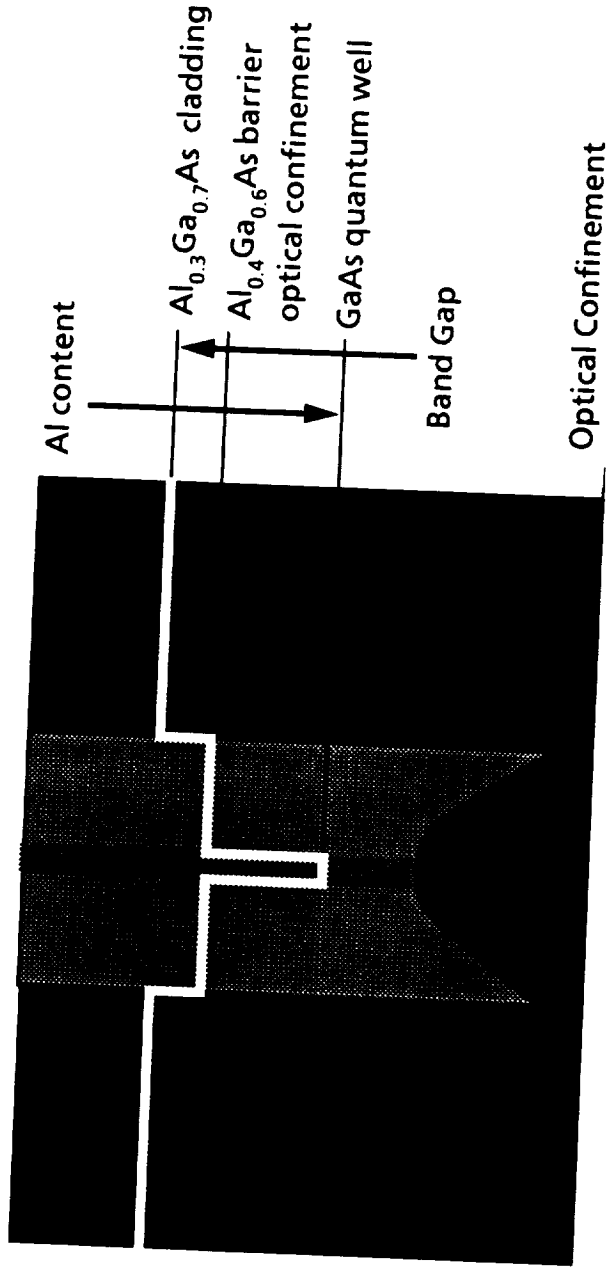
- **Xerox interest--low power**
Stable laser wavelength with modulation--
compatibility with diffractive optical elements
- **Megawatt power drive**
NASA--space-based power transmission
SDI--ranging and tracking

Ridge Guide Semiconductor Diode Laser



- n-GaAs substrate
- p-GaAs cap
- n-AlGaAs cladding
- GaAs active layer and waveguide
- p-AlGaAs cladding and ridge
- near-field emission
- far-field emission

Quantum Well Semiconductor Diode Laser



- n-AlGaAs cladding
- AlGaAs confinement/barrier
- quantum well active layer
- p-AlGaAs cladding and ridge
- Optical field

Limits to Semiconductor Laser Coherent Optical Power

- *Single Spatial Mode Operation*

1 μm transverse X 6 μm lateral

- *Catastrophic Facet Damage*

$$1\text{-}10 \text{ MW/cm}^2 = 10\text{-}100 \text{ mW}/\mu\text{m}^2$$

⇒ *Maximum Coherent Laser Power \approx 600 mW*

⇒ *0.1 W/ μm = 0.1 MW/m of facet length*

Amplifiers

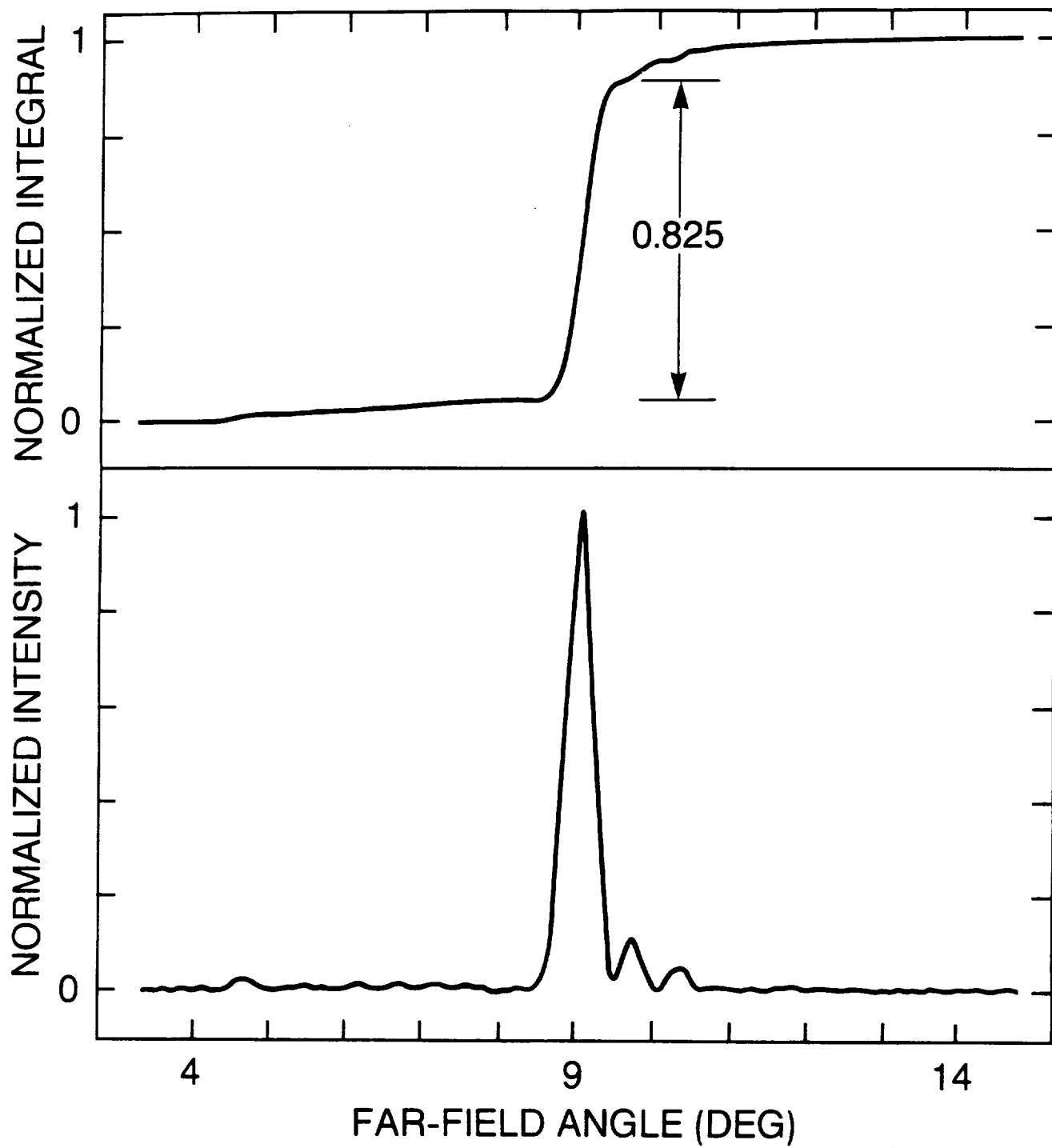
- ***Injection-Locked Laser Amplifier***

$$G_s \approx 1/\sqrt{R_1 R_2}$$

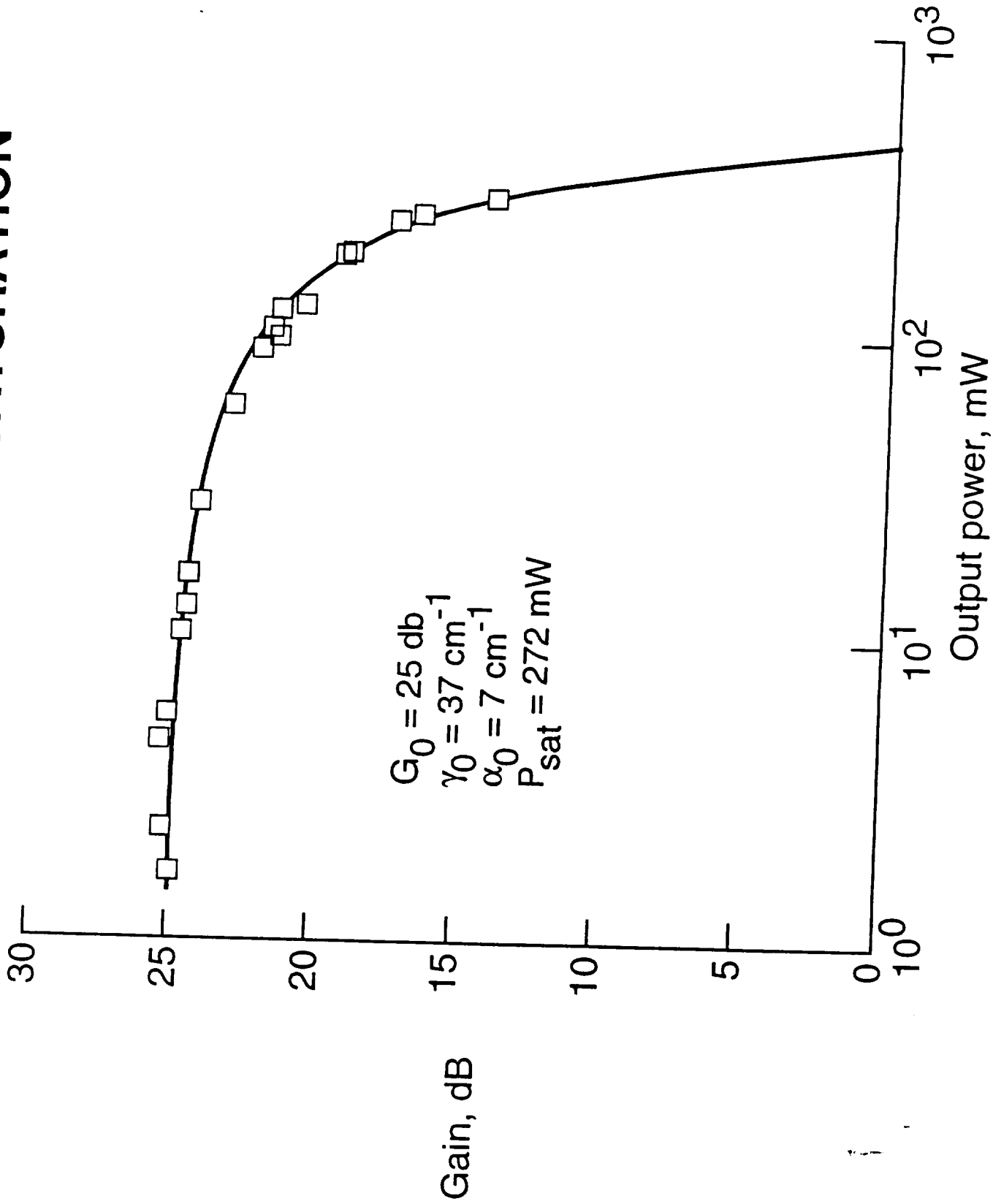
- ***Traveling-Wave Amplifier***

$$G_s \ll 1/\sqrt{R_1 R_2}$$

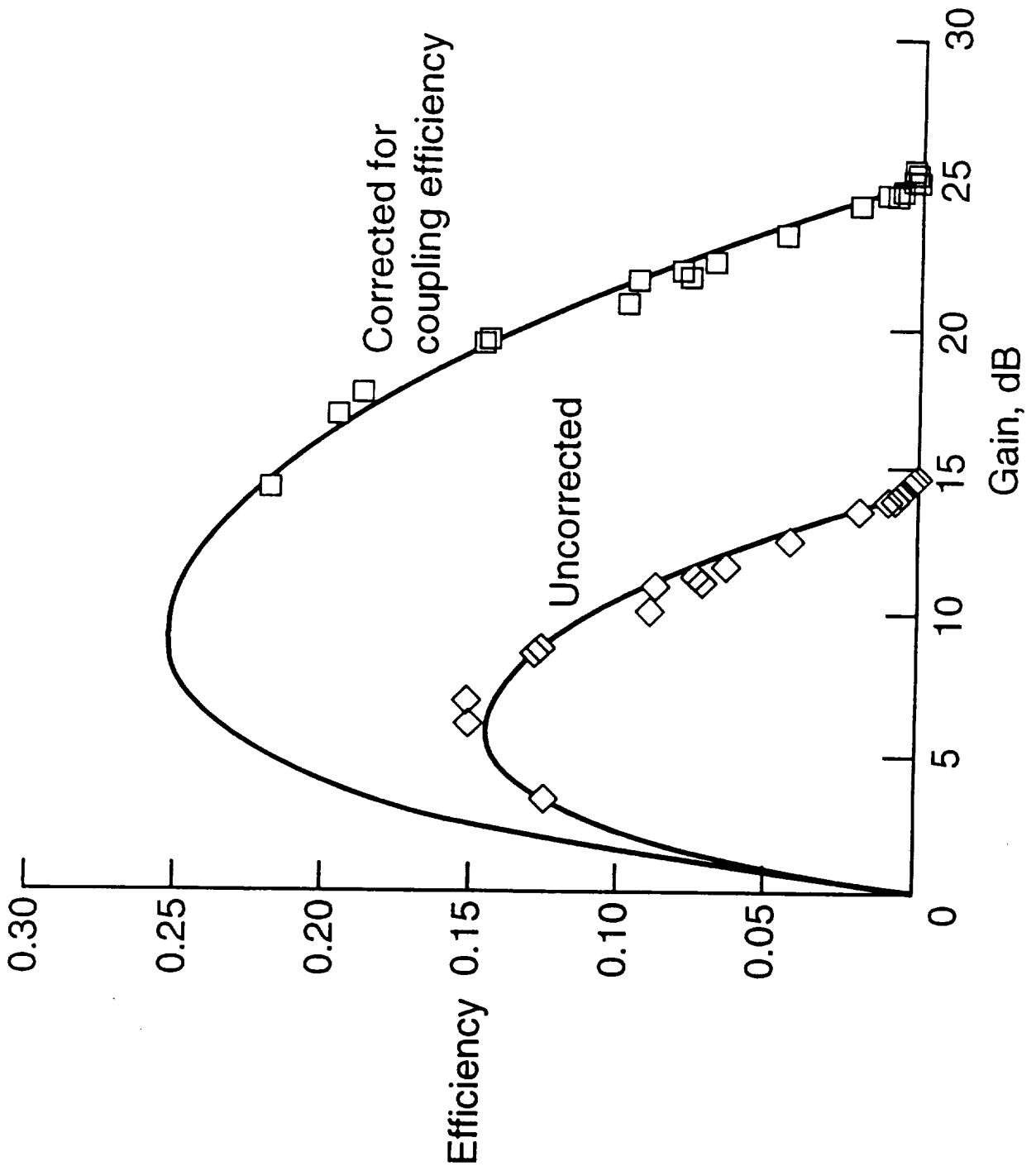
Where G_s is the single-pass gain and R_1, R_2 are the facet reflectivities



SINGLE AMPLIFIER SATURATION



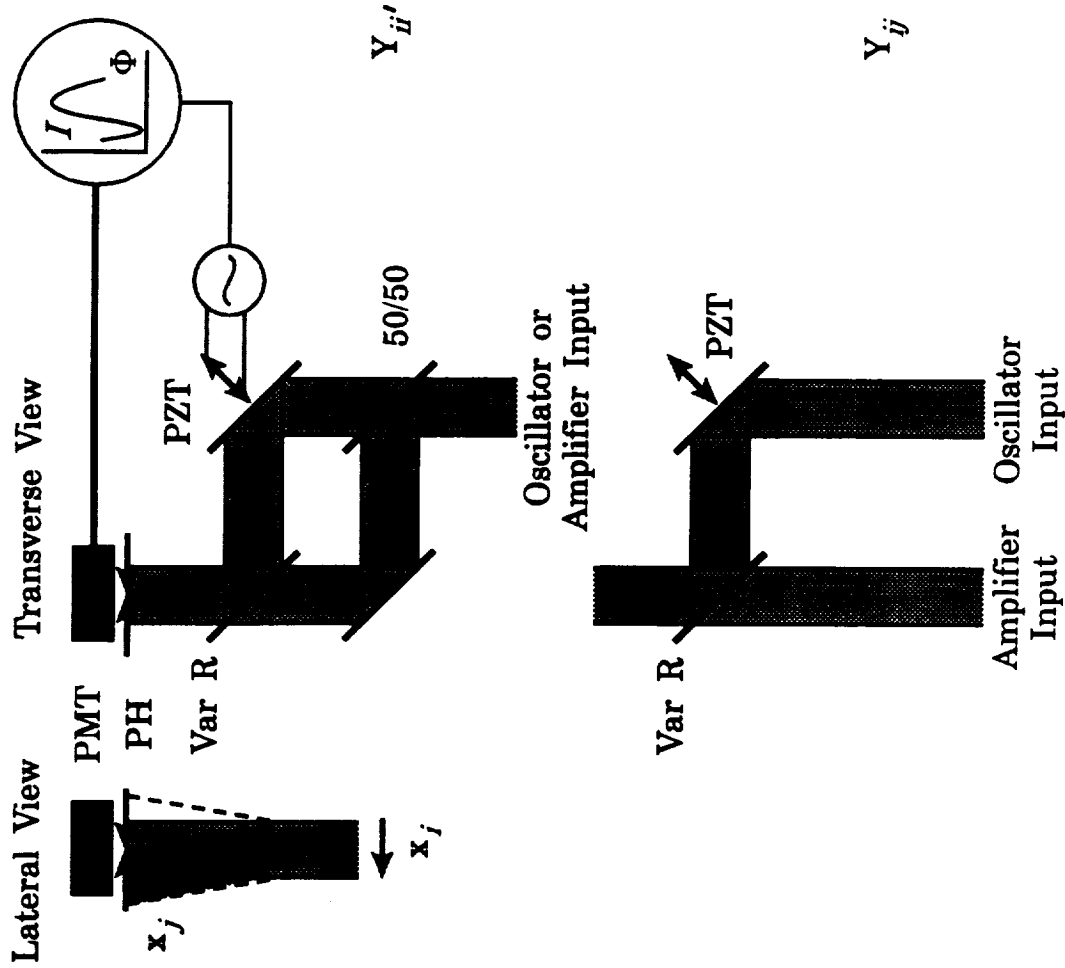
EFFICIENCY VERSUS GAIN

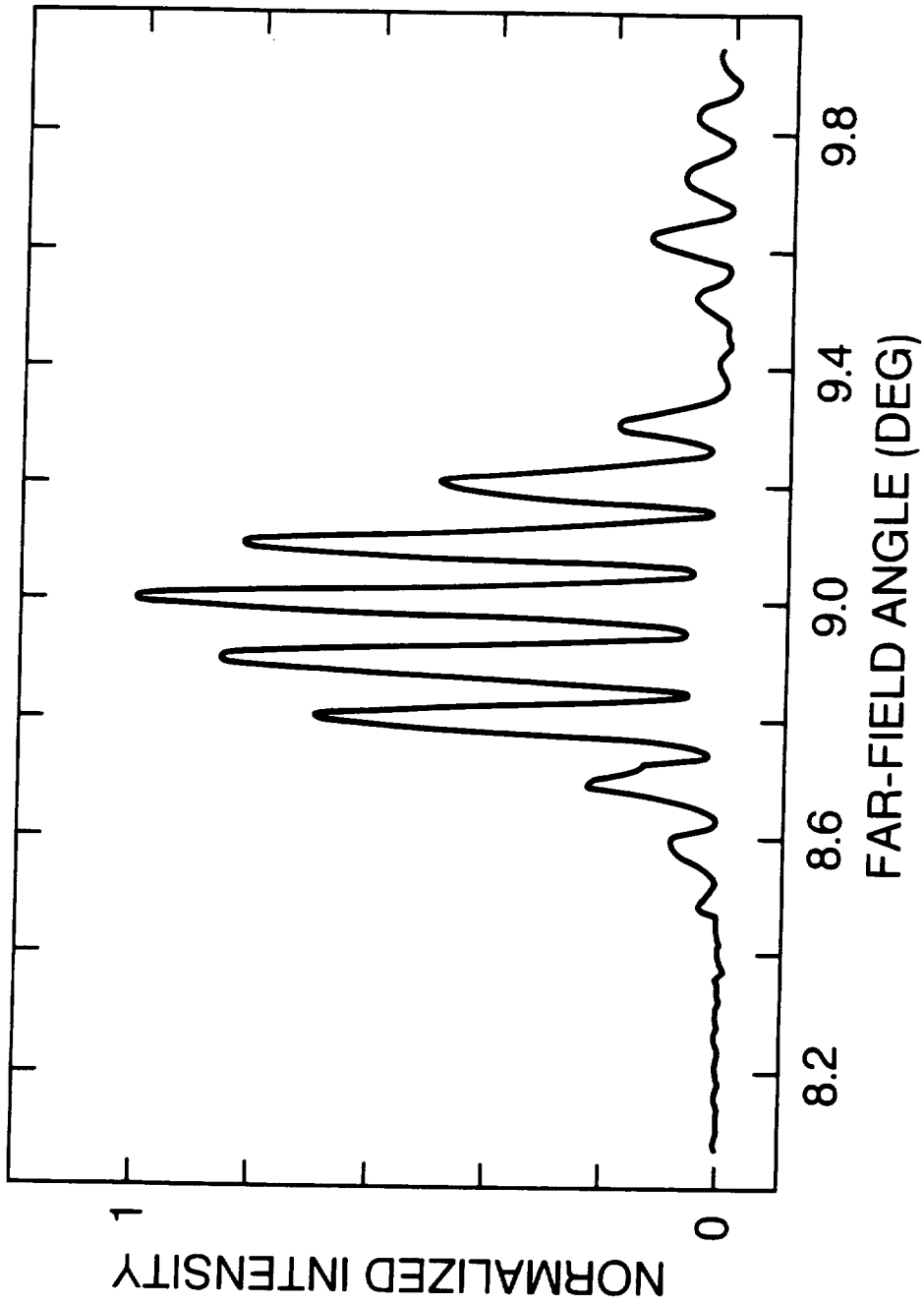


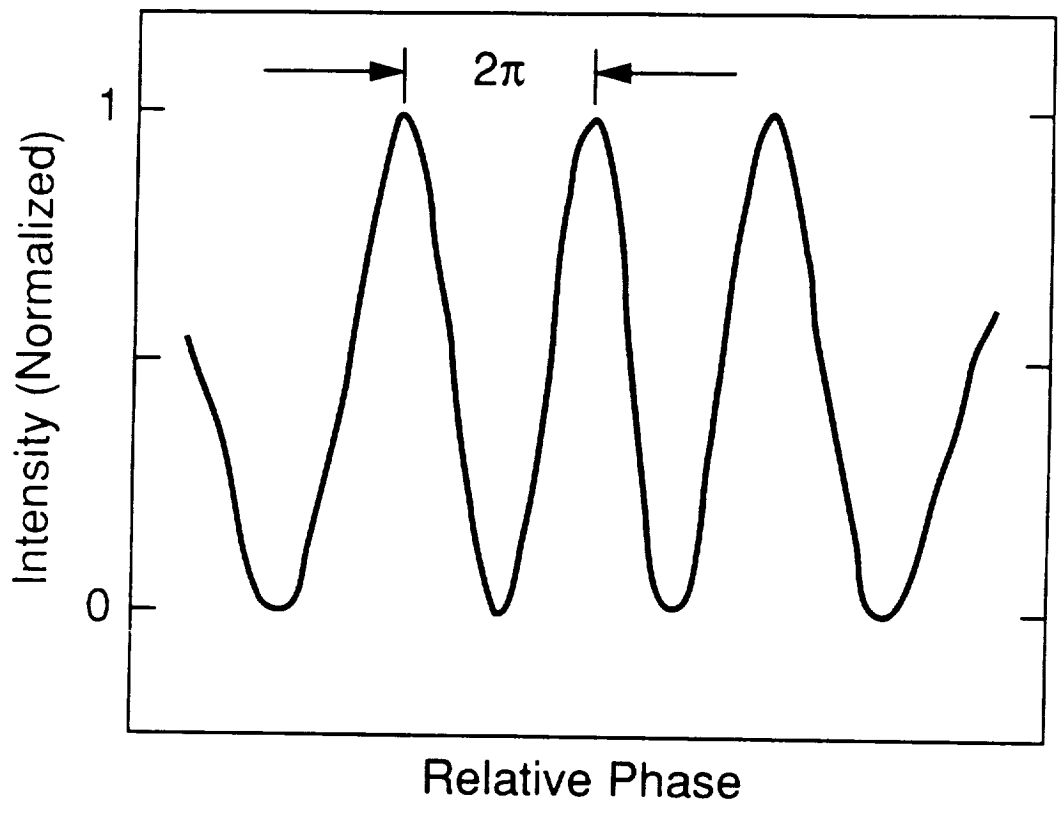
Broad Area Traveling-Wave Amplifier-- Summary

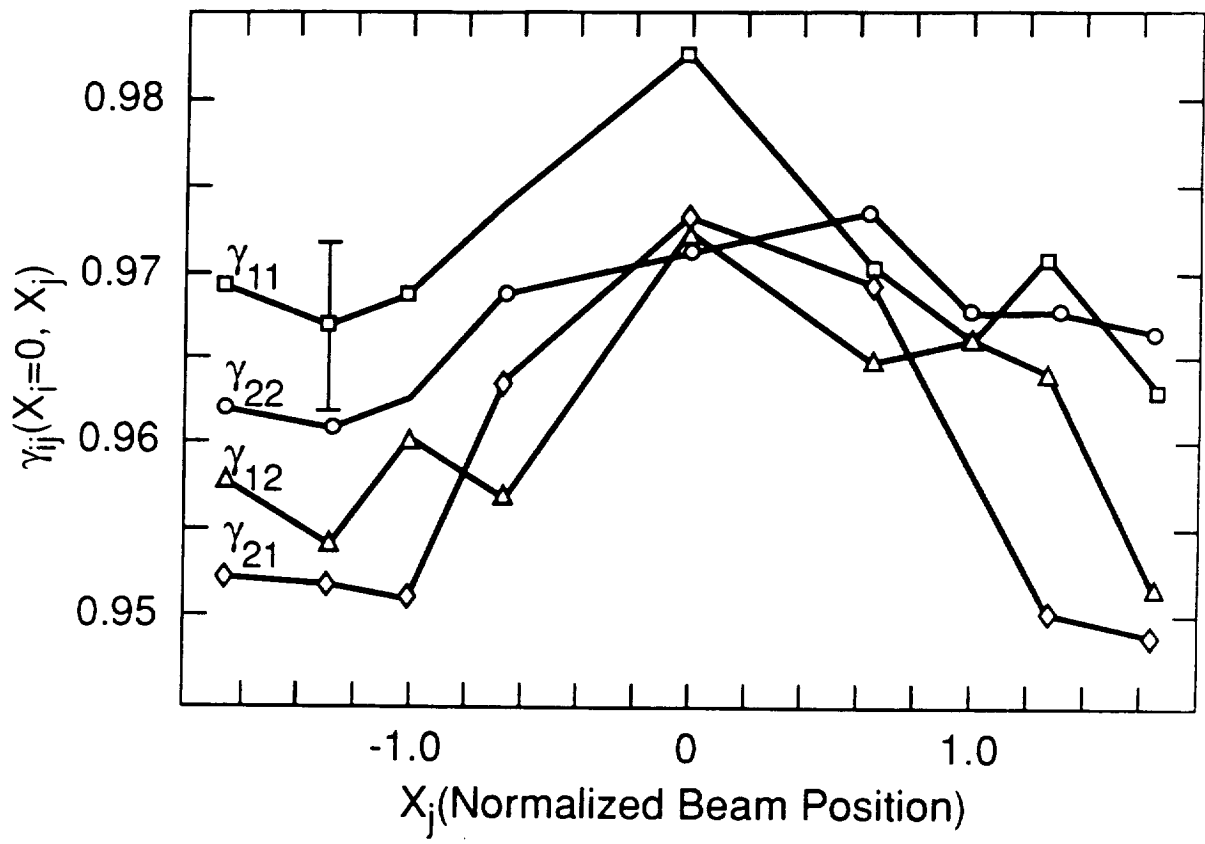
- **Unsaturated Gain 25 dB**
- **Saturation power 2.5 mW/ μm facet length**
- **Internal electrical-to-optical conversion efficiency of 25% at a gain of 9 dB**
- **Diffraction-limited far-field**

Coherence Measurements





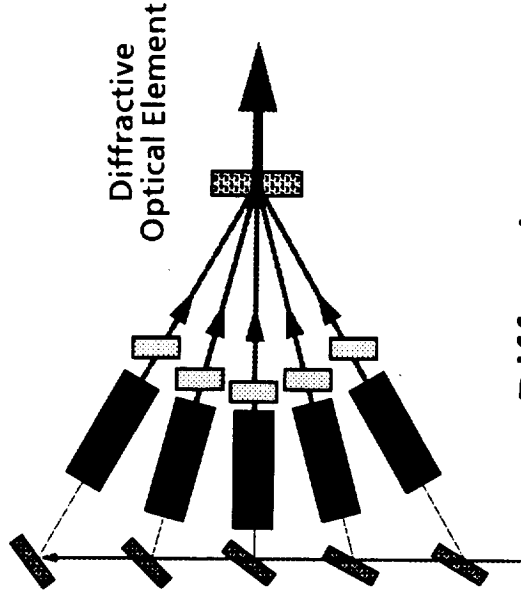
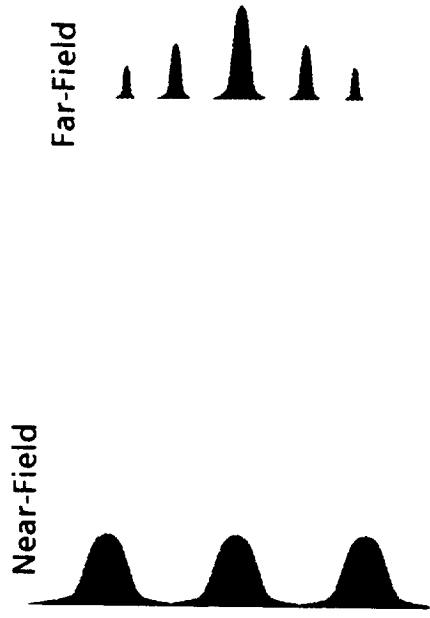




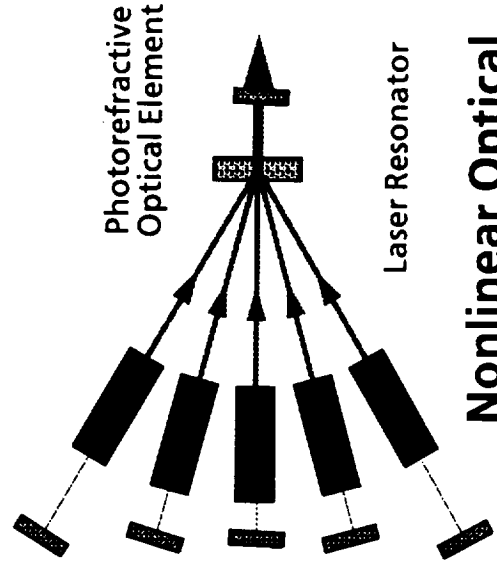
Spatial Coherence--Summary

- ***Self-coherence--0.97***
- ***Mutual coherence for two amplifiers--
0.96***

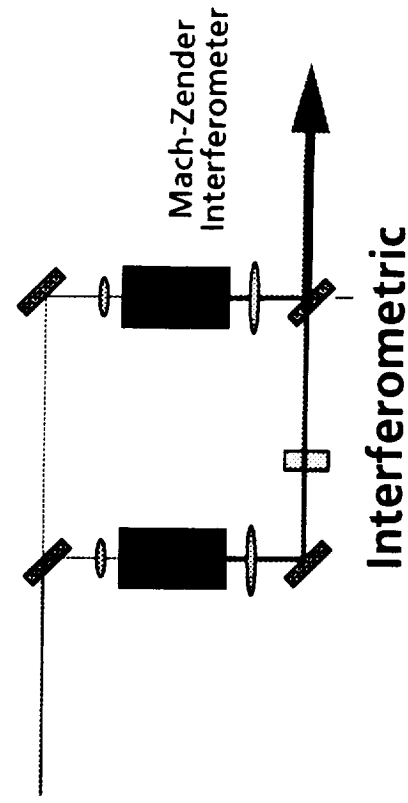
Coherent Summation Methods

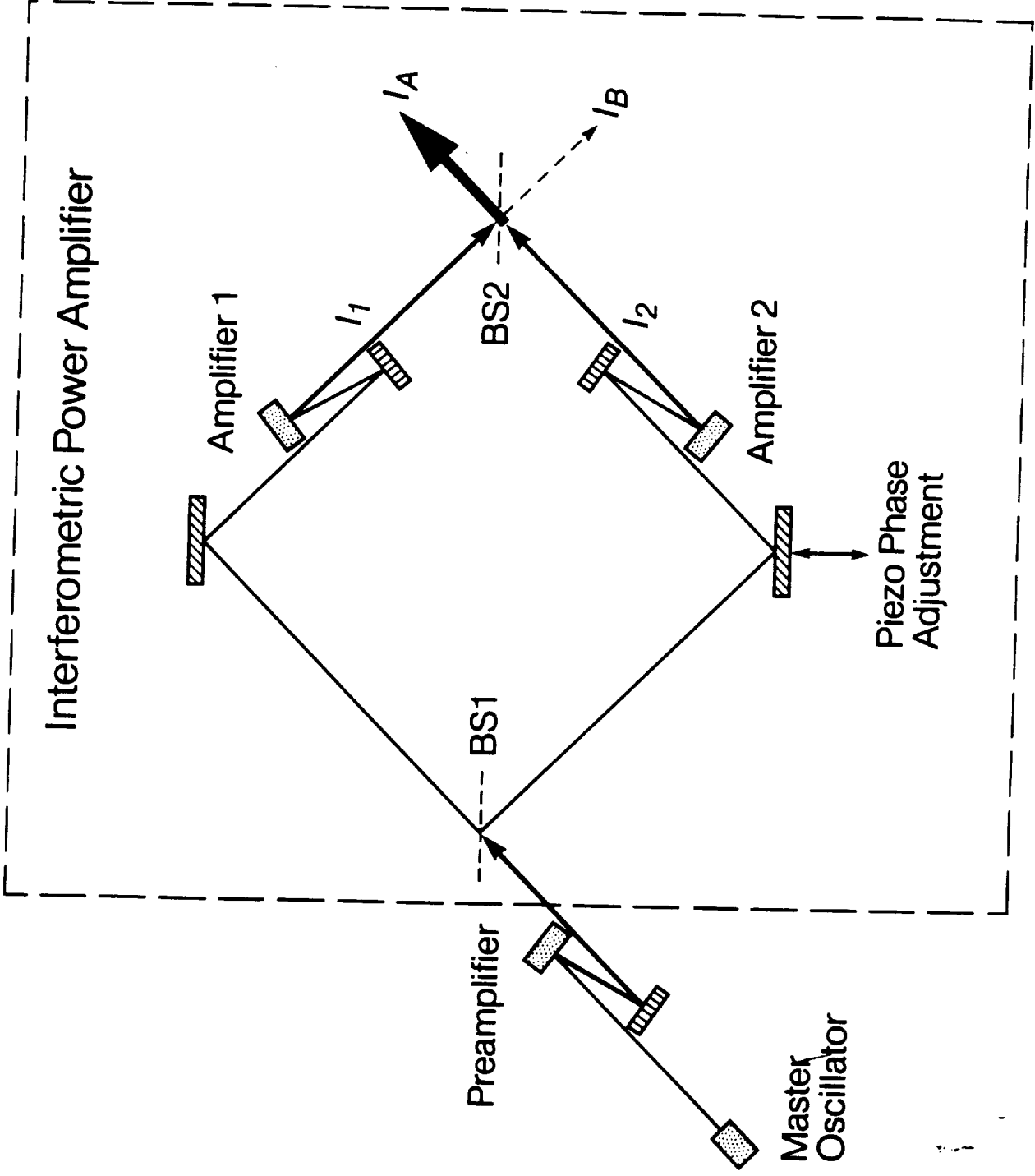


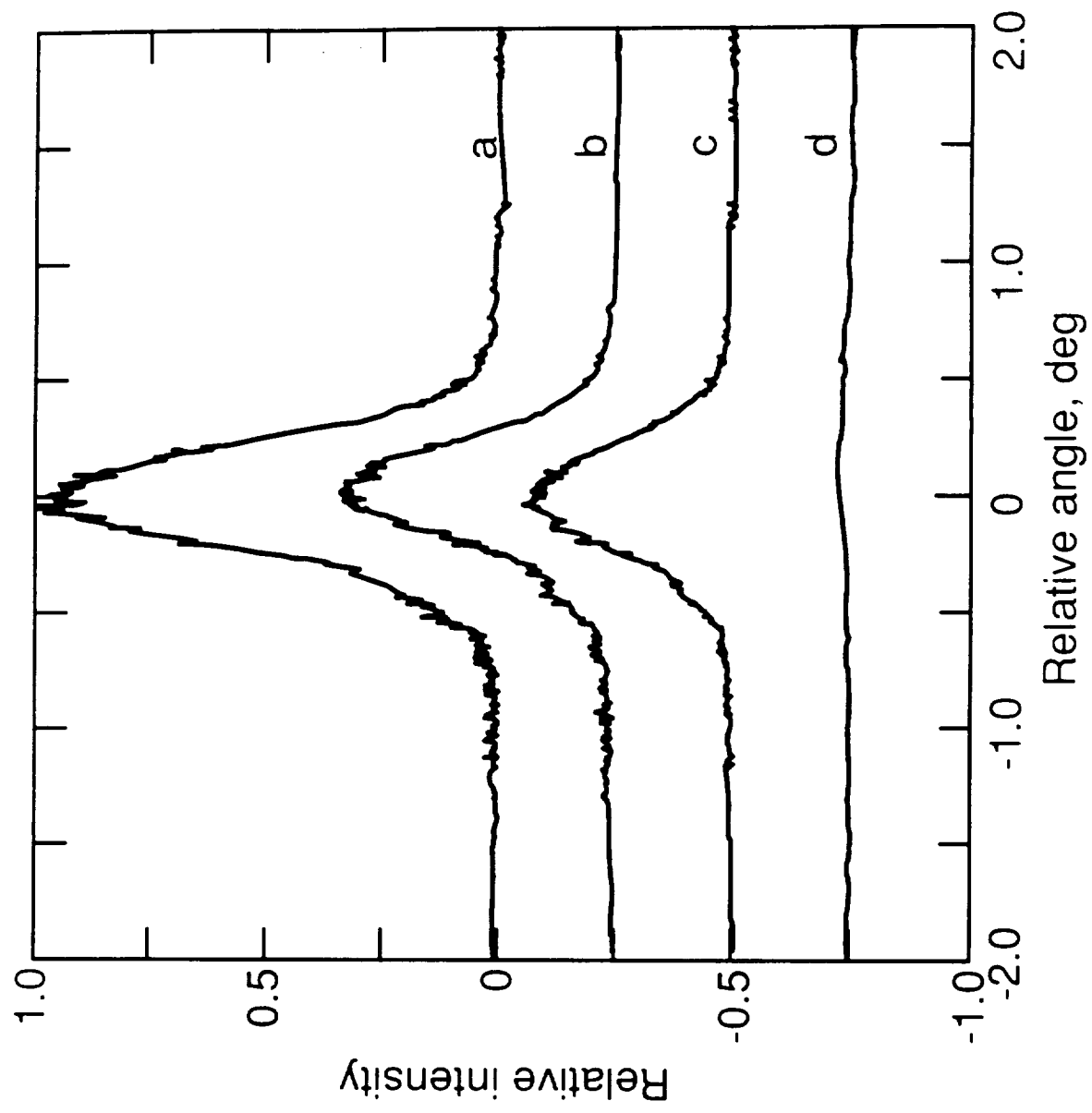
Aperture-Filling

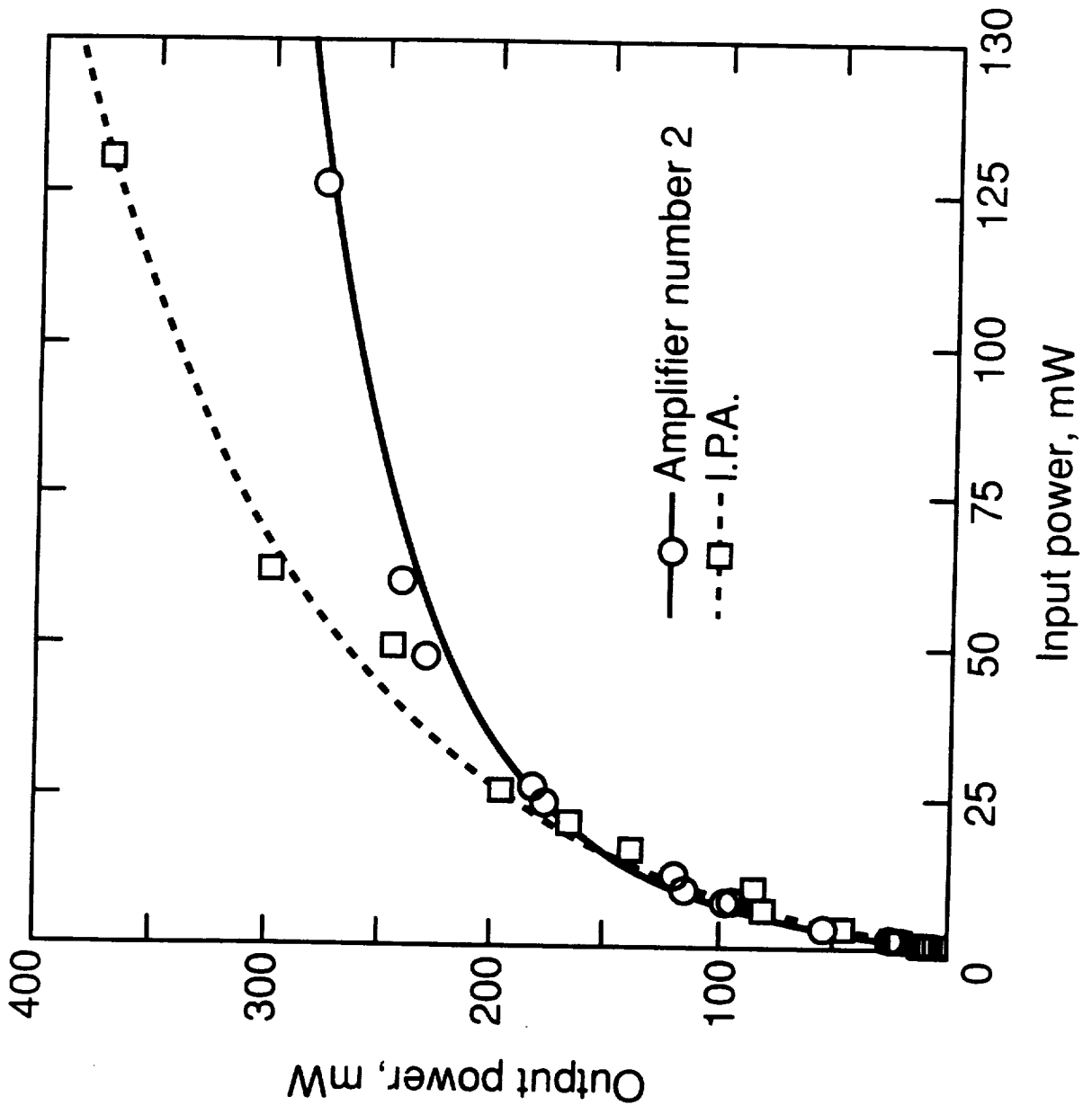


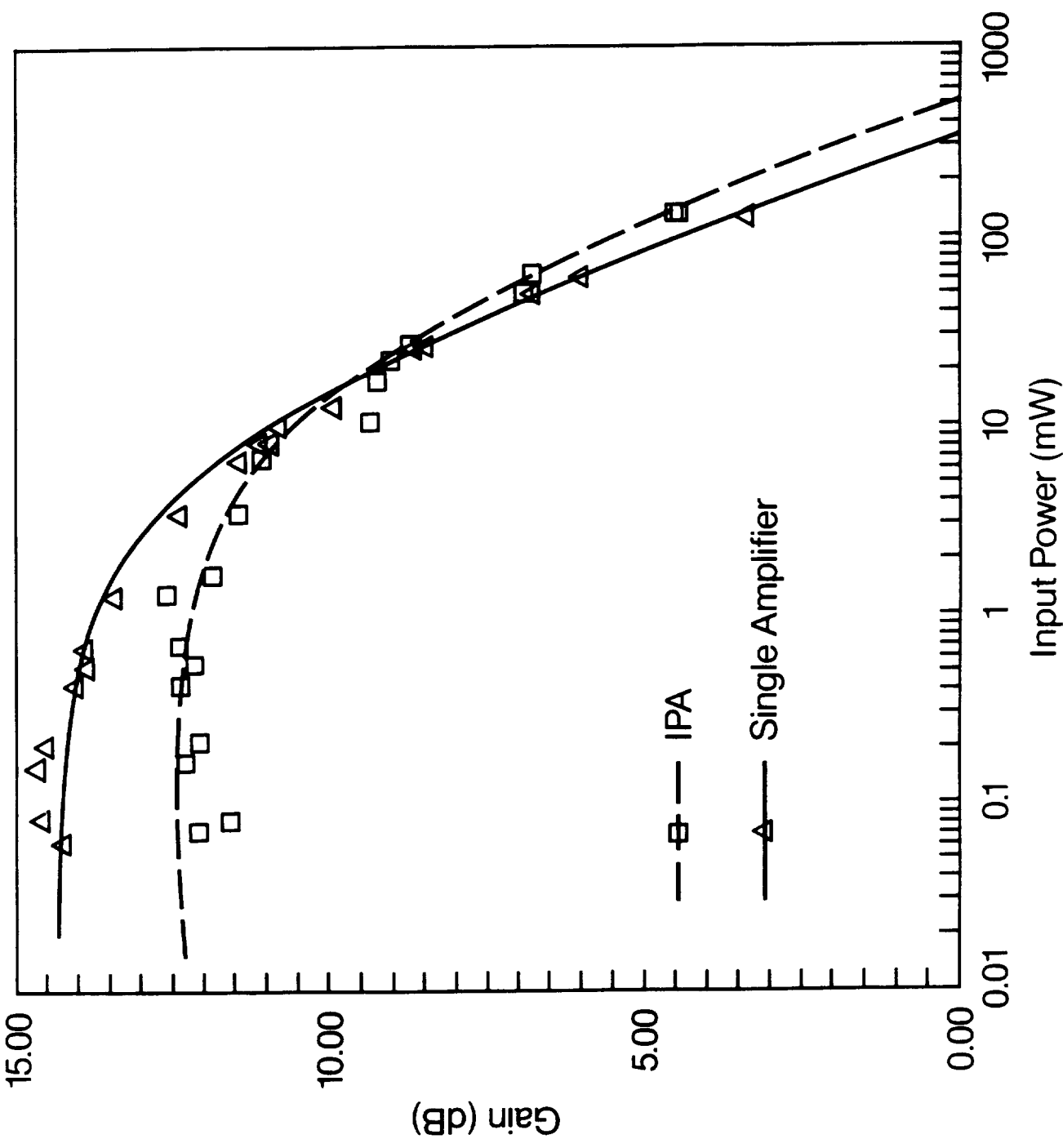
Diffractive







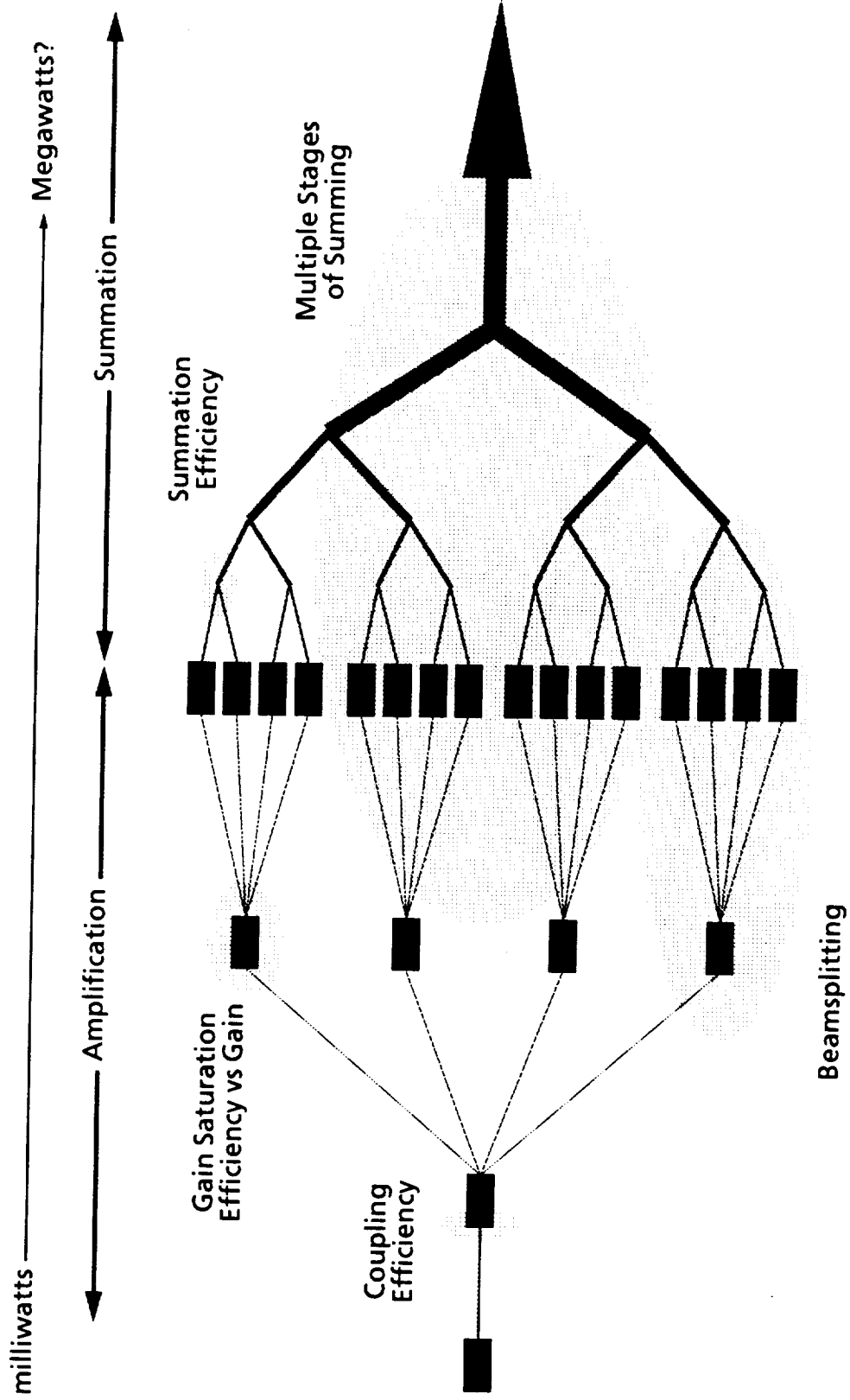




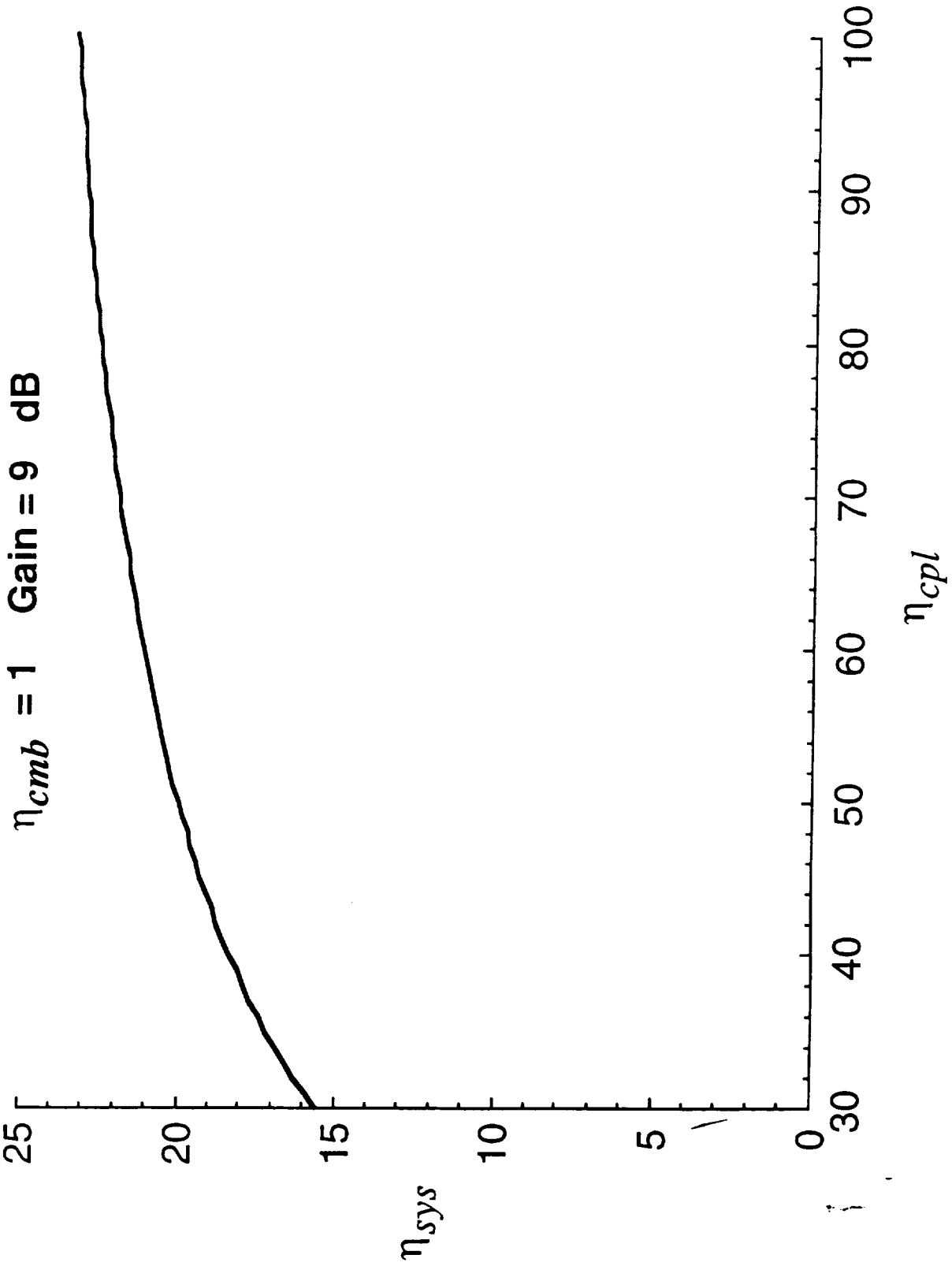
Coherent Summation--Summary

- ***Two-beam summation efficiency of 93%***
- ***372 mW in a diffraction-limited single beam***
- ***1.5-fold enhancement over single amplifier***

System Study

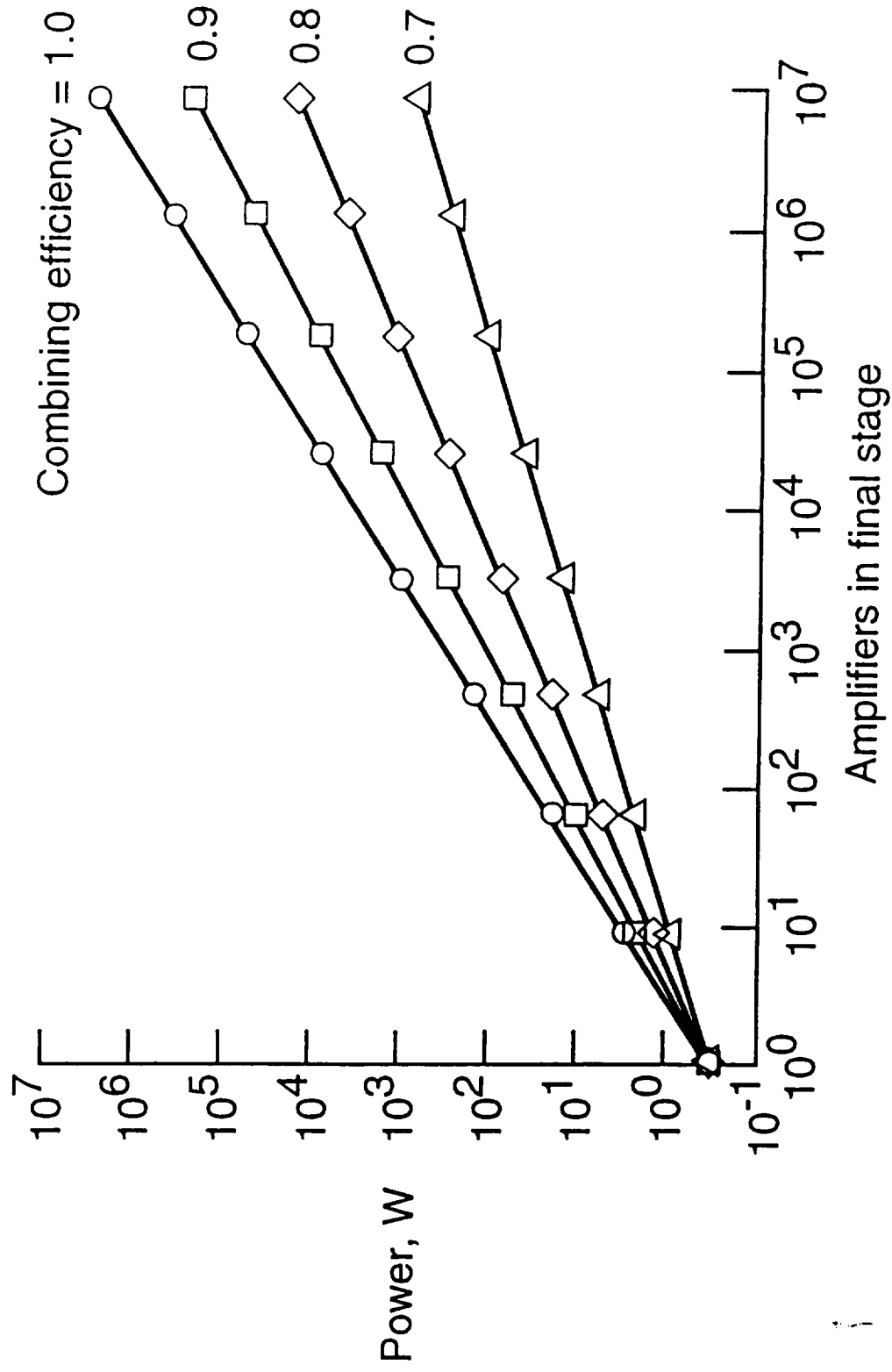


EFFECT OF COUPLING EFFICIENCY ON SYSTEM EFFICIENCY



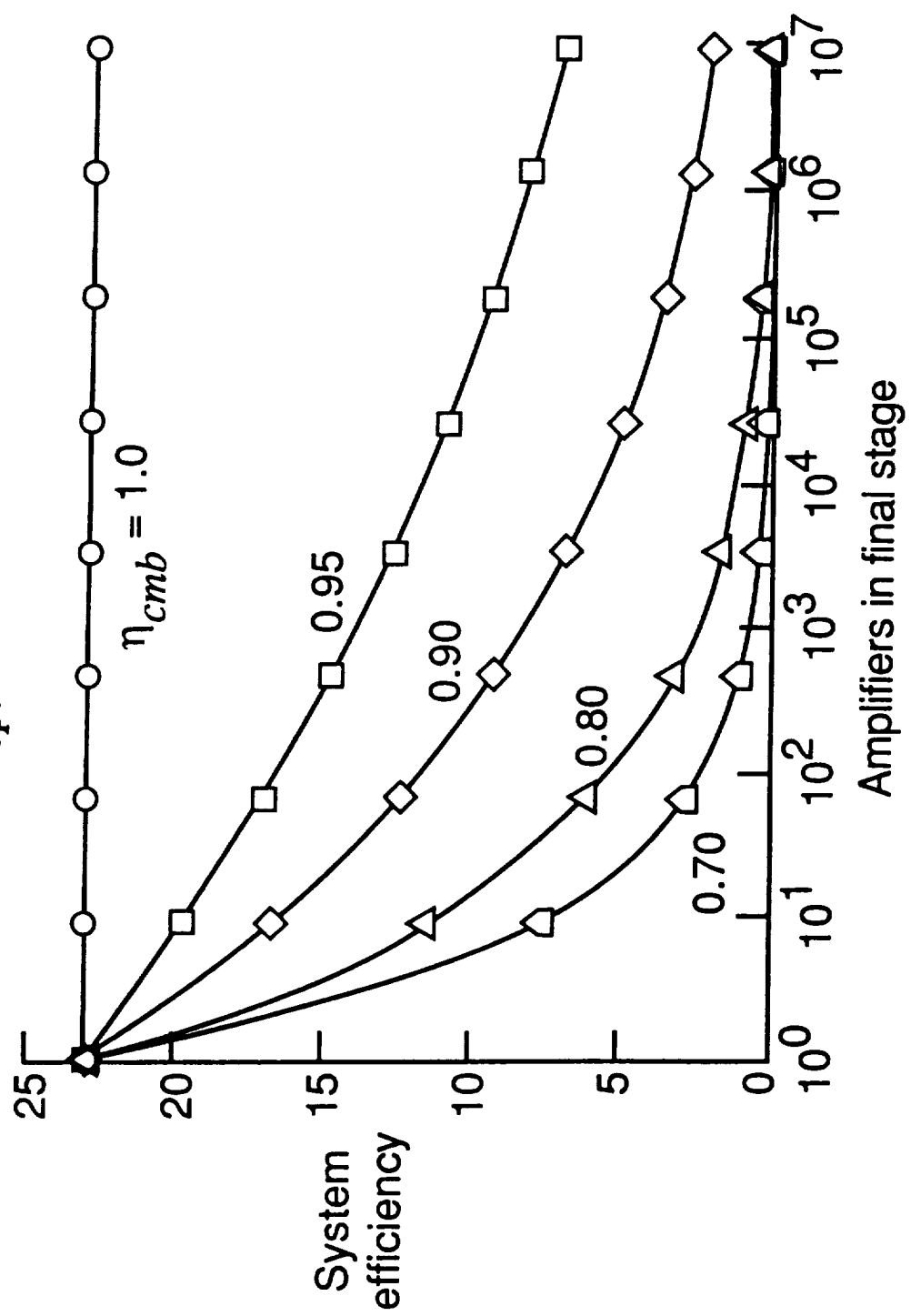
POWER SCALING

$\eta_{cpl} = 0.9$ Gain = 9 dB $P_{sat} = 272$ mW



EFFICIENCY SCALING

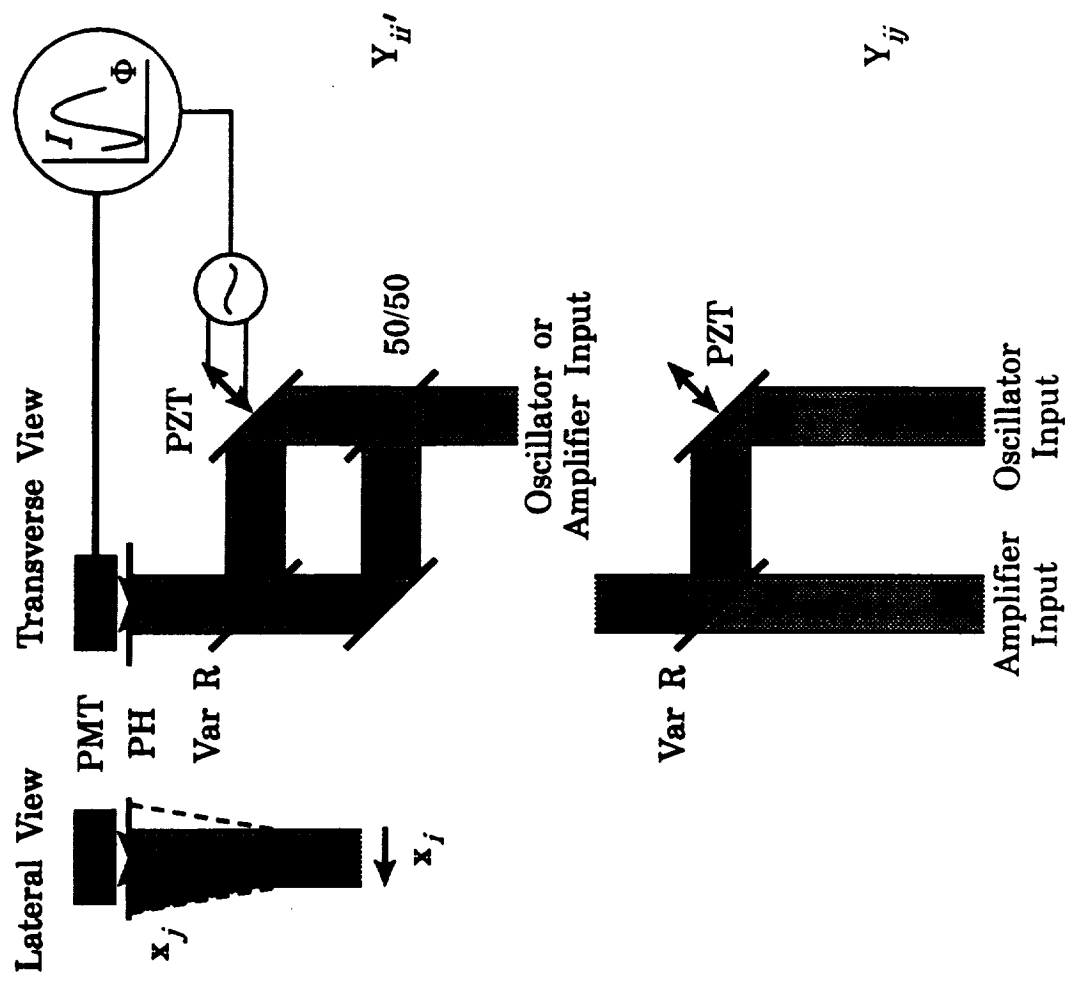
$\eta_{cpl} = 0.9$ Gain = 9 dB



System Study--Summary

- ***Coherent Summation Efficiency is of Primary Concern***
- ***1 MW of coherent optical power might be achieved with 10% system efficiency***
- ***The size and complexity of building such a system will require many innovations***

Coherence Measurements



2. High Power and high spatial coherence broad area power amplifier, J. R. Andrews and G. L. Schuster, Optics Letters, vol. 16, 1991, pp. 913-915

High-power and high-spatial-coherence broad-area power amplifier

John R. Andrews

Xerox Webster Research Center, 800 Phillips Road 0114-20D, Webster, New York 14580

Gregory L. Schuster

National Aeronautics and Space Administration, Langley Research Center MS/493, Hampton, Virginia 23665

Received January 22, 1991

A broad-area AlGaAs amplifier operating cw has delivered 425 mW of total power with 342 mW in a single lobe diverging at 1.02× the diffraction limit (FWHM 0.483°, 87.4-μm actual aperture) for a master oscillator input power of 70 mW. The spatial coherence of the amplifier output is 0.97, and the mutual spatial coherence between the oscillator and amplifier is 0.96.

Recent reports have demonstrated considerable single-lobe power for master oscillator-power amplifier (MOPA) systems including a 160-μm-wide injection-locked amplifier having ~0.45 W in a single lobe with a divergence 1.1× the diffraction limit,¹ a 400-μm-wide amplifier developing 0.51 W in a single lobe with a divergence 1.5× the diffraction limit with the use of two-stage injection locking,² and a 500-μm-wide traveling-wave amplifier having 1 W in a lobe with a divergence ~3.6× the diffraction limit.³ Though the deviation from the diffraction limit is a useful gauge for the wave-front quality of the output beam, the spatial coherence⁴ is more fundamentally related to the efficiency of wave-front transformations, the ability of the beam to carry information, and the ability to combine several beams coherently. It has recently been pointed out that the divergence is not a sensitive measure of the coherence.⁵ There are numerous reports on the mutual coherence of the elements of diode-laser arrays,⁶⁻⁸ a report for injection-locked arrays,⁹ and a report for a traveling-wave amplifier array.¹⁰ The highest values of the coherence, as represented by the fringe visibility V have been >0.86 across a 20-element laser array, 0.6 for the elements of an injection-locked array, and 0.9 for the elements of a traveling-wave amplifier array. A visibility $V = 0.87$ has been reported for the mutual coherence between a diode-laser master oscillator and a single-stripe injection-locked amplifier.¹¹

The research reported here demonstrates a 96-μm-wide amplifier developing 342 mW in a single lobe that diverges at only 1.02× the diffraction limit, a spatial self-coherence for the amplifier of 0.97, and mutual spatial coherence between the oscillator and amplifier of 0.96.

The interference of two quasi-monochromatic beams of intensities I_1 and I_2 at positions within the respective beams of x_1 and x_2 provides information about the coherence between the two beams. The experimentally measurable fringe visibility V at some observation point P in the overlap region between the two beams is given by⁵

$$V(P) = \frac{I_{\max} - I_{\min}}{I_{\max} + I_{\min}} = \frac{2[I_1(x_1)I_2(x_2)]^{1/2}}{I_1(x_1) + I_2(x_2)} \times |\gamma_{12}(x_1, x_2, \tau)|, \quad (1)$$

where γ_{12} is the complex degree of coherence for beams 1 and 2 that depends on the relative positions within the beams at which they overlap at P and the time delay τ between the beams. For τ much less than the coherence time, γ_{12} represents the spatial coherence of the beams. When $I_1 = I_2$ the fringe visibility gives directly the magnitude of the mutual coherence γ_{12} . Some limiting cases of the degree of coherence that are of interest are the mutual coherence between two different beams,

$$0 \leq |\gamma_{12}(x_1, x_2)| \leq 1, \quad (2)$$

and the self-coherence, i.e., the coherence between portions of the same wave front,

$$|\gamma_{11}(x_1 = x_1')| = 1, \quad (3)$$

$$0 \leq |\gamma_{11}(x_1 \neq x_1')| \leq 1. \quad (4)$$

The MOPA system consisted of a single-mode AlGaAs diode laser (Spectra Diode Laboratories SDL5410) delivering 70 mW to the amplifier coupling optics. The double-pass amplifier (Spectra Diode Laboratories SDL-2419) was a 10-stripe gain-guided array that was 96 μm wide and 250 μm long. This is referred to as a broad-area amplifier based on findings that the gain-guided array behaves like a broad-area gain medium with periodic perturbations in the gain due to the localized current sources provided by the array stripes.¹² The rear facet had a high-reflectivity coating, and the front facet had an antireflection coating. The antireflection coating on the front facet raised the threshold current to ~620 mA from a value of 287 mA for the uncoated facet. The anamorphic coupling optics were similar to an earlier paper.¹³ The oscillator lateral beam shape at the entrance face of

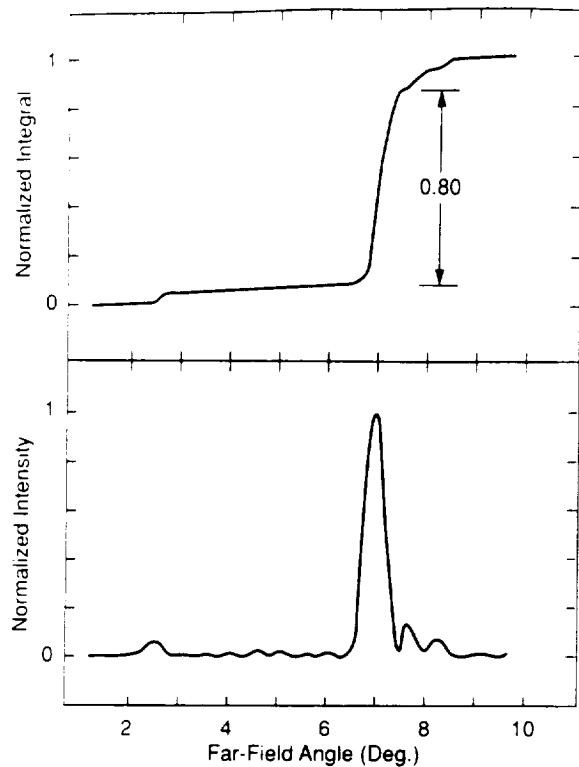


Fig. 1. Far field of the amplifier with 425-mW output power (lower trace). The strong lobe has a divergence (FWHM) of 0.483° , and the power contained within the lobe is 342 mW. The lobe width is $1.02\times$ the diffraction limit for the measured width of the near field, $87.4\ \mu\text{m}$. The upper trace is the normalized integral of the far-field intensity showing 80% of the total intensity in the strong lobe.

the amplifier was approximately Gaussian with a width (FWHM) of $120\ \mu\text{m}$. The oscillator beam was incident at 5° to the amplifier axis so that the amplified beam exited through the spherical and cylindrical coupling optics and could be picked off by a mirror. Far-field measurements of the lateral beam profile were made with a linear charge-coupled-device array. Near-field measurements of the amplifier were made by picking off the amplified beam in front of the cylindrical lens. A Faraday isolator between the oscillator and amplifier provided 35 dB of isolation. The oscillator and amplifier were both operated cw with the use of stabilized current sources and held at constant temperature with the use of thermoelectric cooling.

Coherence measurements were made with a shearing interferometer that had equal path lengths (i.e., path-length difference much less than master oscillator coherence length) in order to ensure that the fringe-visibility measurements were a function of only the spatial coherence. The initial setup of the interferometer gave stable straight-line fringes perpendicular to the p - n junction planes. A phase-shifting method proved most accurate for the determination of the visibility. A photomultiplier was placed behind a $25\text{-}\mu\text{m}$ pinhole, which was then placed in the overlap region of the beams from the two arms of the interferometer. The individual intensities of the two beams transmitted through the pinhole were adjusted to be equal. A mirror in one arm of the interferometer was

mounted on a piezoelectric stack and driven by a sinusoidal voltage waveform to vary the path length of that arm of the interferometer by several wavelengths. The intensity variations as several fringes moved across the pinhole were recorded on a digital oscilloscope. The maximum and minimum intensities recorded were used in the calculation of the fringe visibility. A series of measurements were made by maintaining one of the beams fixed in position and scanning the beam from the other arm of the interferometer across the pinhole; visibility measurements were made for each setting. All measurements were made with fringe spacings large enough that spatial averaging did not reduce the measured visibility.

The total output power of the amplifier was 425 mW with a 70-mW signal from the master oscillator into the amplifier coupling optics and a 671-mA current to the amplifier. The far-field profile for these conditions is shown in Fig. 1. The predominant single lobe with far-field divergence of 0.483° (FWHM) contains 80% of the total power, or 342 mW, as is shown by the integral of the far field in Fig. 1. The measured near-field profile was $87.4\ \mu\text{m}$ in width. This is narrower than the $96\text{-}\mu\text{m}$ actual current-pumped width of the amplifier because of vignetting by the lossy regions on either side of the amplifier. A lobe width of 0.483° is $1.02\times$ the Fraunhofer diffraction limit for a uniformly illuminated $87.4\text{-}\mu\text{m}$ slit. The other features in the far field are also readily understood. The small lobe at 2.5° is the result of diffraction by the grating formed by the gain modulation created by the 10 stripes in the amplifier.^{12,14} The small sidelobes at 7.7° and 8.3° are features that were observable in the near field of the master oscillator and are thus not the result of beam degradation due to the amplifier. The amplified spontaneous emission power along the amplifier axis was $<30\ \text{mW}$.

Four sets of fringe-visibility measurements were made to characterize the spatial coherence of our MOPA system. The measurements were made with 100-mW power out of the master oscillator, 65-mW power incident to the amplifier, and 400-mW total power out of the amplifier. The fringe visibility of the oscillator (designated by the subscript 1) and amplifier (designated by the subscript 2) were measured across their beam profiles x_i with respect to the beam center $x_i = 0$ of either a split-off portion of itself

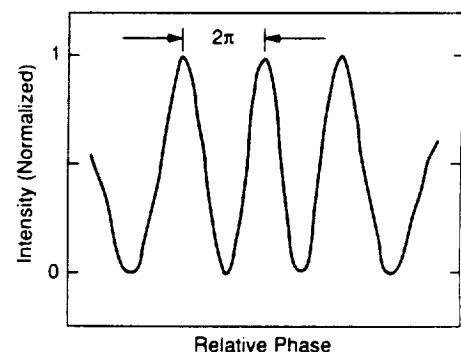


Fig. 2. Intensity fringes obtained from the phase-shifting shearing interferometer. This measurement is of $|\gamma_{12}(x_1 = 0, x_2 = 0)|$ and gives a value of 0.97.

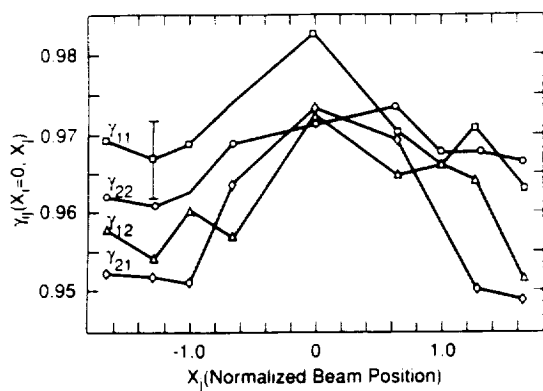


Fig. 3. Measured coherence as a function of the spatial position in one beam for the four coherences described in the text. Representative error bars are shown on one point. The data points are at the beam center and at the 75%, 50%, 30%, and 10% intensity points.

$[\gamma_{11}(x_1 = 0, x_1), \gamma_{22}(x_2 = 0, x_2)]$ or the other beam $[\gamma_{21}(x_2 = 0, x_1), \gamma_{12}(x_1 = 0, x_2)]$. An example of the experimentally acquired fringes for the measurement of $|\gamma_{12}(x_1 = 0, x_2 = 0)|$ is shown in Fig. 2. The fringe visibilities for the four sets of coherences are shown in Fig. 3, measured at the beam center and at the 75%, 50%, 30%, and 10% intensity points. The position parameter x_i is normalized to the beam HWHM. The observed visibility ranges from 0.98 to 0.95. The values of $|\gamma_{11}(x_1 = 0, x_1 = 0)| = 0.98$ and $|\gamma_{22}(x_2 = 0, x_2 = 0)| = 0.97$ both differ from the ideal expectation of 1.0. Two experimental factors, (1) the inability to identify and overlap the corresponding points on the split wave front perfectly and (2) light scattering from dust in the two arms of the interferometer, are thought to be the causes of the deviation of the measured values from the ideal. In all cases there is a general decrease in the observed fringe visibility at the edges of the beam. A contribution of a few percent or less of a higher-order spatial mode in the master oscillator would be sufficient to explain this observation fully.¹⁵ Other factors, such as increased contribution of spontaneous emission to the intensity, might also contribute to the slight loss of coherence away from the center of the beam. A useful measure of the fraction of the light in one beam that is coherent with a point in the second beam is the intensity-weighted coherence Γ_{ij} :

$$\Gamma_{ij} \equiv \frac{\sum_j I_j(x_j) \Delta x_j |\gamma_{ij}(x_i = 0, x_j)|}{\sum_j I_j(x_j) \Delta x_j}, \quad (5)$$

where $I_j(x_j)$ is the intensity of the beam at a position in the profile x_j and Δx_j is the measurement interval. For the four cases examined here, $\Gamma_{11} = 0.97$, $\Gamma_{22} = 0.97$, $\Gamma_{12} = 0.96$, and $\Gamma_{21} = 0.96$. The loss of 0.01 in the mutual coherence relative to the self-coherence seems surprisingly small in light of earlier results.⁵⁻¹¹ Possible explanations for any loss of coherence include the experimental factor of light scattering from the addi-

tional optics coupling into and out of the amplifier arm of the interferometer and the more fundamental coherence degradations due to amplified spontaneous emission and the noise dynamics of the amplifier. In any case the small loss in coherence induced by this high-power amplifier indicates that multiple amplifier chains² and amplifier arrays^{9,16,17} are practical techniques for generating highly coherent beams of high power.

The results described here demonstrate that high-power diffraction-limited single-lobe output with high coherence can be obtained from a single-mode master oscillator, broad-area power amplifier system. The spatial-coherence values reported here are, to our knowledge, the highest reported for injection-locked or traveling-wave MOPA's. The high power and high spatial coherence are particularly important for the realization of coherent beam-combining systems for power scaling.^{16,17}

Note added in proof: A paper published after submission of this Letter has reported values of $\Gamma_{12} = 0.96$ for a pair of injection-locked amplifiers.¹⁸

References

1. L. Goldberg and M. K. Chun, *Appl. Phys. Lett.* **53**, 1900 (1988).
2. L. Y. Pang, E. S. Kintzer, and J. G. Fujimoto, *Opt. Lett.* **15**, 728 (1990).
3. C. D. Nabors, R. L. Aggarwal, H. K. Choi, C. A. Wang, and A. Mooradian, in *Proceedings of the LEOS Annual Meeting* (IEEE Lasers and Electro-Optics Society, Piscataway, N.J., 1990), paper SDL3.5.
4. M. Born and E. Wolf, *Principles of Optics*, 5th ed. (Pergamon, New York, 1975), Chap. 10.
5. N. W. Carlson, V. J. Maslin, M. Lurie, and G. A. Evans, *Appl. Phys. Lett.* **51**, 643 (1987).
6. L. J. Mawst, D. Botez, M. Jansen, T. J. Roth, and J. J. Yang, *IEEE Photon. Technol. Lett.* **2**, 249 (1990).
7. G. C. Dente, K. A. Wilson, T. C. Salvi, and D. Depatie, *Appl. Phys. Lett.* **51**, 9 (1990).
8. C.-P. Cherrng, T. C. Salvi, M. Osinski, and J. G. McInerney, *Appl. Opt.* **29**, 2701 (1990).
9. M. Jansen, J. J. Yang, L. Heflinger, S. S. Ou, M. Sergant, J. Huang, J. Wilcox, L. Eaton, and W. Simmons, *Appl. Phys. Lett.* **54**, 2634 (1989).
10. M. S. Zediker, H. R. Appelman, B. G. Clay, J. R. Heidel, R. W. Herrick, J. Haake, J. Martinosky, F. Streumph, and R. A. Williams, *Proc. Soc. Photo-Opt. Instrum. Eng.* **1219**, 197 (1990).
11. S. Kobayashi and T. Kimura, *IEEE J. Quantum Electron.* **QE-17**, 681 (1981).
12. J. R. Andrews, T. L. Paoli, and R. D. Burnham, *Appl. Phys. Lett.* **51**, 1676 (1987).
13. J. R. Andrews, *J. Appl. Phys.* **64**, 2134 (1988).
14. J. R. Andrews, *Appl. Phys. Lett.* **48**, 1331 (1986).
15. P. Spano, *Opt. Commun.* **33**, 265 (1980).
16. J. R. Andrews, *Opt. Lett.* **14**, 33 (1989).
17. J. R. Leger, G. J. Swanson, and W. B. Veldkamp, *Appl. Opt.* **26**, 4391 (1987).
18. R. L. Brewer, *Appl. Opt.* **30**, 317 (1991).

3. Coherent summation of saturated AlGaAs amplifiers,
G. L. Schuster and J. R. Andrews, Optics Letters, vol. 18,
1993, pp. 619-621

Coherent summation of saturated AlGaAs amplifiers

Gregory L. Schuster

National Aeronautics and Space Administration, Langley Research Center, MS/493, Hampton, Virginia 23665

John R. Andrews

Xerox Webster Research Center, 800 Phillips Road 0114-20D, Webster, New York 14580

Received January 13, 1993

Coherent summation of the output of two saturated traveling-wave amplifiers, each injected from a common semiconductor laser and all operated cw, has resulted in a single diffraction-limited beam containing 93% of the power originally contained in the two individual amplified beams. The 372 mW of power in a single diffraction-limited lobe is a 1.5-fold enhancement over the power available from a single amplifier.

Semiconductor laser arrays¹ and broad-area amplifiers^{2,3} can now deliver powers in the range 1–3 W cw while maintaining high spatial coherence. Advances in coherent summation are complementary to efforts at increasing the power of semiconductor lasers and amplifiers in that coherent summation offers a means, independent of specific device optimizations, to combine the power from several mutually coherent high-power sources into a single beam. Three families of coherent summation methods have been explored: collinear interferometric summation,^{4–8} aperture filling,^{9–15} and two-wave mixing.^{16,17} The mutual coherence among the beams to be summed can be created by placing all the gain elements inside a laser resonator^{4,5,10,11} or through extracavity amplification of mutually coherent wave fronts.^{6–8,12–15} The three summation methods share the requirement of mutual coherence and wave-front matching of the beams to be combined.

Among the collinear interferometric summation methods, binary phase gratings have been used to sum two injection-locked Nd:YAG lasers with an efficiency of 0.75.⁶ Two-wave mixing of two injection-locked AlGaAs lasers in BaTiO₃ has resulted in summation efficiencies as high as 0.80, yielding 98 mW of power in a diffraction-limited single lobe.¹⁶ The interferometric power amplifier (IPA), consisting of a Mach–Zehnder interferometer with a semiconductor amplifier in each interferometer arm, has demonstrated a combining efficiency of 0.83, for a total output power of 8.3 mW (Ref. 7) and 110 mW with a combining efficiency of 0.85.⁸

In this Letter we report on experiments demonstrating collinear coherent summation with a Mach–Zehnder IPA. The IPA sums the output of two amplifiers into a diffraction-limited lobe with an efficiency of 0.93 and an output power in the single lobe of 372 mW. This is a 1.5-fold power enhancement over the power obtainable from a single amplifier. To our knowledge, this is the highest-efficiency interferometric summation with semiconductor gain elements and the highest single-lobe power obtained by interferometric summation reported to date.

Collinear interferometric summation⁷ can be accomplished when two mutually coherent beams with intensities I_1 and I_2 intersect on the surface of a beam splitter (Fig. 1). The beam-splitter surface bisects the intersection angle between the two beams, resulting in two beams I_A and I_B exiting the beam splitter that are the coherent sum of the two input beams,

$$I_A = I_1R + I_2T + 2\gamma_{12}\sqrt{I_1RI_2T}\cos(\Delta\phi), \quad (1)$$

$$I_B = I_1T + I_2R + 2\gamma_{12}\sqrt{I_1TI_2R}\cos(\Delta\phi + \pi), \quad (2)$$

where R and T are the reflectivity and transmission of the beam splitter, γ_{12} is the degree of mutual coherence between the two beams 1 and 2, and $\Delta\phi$ is the phase difference between the two beams. If $\Delta\phi = 0$, $\gamma_{12} = 1$, $R = T$, and $I_1 = I_2$, then

$$I_A = I_1 + I_2, \quad (3)$$

$$I_B = 0. \quad (4)$$

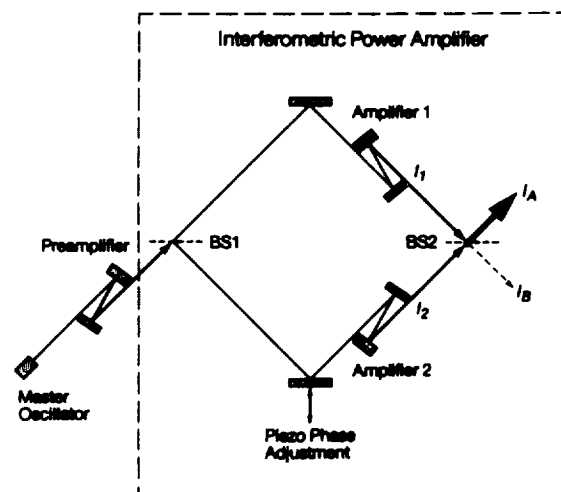


Fig. 1. Experimental setup. The line weight in the light paths is an indication of the relative intensities in each path. The beam splitters are designated BS1 and BS2. The coupling optics are not shown.

The mutually coherent beams 1 and 2 are combined into a single beam A containing all the power originally in beams 1 and 2. If $\gamma_{12} < 1$, the spatial-mode profiles of beams 1 and 2 are not perfectly matched, or the intensities and beam splitting are not properly matched,⁷ the summation will not be complete. A measure of the efficiency Ω of summation is

$$\Omega \equiv \frac{I_A}{I_1 + I_2} \quad (5)$$

To understand how the IPA can lead to power enhancements over a single amplifier, it is necessary to examine the power output of amplifiers with saturated gain.⁹ Compare the power output of a single amplifier P_{amp} with the power output of a two-arm IPA P_{IPA} for identical injection power from the master oscillator P_{in} and all individual amplifiers operating at the same small-signal gain G_0 :

$$P_{\text{amp}} = P_{\text{sat}} \frac{G}{G-1} \ln(G_0/G), \quad (6)$$

where P_{sat} is the saturation power, the actual gain G is

$$G \equiv P_{\text{amp}}/P_{\text{in}}, \quad (7)$$

and P_{in} is the injected power. For the IPA with two identical amplifiers and equal beam splitting,

$$P_{\text{IPA}} = 2\Omega P_{\text{amp}}[f(P_{\text{in}}/2)], \quad (8)$$

where $P'_{\text{amp}}[f(P_{\text{in}}/2)]$ describes the use of Eq. (6), where $P_{\text{in}}/2$ replaces P_{in} in Eq. (7). From Eqs. (6)–(8), it is apparent that, when the single amplifier is unsaturated, it will deliver more output power than the IPA when the coherent summation process has an efficiency $\Omega < 1$. However, as the injected power increases, both the single amplifier and the IPA saturate. Because the injection power is distributed among the amplifiers of the IPA, the IPA will undergo less gain saturation. Thus the gain versus injected power curves for the IPA and the single amplifier cross at some value of the gain. This crossover point can be derived for the ideal case of identical amplifiers and equal beam splitting if Eqs. (6) and (8) are set equal and rearranged to provide the following relationship:

$$\frac{G}{G_0} = \Omega \left(\frac{2\Omega}{2\Omega-1} \right). \quad (9)$$

For greater gain saturation than that given by Eq. (9), the IPA will have higher-power delivering capabilities than a single amplifier.

The experimental schematic is shown in Fig. 1. The master oscillator was a single-mode AlGaAs laser, and all the amplifiers were 10-stripe gain-guided arrays with an aperture width of 100 μm and a length of 250 μm . The amplifier had nominal front-facet reflectivity $R_1 = 0.03$ and rear-facet reflectivity $R_2 = 0.97$. The apparent threshold current was > 600 mA. The master oscillator and all gain elements were operated cw. The amplifiers were operated in a double pass, 5° off axis. The

preamplifier output was split into two beams at BS1. A mirror mounted on a piezoelectric stack in one arm of the interferometer provided relative phase adjustment at BS2. The outputs from the two amplifiers were coherently summed at the final beam splitter BS2 when the relative phase delay between the two arms was set to zero. The summed output at A was monitored by a line-scan CCD camera. The amplifiers used in these experiments, although nominally the same as the amplifier described in Ref. 18, were only capable of lower individual output powers for coherent operation due to individual device variations.

The far field of the coherently summed output of amplifiers 1 and 2 is shown in Fig. 2, curve a. The in-phase far field had a maximum output power of 372 mW in a diffraction-limited lobe. The far field for the out-of-phase condition shows nearly complete cancellation of the intensity (Fig. 2, curve d) demonstrating the high quality of the mode matching and high mutual coherence of the two amplified beams. The far fields of the individual amplifiers had diffraction-limited central lobes containing 92% of the total power for amplifier 1 and 80% of the total power for amplifier 2. The far fields from the amplifiers in each of the arms of the interferometer are shown in curves b and c of Fig. 2. Before BS2, the amplifier output powers in the central lobe were 206 and 195 mW for amplifier currents of 600 mA each. The corresponding interferometer combining efficiency was $\Omega = 0.93$. The divergence of the in-phase summed lobe is equivalent to that of the individual amplifiers. The individual amplifiers were operated at overall gains of 7.0 and 6.0 dB, whereas the small signal gains were 12.3 and 14.3 dB. Based on the estimated coupling efficiency, the internal gains are 10 dB higher than the overall gains.

The IPA output power for the in-phase condition (coherent summation) is shown in Fig. 3 as a function of input power. This can be compared with the

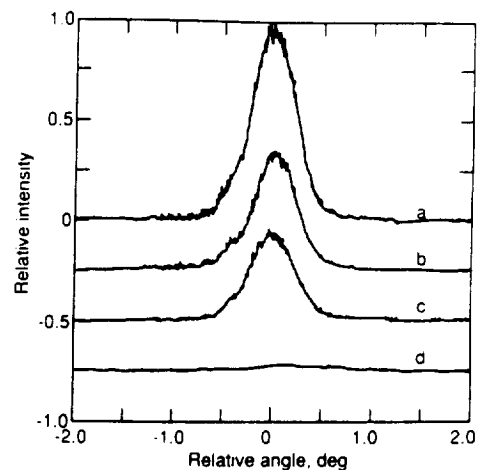


Fig. 2. Far-field profiles for the IPA. The vertical scale is identical for all profiles, and the baselines are offset for clarity. Curve a, coherently summed far field from two amplifiers with 372-mW single-lobe power; curve b, far field of amplifier 1 with 206-mW single-lobe power; curve c, far field of amplifier 2 with 195-mW single-lobe power; curve d, coherently summed out-of-phase profile.

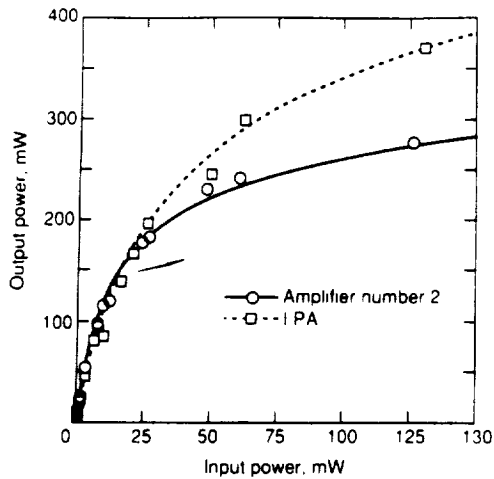


Fig. 3. Total output power of a single amplifier (○) operated at 550 mA and the output power of the IPA (□) as a function of the total input power. The solid curve is a theoretical fit for the individual amplifier that includes gain saturation, and the dashed curve is a theoretical fit for the IPA power that includes the efficiency of the coherent summation.

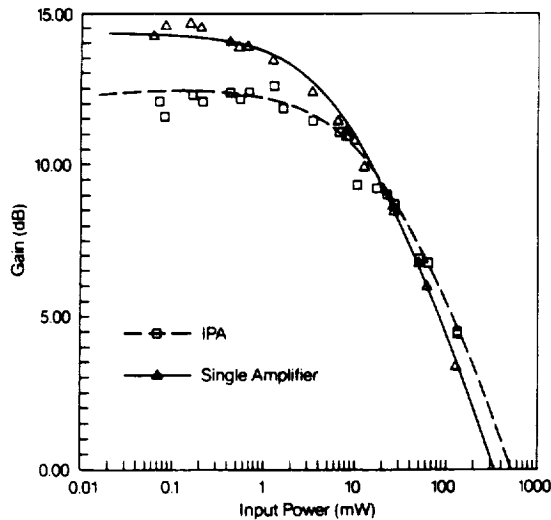


Fig. 4. Gain saturation of the single amplifier (△) and the IPA (□). The curves are theoretical fits as in Fig. 3.

output power of a single amplifier (before spatial filtering of the diffractive sidelobes) (Fig. 3). At high output powers, the IPA gives up to 1.3 times the total power and 1.5 times the single-lobe power of an individual amplifier for a given total injected power owing to reduced gain saturation. The data shown in Fig. 3 are replotted as gain versus the logarithm of the input power in Fig. 4 to demonstrate more clearly the crossover predicted by Eqs. (6)–(8). The calculated curves shown in Figs. 3 and 4 use the extensions of Eqs. (6)–(8) that include amplifier internal losses¹⁹ and $\Omega = 0.93$. The vertical distance between the two saturation curves in Fig. 4 allows determination of the power-output enhancement as

a function of the gain saturation. Deeper saturation leads to a larger power enhancement for the IPA, i.e., a larger difference in the gain. Because of the non-linear characteristics of the gain saturation, doubling the number of amplifiers does not necessarily lead to a doubling of the output power for a given input power.

Coherent summation of two AlGaAs amplifiers in an interferometric power-amplifier configuration has been done with 93% summation efficiency and resulted in 372 mW of power in a single diffraction-limited lobe. Coherent summation of an array of gain elements provides a means to increase the available optical power by at least a factor of 1.5 over a single equivalent gain element.

References

1. C. Zmudzinski, L. J. Mawst, D. Botez, C. Tu, and C. A. Wang, *Electron. Lett.* **28**, 1543 (1992).
2. J. N. Walpole, E. S. Kintzer, S. R. Chinn, C. A. Wang, and L. J. Missaggia, *Appl. Phys. Lett.* **61**, 740 (1992).
3. L. Goldberg, D. Mehuys, and D. C. Hall, *Electron. Lett.* **28**, 1082 (1992).
4. R. H. Rediker, R. P. Schloss, and L. J. Van Ruyven, *Appl. Phys. Lett.* **46**, 133 (1985).
5. J. R. Leger, G. J. Swanson, and W. B. Veldkamp, *Appl. Opt.* **26**, 4391 (1987).
6. J. Harrison, G. A. Rines, P. F. Moulton, and J. R. Leger, *Opt. Lett.* **13**, 111 (1988).
7. J. R. Andrews, *Opt. Lett.* **14**, 33 (1989).
8. W. Wang, K. Nakagawa, S. Sayama, and M. Ohtsu, *Opt. Lett.* **17**, 1593 (1992).
9. G. J. Swanson, J. R. Leger, and M. Holz, *Opt. Lett.* **12**, 245 (1987).
10. J. R. Leger, M. L. Scott, and W. B. Veldkamp, *Appl. Phys. Lett.* **52**, 1771 (1988).
11. V. Diadiuk, Z. L. Liau, J. N. Walpole, J. W. Caunt, and R. C. Williamson, *Proc. Soc. Photo-Opt. Instrum. Eng.* **1219**, 366 (1990).
12. D. F. Welch, R. Waarts, D. Mehuys, R. Parke, D. Scifres, R. Craig, and W. Streifer, *Appl. Phys. Lett.* **57**, 2054 (1990).
13. G. A. Evans, N. W. Carlson, J. M. Hammer, M. Lurie, J. K. Butler, S. L. Palfry, R. Amantea, L. A. Carr, F. Z. Hawrylo, E. A. James, C. J. Kaiser, C. J. Kirk, W. F. Reichert, S. R. Chinn, J. R. Shealy, and P. S. Zory, *Appl. Phys. Lett.* **53**, 2123 (1988).
14. M. S. Zediker, H. R. Appelman, B. G. Clay, J. R. Heidel, R. W. Herrick, J. Haake, J. Martinosky, F. Streumpf, and R. A. Williams, *Proc. Soc. Photo-Opt. Instrum. Eng.* **1219**, 197 (1990).
15. M. Jansen, J. J. Yang, L. Heflinger, S. S. Ou, M. Sergeant, J. Huang, J. Wilcox, L. Eaton, and W. Simmons, *Appl. Phys. Lett.* **54**, 2534 (1989).
16. W. R. Christian, P. H. Beckwith, and I. McMichael, *Opt. Lett.* **14**, 81 (1989).
17. J. M. Verdiell, H. Rajbenbach, and J. P. Huignard, *IEEE Photon. Technol. Lett.* **2**, 568 (1990).
18. J. R. Andrews and G. L. Schuster, *Opt. Lett.* **16**, 913 (1991).
19. A. Siegman, *Lasers* (University Science, Mill Valley, Calif., 1986), p. 324.

4. Modeling and Optimization of Quantum Well Laser Amplifiers, Sinan Batman, draft of a Masters Thesis to be submitted to the Department of Electrical Engineering, Rochester Institute of Technology

MODELING AND OPTIMIZATION OF QUANTUM WELL LASER AMPLIFIERS

by

Sinan Batman

A Thesis Submitted

in

Partial Fulfillment

of the

Requirements for the Degree of

MASTER OF SCIENCE

in

Electrical Engineering

Approved by:

Prof._____

Prof._____

Prof._____

**DEPARTMENT OF ELECTRICAL ENGINEERING
COLLEGE OF ENGINEERING
ROCHESTER INSTITUTE OF TECHNOLOGY
ROCHESTER, NEW YORK
MAY 1993**

Symbol definitions

<u>Symbol</u>	<u>Definition</u>	<u>Value</u>	<u>Units</u>
$g_S(z)$	modal gain as a function of position		cm^{-1}
$N_d^0(z)$	transparency electron density at reference temperature		cm^{-3}
$N_d^0(T)$	temperature dependent transparency electron density		cm^{-3}
N_w	number of quantum wells		
Γ	optical confinement per well		
G_0	gain constant		cm^{-1}
τ_{sp}	spontaneous emission lifetime		s
d	thickness of junction		cm
e	electron charge	$1.6 \cdot 10^{-19}$	Coulomb
J	current density		A/cm^2
c	speed of light in vacuum	$3.0 \cdot 10^{10}$	cm/s
n_g	group index	3.3	
$N_e(z)$	electron density as a function of position		cm^{-3}
$S(z)$	photon density as a function of position		cm^{-3}
ΔT	change in temperature relative to the reference value		$^{\circ}\text{K}$
T_0	characteristic temperature	150	$^{\circ}\text{K}$
R_{th}	thermal resistance		$^{\circ}\text{K}/\text{W}$
R_s	serial resistance		Ω
V_f	forward voltage	1.5	V
L	length of the amplifier		cm
D	width of the amplifier		cm

<u>Symbol</u>	<u>Definition</u>	<u>Value</u>	<u>Units</u>
P_{el}	electrical power fed to the amplifier		W
P_{in}	optical power injected to the amplifier		W
P_{out2}	optical power transmitted from facet 2		W
P_{out1}	optical power transmitted from facet 1		W
P_{av}	fraction of electrical power transforming to heat		W
P_{max}	facet damage limit for power density		W/cm ²
G_s	single pass gain		
R_1, R_2	front and back facet reflectivities		
β	optical mode propagation constant		cm ⁻¹
h	planck's constant		
α	distributed losses		cm ⁻¹
λ	lasing wavelength		cm
j_0	transparency current density		A/cm ²
b	gain - current coefficient		cm/A
$a^{(\pm)}$	injected / reflected amplitude		
$b^{(\pm)}(z)$	forward/backward travelling amplitudes		
$c^{(\pm)}$	transmitted and amplified optical amplitude		

Laser Amplifiers

Definition

Optical amplifiers can be divided into two different categories: Coherent optical amplifiers and incoherent optical amplifiers. Coherent optical amplifiers are devices that increase the amplitude of an optical field while maintaining its phase. If the input optical field is monochromatic, the output will also be monochromatic, with the same frequency. In contrast, an amplifier that increases the intensity of an optical wave without preserving the phase is called an incoherent optical amplifier. This thesis is concerned with coherent optical amplifiers, namely quantum well structures. Such amplifiers are used in many applications; examples include the amplification of weak optical pulses for use in long distance fiber communications, the amplification of highly intense optical pulses for laser-fusion applications or the amplification of continuous wave optical field from a master oscillator in a MOPA system.

Coherent amplification is achieved through amplification by the stimulated emission of radiation. That is a photon in a given mode induce an atom at a higher energy level to undergo a transition to a lower energy level, emitting a second photon into the same mode (a photon with the same direction, frequency and polarization). The two photons, in turn, can stimulate the emission of two additional photons with the same properties and so on. The requirement for stimulated emission being the incident photon to have a nearly equal energy to the corresponding atomic transition, the process is restricted to a band of frequencies determined by the atomic linewidth. Thus, the primary frequency selection in optical amplifiers is due to the energy level differences of the laser material

used. Optical cavities may be used to assure auxiliary frequency tuning in contrary to electronic amplifiers where the frequency tuning is achieved through an internal resonant circuit making use of inductors and capacitors.

In thermal equilibrium the number of atoms in the lower energy level is higher than the number of atoms in a higher level, resulting into the domination of absorption by the low energy atoms over the stimulated emission through the minority high energy atoms. To achieve amplification, the inequality mentioned above has to be reversed with the help of an external source of power resulting into a nonequilibrium situation. An elementary diagram describing the operation of a laser amplifier is illustrated below (see figure 1.1).

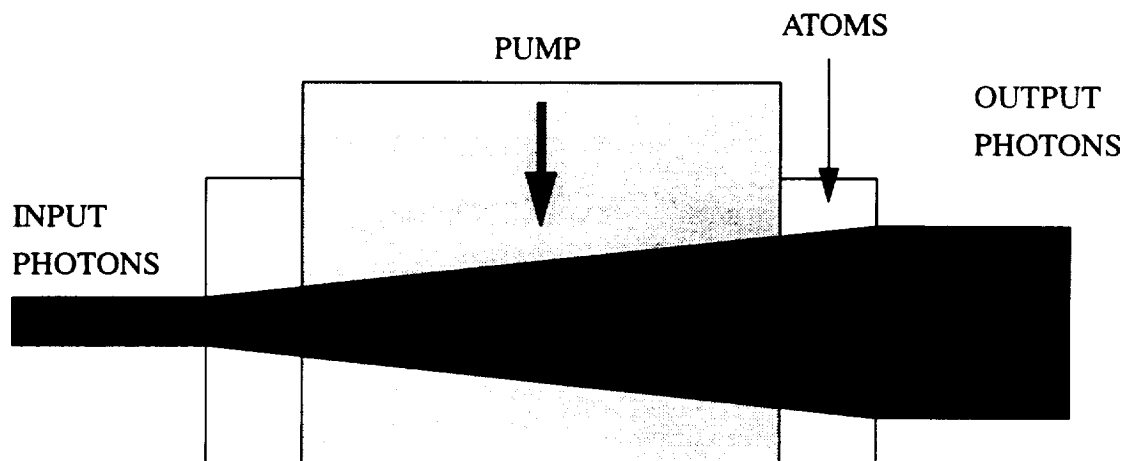


Figure 1.1 : Simplified illustration of amplification along a traveling wave amplifier

Characterization criterias for optical amplifiers

Real coherent amplifiers are characterized by a gain and phase shift that are frequency dependent. Furthermore, for a sufficiently large input photon density the amplifier exhibit saturation which results into a non-proportional relationship between input and output powers. Also saturation may

result into generation of harmonic components. Finally a noise is always present in the output.

An amplifier may therefore be characterized by the following:

- Gain
- Bandwidth
- Phase shift
- Power source
- Nonlinearity and gain saturation
- Noise

Examples of laser amplifiers

Laser amplification can happen in a variety of materials. Usually each system has interacting energy levels influencing the electron populations of the transition of interest. The operations of most of these amplifiers can be modelled as a three or a four level system. Examples are the three-level ruby laser amplifier, the four-level neodymium-doped yttrium-aluminium garnet laser amplifier, and the three-level erbium-doped silica fiber laser amplifier. Besides the solid state lasers mentioned above gas and liquid lasers can also be used to achieve amplification.

Pumping may be implemented using many methods, including the use of electrical, optical and chemical means. Gas lasers usually requires a direct current (dc) or a radio-frequency (RF) discharge current for pumping. The solid-state silica fiber laser requires optical pumping which may be achieved through a semiconductor (injection diode). Finally semiconductor laser amplifiers use direct current (dc) or ~~alternative current (ac)~~ for pumping in a cw or pulsed mode of operation res-

pectively.

Optical Amplification by semiconductor lasers

After the invention of semiconductor laser [1] in 1962, the coherent light properties of the device became the focus of extensive research [2]. Due to the inherent nature of optical amplification, semiconductor lasers can be utilized as optical amplifiers besides oscillators. It acts as a “linear” amplifier when the supplied current is below the oscillation threshold and as a nonlinear amplifier through injection locking when it is operated above threshold.

In the linear mode, it is possible to classify the amplifier into two types: the Fabry-Perot (FP) and travelling wave (TW) type, differing from each other at the reflectivities at both end mirrors. The travelling wave amplifier has very low facet reflectivities resulting into the incident light being amplified in a single pass without suffering any reflection. This kind of amplifiers causes a smooth increase in spontaneous emission with increasing electrical power, making difficult to differentiate amplification below the threshold from amplification above the threshold. Fabry-Perot type amplifiers however, are characterized by considerable facet reflectivity resulting into a regenerative resonant amplification between both end mirrors.

The principle underlying the operation of a semiconductor laser amplifier is the same as that for other laser amplifiers: population inversion. It is achieved through artificial pumping of electrons to higher energy levels by electrical current injected in a p-n junction diode. Application of a forward bias voltage results into the injection of carriers pairs into the active region, where they recombine through stimulated emission.

The theory behind semiconductor laser amplifier is somewhat more complicated than the amplifier

structure mentioned earlier because the transitions occur between bands of closely spaced energy levels rather than well-separated discrete levels. However, the semiconductor laser amplifier may be viewed as four level laser system (see the appendix A), in which the upper two levels lie in the conduction band and the lower two levels lay in the valence band.

These amplifiers have both advantages and disadvantages. Although they are very small in size so that they can easily be incorporated into optoelectronic integrated circuits and their bandwidths can be as large as 10 THz (greater than optical fibers), the coupling loss is very high (3dB to 5dB) and they are temperature and polarization sensitive.

Motivation for Heterostructures

The complex dependence of the gain coefficient on the injected-carrier concentration makes the analysis of the semiconductor amplifier somewhat difficult. Because of this, it is customary to adopt an empirical approach in which the peak gain coefficient g_s is assumed to be linearly related to the injected carrier concentration N_{el} for values of N_{el} close to the operating point (similar to the small signal treatment for electronic amplifiers). The dependence of the peak gain coefficient g_s on N_{el} may then be modeled by the linear equation

$$g_s = G_o \left(\frac{N_{el}}{N_{el}^0} - 1 \right) \quad (1)$$

The parameters α and N_{el}^0 are chosen to satisfy the requirement that when the injected carrier concentration is zero, the peak gain coefficient is equal to minus alpha which is the absorption coeffi-

cient of the semiconductor and when the injected carrier density is equal to transparency current density, the medium becomes transparent, that is g_s is equal to zero. It is clear from the equation that, depending upon whether we are operating below or above transparency, the amplifier acts as a strong absorber and strong amplifier respectively.

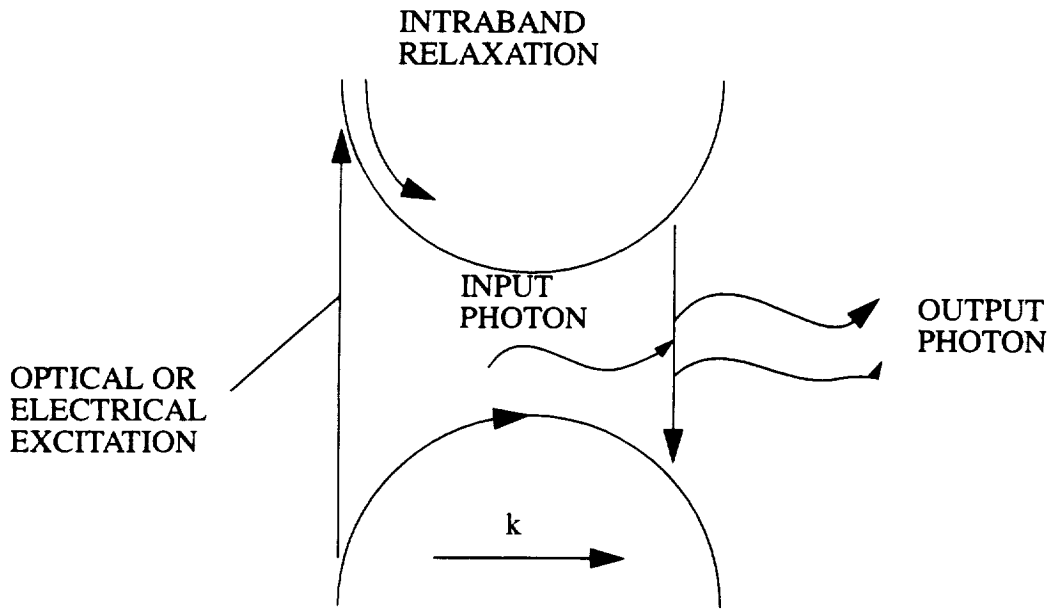


Figure 1.2 : The energy-band diagram of a forward-biased heavily doped p-n junction

The energy-band diagram of a forward-biased heavily doped p-n junction is illustrated below (see figure 1.2). The conduction and valence bands quasi-Fermi levels E_{fc} and E_{fv} lie within the conduction and valence bands respectively and a state of quasi-equilibrium exists in the active region. The quasi-fermi levels are sufficiently well separated so that a population inversion is achieved and net gain may be obtained over the bandwidth $E_g \leq h\nu \leq E_{fc} - E_{fv}$ within the active region. The thickness d of the active region in a semiconductor homostructure laser is a very important parameter that is determined principally by the diffusion lengths of the minority carriers at both sides of

the junction. Due to the proportionality between electron densities and injected current density at low input optical powers, equation (1) can be rewritten as

$$g_s = G_0 \left(\frac{J}{J_0} - 1 \right) \quad (2)$$

where J and J_0 can be expressed as

$$(J, J_0) = \frac{ed}{\tau_{sp}} (N_{el}, N_{el}^0) \quad (3)$$

It is seen from the above equations that transparency current density J_0 is directly proportional to the junction thickness d , so that a narrower active region would result in a lower current density to achieve transparency. The amplifier however would still experience the same gain at a much lower current density. The new device would consequently require a much easily achievable electrical power and would be much more efficient. However, reducing the size of the junction causes some problems, namely the diffusion of electrons and holes out of this smaller region, their diffusion lengths being greater. A solution to the problem of confining electrons and photons into an active region that is smaller than their diffusion lengths is to use a heterojunction device which would also confine the optical beam to an active region which is smaller than its wavelength.

Heterostructures

The concept of the heterostructure is to form heterojunction potential barriers on both sides of the p-n junction to provide a potential well that limits the distance over which the minority carriers may

diffuse. This confinement results in active regions of thickness as small as $0.1 \mu\text{m}$ (even thinner confinement regions, $\approx 0.01 \mu\text{m}$ were achieved with quantum wells).

It is also possible to achieve optical confinement of the electromagnetic beam simultaneously, by selecting the material of the active region in such a way that its refractive index is slightly greater than that of the surrounding layers so that the structure acts as an optical waveguide like core guided fiber optic cables.

A typical heterostructure device would have three layers of different lattice-matched materials:

Layer 1 : p-type, energy gap E_{g1} , refractive index n_1

Layer 2 : p-type, energy gap E_{g2} , refractive index n_2

Layer 3 : n-type, energy gap E_{g3} , refractive index n_3

The energy gap of the active region is chosen to be smaller than the sandwiching layers to insure carrier confinement and its refractive index is chosen to be slightly higher to achieve light confinement.

The advantages of using a heterostructure device instead of a homostructure are:

- Increased amplifier gain for a given electrical power due to the ease of reaching transparency.
 - Increased amplifier gain due to the increase of the proportion of light being amplified resulting from the enhanced optical confinement
 - Reduced absorption from the cladding layers, their gap energy being larger than photon energy
- The energy band diagram and refractive index as a function of position for a double heterostructure semiconductor laser is illustrated in figure 1.3.

When the thickness of the active layer is made sufficiently small (i.e. smaller than the de Broglie wavelength of a thermalized electron, $\approx 50 \text{ nm}$ in GaAs), the understanding of the physics of the device necessitates quantum mechanics due to the shrinking in size. Since the energy gap of the

surrounding layers are larger than the active region, the latter start acting as a quantum well resulting into a different energy-momentum relationship than the usual heterostructure.

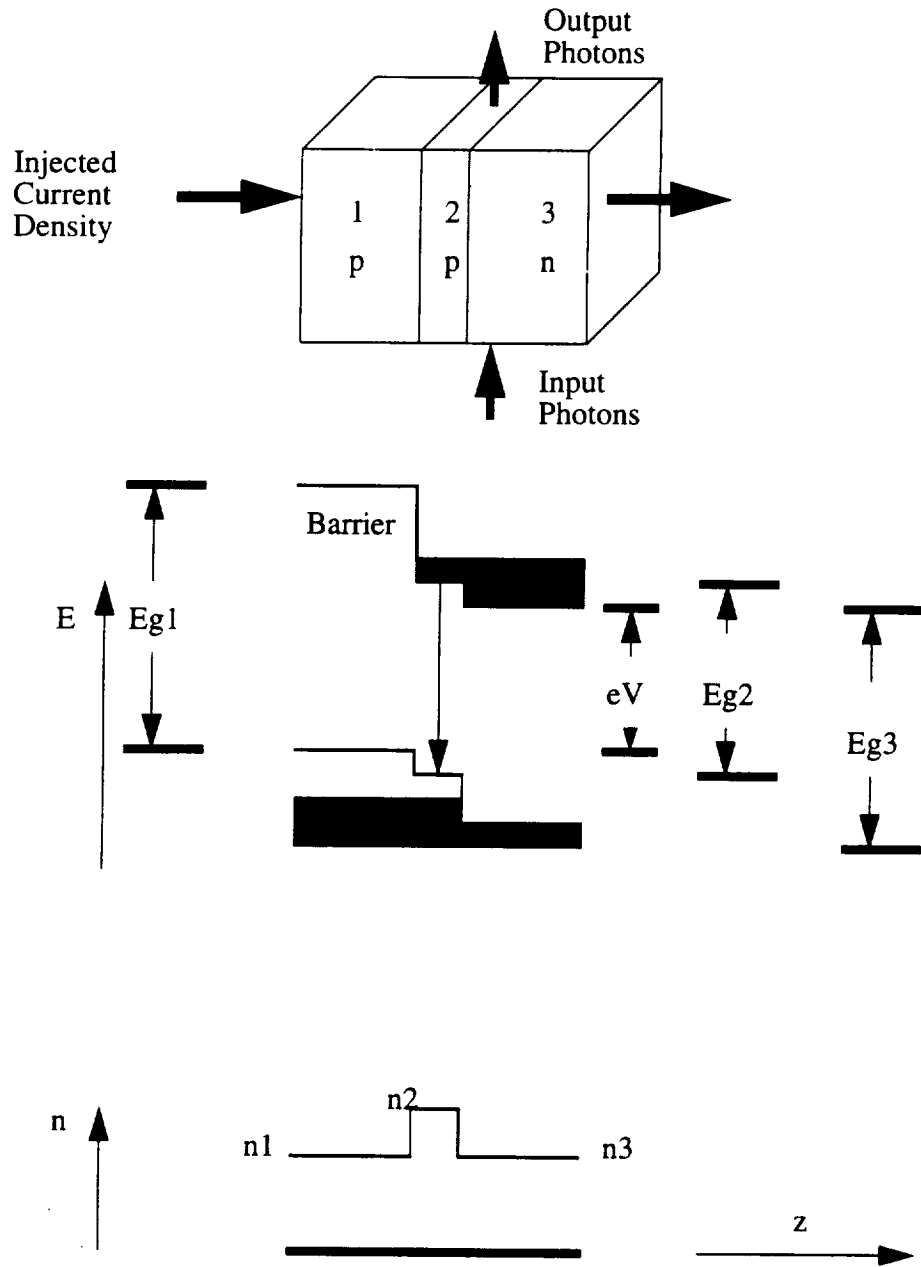


Figure 1.3 : The energy band diagram and refractive index as a function of position for a double heterostructure semiconductor laser.

Quantum well laser amplifiers

Except for the thickness of its active layer, quantum well lasers are identical to the conventional heterostructure lasers. The diagram of a graded index separate confinement GaAlAs heterojunction quantum well laser is illustrated in figure 1.4.

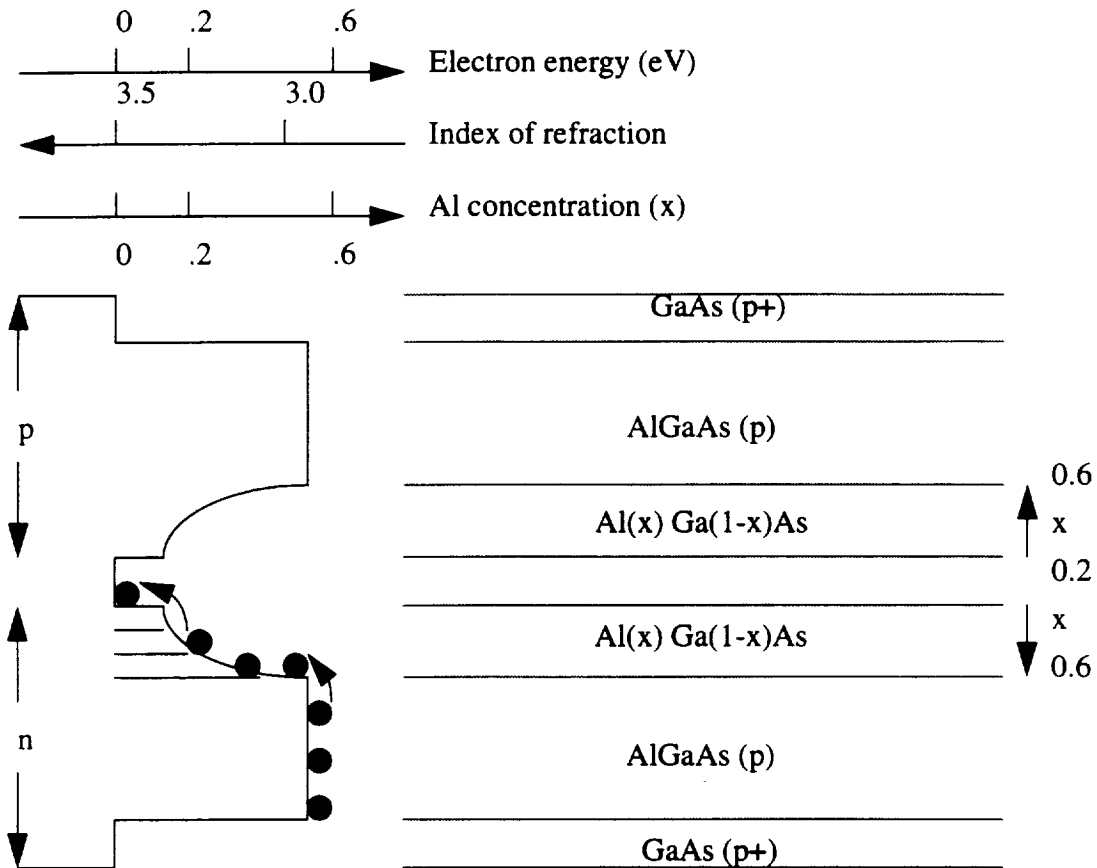


Figure 1.4 : Anatomy of a graded index separate confinement GaAlAs heterojunction quantum well laser

The function of the graded region is to enhance the advantages of using a heterostructure with respect to a homostructure laser, that is, it enhances dielectric waveguide properties of the laser and

confines and guides electrons and holes to the well.

It has been mentioned earlier that quantum well lasers have a different energy-momentum relationship than the bulk material. The energy levels E_q of an electron of mass m_c or a hole of mass m_v confined to a one dimensional infinite rectangular well of width d can be found by solving the Schrödinger equation as

$$E_q = \frac{1}{8m} \left(\frac{hq}{d} \right)^2 \quad (4)$$

where $q=1,2,\dots$ and m designates an electron's or a hole's mass. Remark that increasing the width of the well results in an increase in the separation between adjacent energy levels.

As shown in the figure 1.5, electrons and holes are confined to the active region in x direction. However in the y - z plane, they extend to a much larger dimension and can be treated as if they were in bulk semiconductor.

The energy-momentum relationship in the conduction band can be written as

$$E = E_c + \frac{\hbar^2 k_1^2}{2m_c} + \frac{\hbar^2 k_2^2}{2m_c} + \frac{\hbar^2 k_3^2}{2m_c} \quad (5)$$

where $k_1=q_1\pi/d_1$, $k_2=q_2\pi/d_2$, $k_3=q_3\pi/d_3$ and $q_1, q_2, q_3=1,2,\dots$. Remark that since the active layer thickness is much smaller than the surrounding layers thicknesses, the separation between the discrete values of \vec{k} in x - z plane is much more important than the ones in x - y and y - z planes. Eventually, k_2 and k_3 may be approximated as a continuum in which case equation (5) can be rewritten as

$$E = E_c + E_{q1} + \frac{\hbar^2 k^2}{2m_c} \quad (6)$$

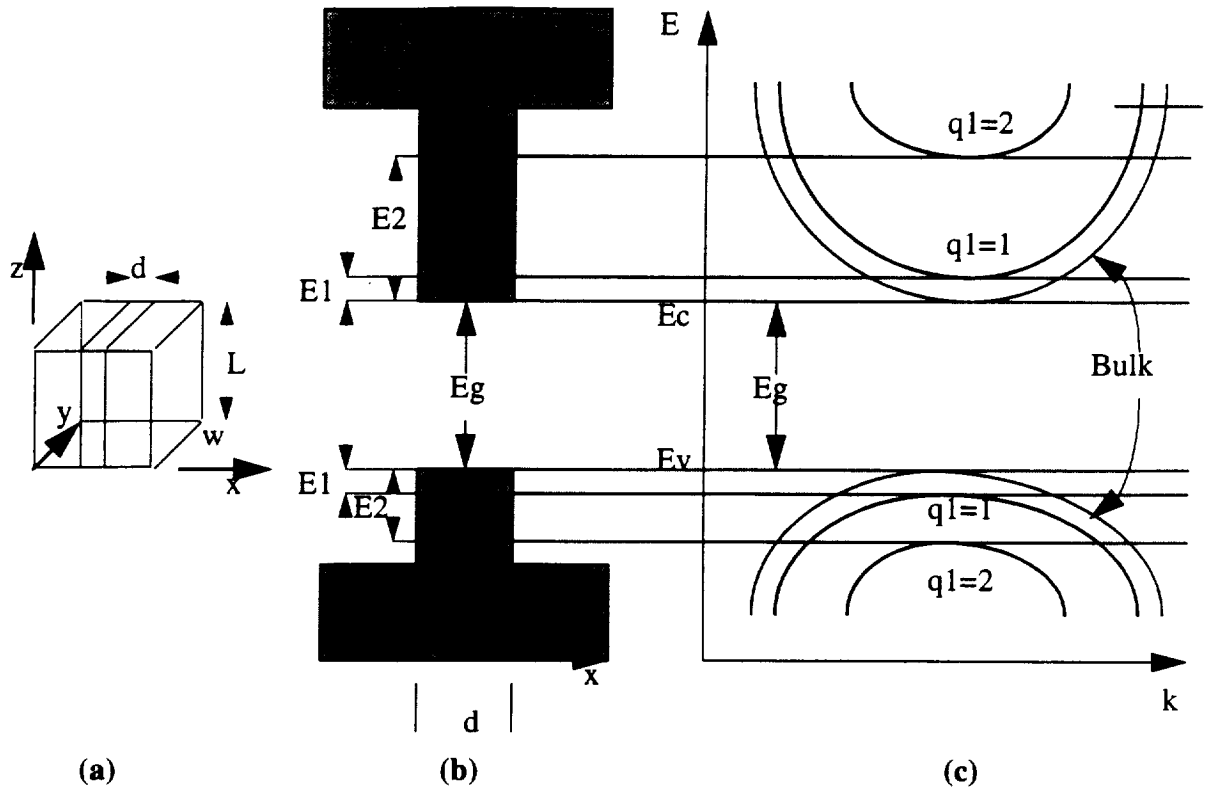


Figure 1.5 : (a) Geometry of quantum-well structure (b) Energy level Diagrams in the quantum well (c) Cross section of E-k relation in the direction of k_2 and k_3

where $q_1=1,2,3,\dots$, and $k = \sqrt{|\vec{k}_2|^2 + |\vec{k}_3|^2}$. In the above equation q_1 is the quantum number denoting the subband with minimum energy $E_c + E_{q_1}$. The valence band could be treated similarly.

For the bulk semiconductor the energy is a parabolic function of the three dimensional momentum vector and the difference between each value of the momentum in each direction has comparable magnitudes unlike the quantum well structure for which the momentum vector k_1 takes well separated values.

For the bulk semiconductor the density of states can be written as (see appendix for derivation)

$$\rho(k) = \frac{k^2}{\pi^2} \tag{7}$$

From the equation above, the density of electrons and holes near the conduction and valence bands respectively follow as (see appendix for derivation)

$$\rho_c(E) = \frac{(2m_c)^{3/2}}{2\pi^2 \hbar^3} (E - E_c)^{1/2} \quad (8)$$

for $E \geq E_c$ and

$$\rho_v(E) = \frac{(2m_v)^{3/2}}{2\pi^2 \hbar^3} (E_v - E)^{1/2} \quad (9)$$

for $E \leq E_v$, where m_c and m_v stands for the effective averaged masses of electrons and holes respectively.

For the case of quantum well laser, the density of state functions are obtained from the magnitude of the two dimensional wavevector (k_2, k_3) and therefore they are linearly dependent on it. The expression for the density of state per unit volume follows as :

$$\rho(k) = \frac{k}{\pi d_1} \quad (10)$$

The electron density of states as a function of the energy $\rho_c(E)$ is related to the density of state function with the relation (see appendix for details).

$$\rho_c(E) dE = \rho(k) dk = \frac{k}{\pi d_1} dk \quad (11)$$

Taking the derivative of the right hand side of equation (6) with respect to the two dimensional wavevector k yields

$$\frac{dE}{dk} = \frac{\hbar^2 k}{m_c} \quad (12)$$

Putting (12) into (11) yields

$$\rho_c(E) = \frac{m_c}{\pi \hbar^2 d_1} \quad (13)$$

for $E > E_c + E_{q_1}$ and 0 otherwise for $q_1 = 1, 2, \dots$. It can be seen from the above equation that when $E > E_c + E_{q_1}$ the density of state per unit volume is constant for each quantum number q_1 . Since to obtain the overall density of state function one has to add the density of state functions corresponding to each quantum level q_1 , the former exhibits a staircase like shape as shown in figure 1.6. This property is also true for the density of states in the valence band.

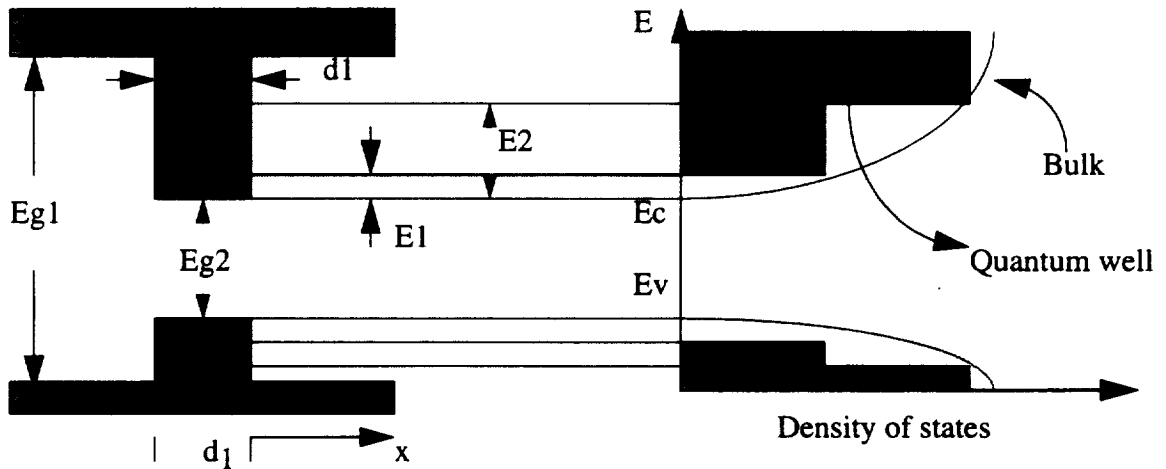


Figure 1.6 : Density of states for a quantum-well structure and for a bulk semiconductor

In a quantum well laser, photons interact with electrons and photons somewhat similarly to the bulk semiconductor. The transitions conserve energy and momentum between conduction and valence bands. Different from the bulk semiconductor, the transitions in the quantum well laser also conserve the quantum number q , that is they are allowed within the band $q \uparrow = i$ in the valence band and $q \downarrow = i$ in the conduction band, where i denotes the subband number. The expressions derived for gain coefficient and transition probabilities in the bulk material also apply to the quantum well when the bandgap energy E_g is replaced with the energy gap between the subbands, $E_{gq} = E_g + E_q + E'_q$ and a constant density of states is used rather than one that varies as the square root of the energy. The total gain coefficient is obtained by summing up all subband gain coefficients.

At this point we can rewrite the joint density of states function in terms of frequency as

$$\rho(\nu) = \frac{\hbar m_r}{m_c} \frac{m_c}{\pi \hbar^2 d_1} = \frac{2m_r}{\hbar d_1} \quad (14)$$

when $\hbar\nu > E_g + E_q + E'_q$, and 0 otherwise. The transition from equation (11) is straightforward using the relationship

$$\rho_c(\nu) = \left(\frac{dE}{d\nu} \right) \rho_c(E) = \left(\frac{\hbar m_r}{m_c} \right) \rho_c(E) \quad (15)$$

when the transitions from all subbands are considered the joint density of states looks like staircase distribution as it is illustrated in the preceding figure.

Gain coefficient

As in the case of bulk semiconductor (see Appendix B), the gain coefficient of the quantum well structure is given by the expression

$$g_s(\nu) = \frac{\lambda^2}{8\pi\tau_r} \rho(\nu) f_g(\nu) \quad (16)$$

where $f_g(\nu)$ is the Fermi inversion factor identical for bulk and quantum well lasers. Thus the only difference between the two gain coefficients is the joint density of states function. The effect of different density of state function on the gain coefficient is illustrated in figure 1.7, where it is assumed that the higher levels of the laser are not excited. The step wise density of state function of the quantum well structure results into a smaller peak gain and narrower bandwidth.

The dependence of the peak gain on current density supplied to the quantum well can be inferred from the graph. An increase in the electron density will result into the generation of excess holes and electrons which will increase the gap between the quasi-Fermi levels. When the value of the current density J is high enough so that $E_{fc} - E_{fv}$ barely exceeds the gap E_{g1} between the $q=1$ levels, the medium starts experiencing gain which will sharply increase up to its saturation value given by

$$g_p = \frac{\lambda^2 m_r}{2\tau_r h l} \quad (17)$$

If J is further increased, the spectral width will be broadened leaving the peak gain unchanged. In case the amount of pumping is at such a level that the difference $E_{fc} - E_{fv}$ cross over E_{g2} , the levels

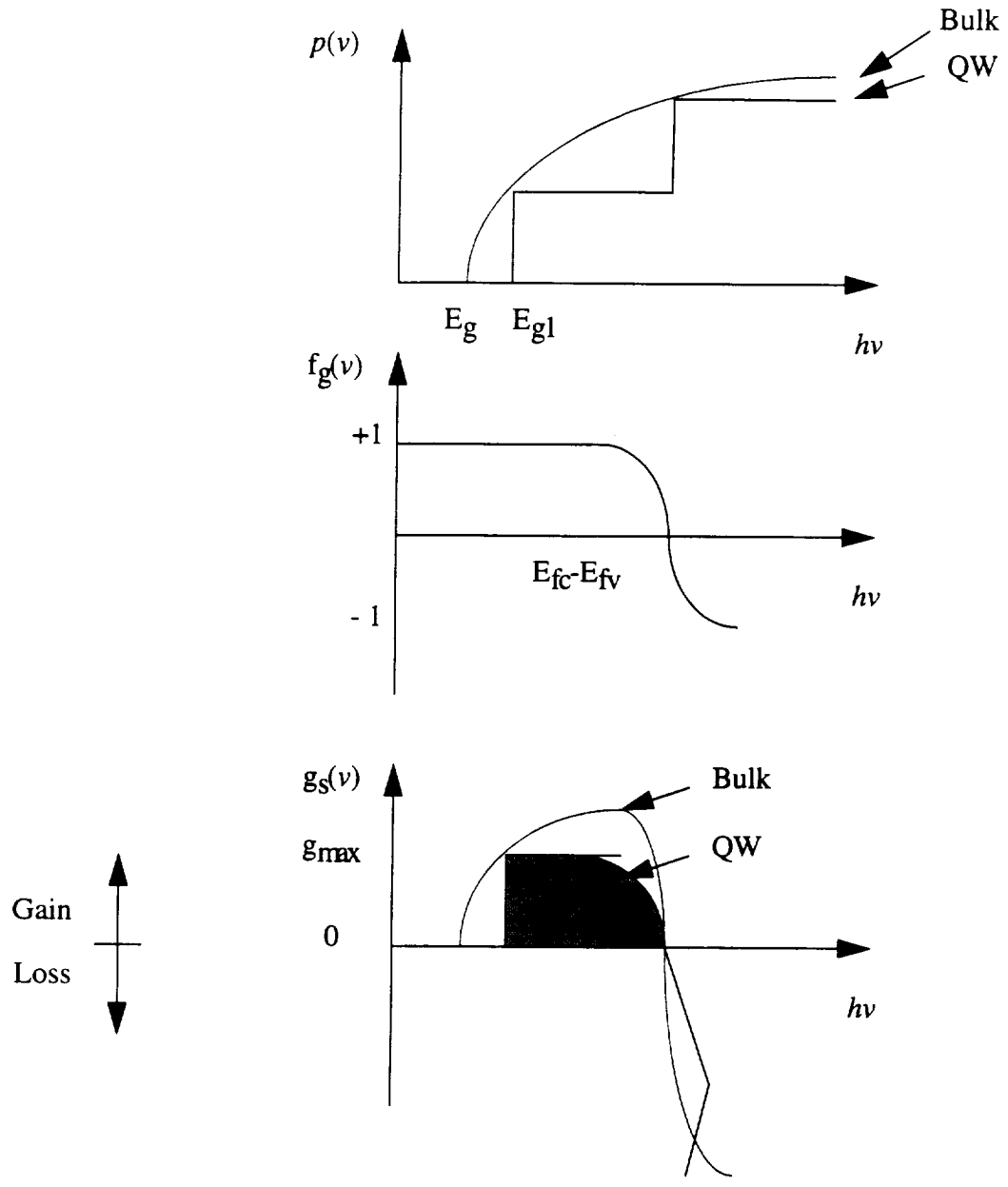


Figure 1.7 : Density of states, Fermi inversion factor, and gain coefficient in quantum well and bulk structures.

$q=2$ becomes excited and the peak gain coefficient experiences a second jump. The described variation of the peak gain coefficient with current density is shown in figure 1.8. Note that if $q=1$ levels are excited only the relationship could be considered as pseudo-logarithmic.

The semi-classical theory presented above displays the major differences between quantum well and double heterostructure devices. A more elaborate treatment can be found in papers where a pure quantum mechanical approach is used. But, the possible (and adequate) representation of the behaviour of the quantum well material gain with injected current density by a semi-logarithmic-function makes such an approach unnecessarily complex and timewise expensive

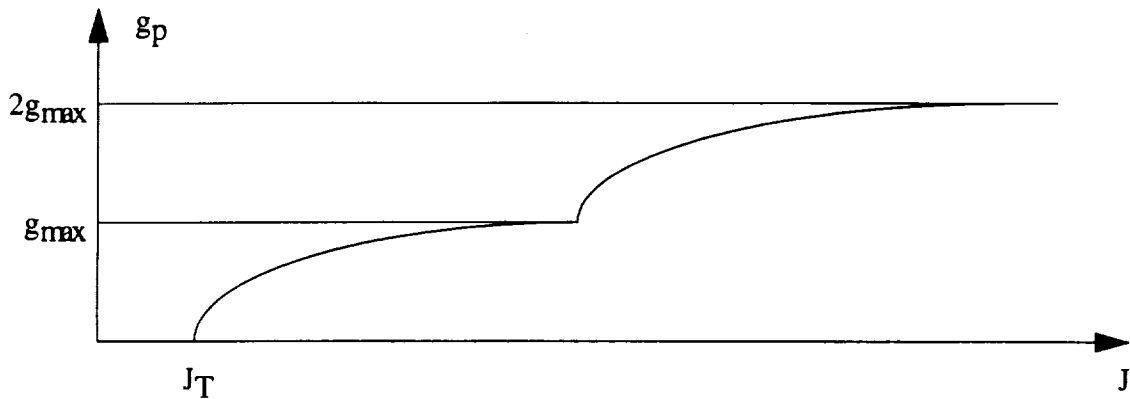


Figure 1.8 : Schematic relationship between peak gain coefficient and current density

Amplifier Model

The amplifier model chosen has to be able to predict closely the gain and efficiency of the amplifier in any operating condition necessitated by the optimization algorithm without increasing the mathematical complexity with unnecessary details. The model parameters should be easily determined from experiment and the set of equations used shouldn't become transcendental at any operating condition.

Rate Equations

Mathematically, semiconductor laser amplifiers are usually described by time dependent rate equations dealing with temporal changes in electron and photon densities in the active region of the device ignoring their spatial variation along the amplifier. Such method is used to describe amplifiers with high facet reflectivities for which the spatial distribution of electrons and photons are relatively even. However, to deal adequately with any kind of reflectivity (especially with zero reflectivity due to anti-reflective coating at facets), one has to use time and space dependent travelling-wave equations.

Rate Equations in the absence of excitation

In the absence of input optical field the dynamics of amplification can be described by the following two rate equations corresponding to the variation of spontaneously emitted photon and electron densities along the amplifier.

$$\frac{d}{dt}N_{el}(z) = \frac{J}{eN_w d} - \frac{N_{el}(z)}{\tau_{sp}} - \frac{c}{n_g N_w \Gamma} \sum_{\nu=1}^{\infty} g_{\nu}(z) S_{\nu}(z) \quad (18)$$

$$\frac{d}{dt}S_\nu(z) = \frac{\xi}{\tau_{sp}}D_\nu N_{el}(z) - \frac{S_\nu(z)}{\tau_{ph}} + \frac{c}{n_g}g_\nu(z)s_\nu(z) \quad (19)$$

The second term on the right side of equation (18) can be related to the loss coefficient of the guided mode as

$$\alpha = \frac{n_g}{c\tau_{ph}} \quad (20)$$

The first term in the right hand side of equation (17) is the contribution of pumping electrons to the electron population. The second term accounts for the rate at which the excess electron population decays through spontaneous emission. The last term represents the saturation effect resulting from the depletion of electron population following the electron hole combination.

The first term at the right hand side of equation (18) accounts for the increase in the amount of spontaneously emitted photons at frequency ν following the spontaneous decay of the corresponding proportion of electrons in the conduction band. The distribution function D_ν is used to assure that the electron distribution at all wavelengths tends to increase or decrease at all wavelengths when photons are emitted or absorbed (homogeneous broadening).

The steady state solution of the rate equations can be obtained by letting the left hand sides of equations (17) and (18) equal to zero. Then the electron density can be obtained from equation (17) as

$$N_{el}(z) = \frac{\tau_{sp}}{(dN_w)}e^J - \frac{\tau_{sp}c}{n_g(\Gamma N_w)} \sum_{\nu=1}^{\infty} g_\nu(z)S_\nu(z) \quad (21)$$

The summation in the right hand side of equation (20) is multiplied by two to account for noise photons with two possible polarizations.

The solution for equation (18) necessitates that the spontaneously emitted photons be expressed as

a superposition of photon densities moving in positive and negative z-directions as

$$S_\nu(z) = S_\nu^{(+)}(z) + S_\nu^{(-)}(z) \quad (22)$$

and that the total derivative at the left of equation (18) be decomposed as

$$\frac{d}{dt} S_\nu^{(\pm)}(z) = \frac{\partial}{\partial t} S_\nu^{(\pm)}(z) \pm \frac{c}{n_g} \frac{\partial}{\partial z} S_\nu^{(\pm)}(z) \quad (23)$$

This way equation (18) can be written as two differential equations, one for each propagation direction. At steady state, the derived rate equations follow as

$$\frac{\partial}{\partial z} S_\nu^{(+)}(z) = \frac{\xi n_g}{2c\tau_{sp}} D_\nu N_{el}(z) + (g_\nu(z) - \alpha) S_\nu^{(+)}(z) \quad (24)$$

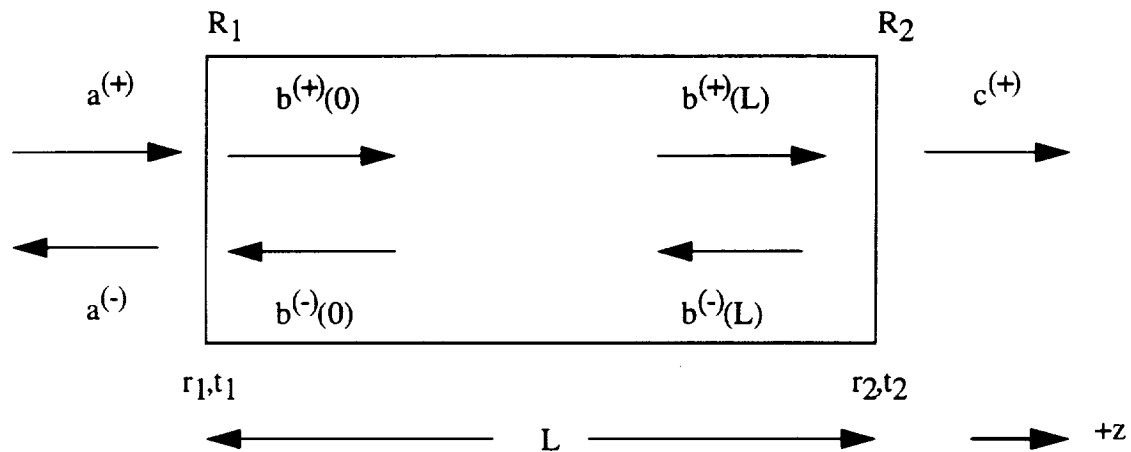
$$\frac{\partial}{\partial z} S_\nu^{(-)}(z) = \left(-\frac{\xi n_g}{2c\tau_{sp}} \right) D_\nu N_{el}(z) + (\alpha - g_\nu(z)) S_\nu^{(-)}(z) \quad (25)$$

Proper integration of equations (23) and (24) will yield the solution in the form of integral equations. The detailed development of the solution is not essential for this paper because in the range, the simulations are performed, spontaneously emitted photon densities are negligible compared to the injected signal density. The interested reader can find the solutions in Marcuse's paper.

Rate equations in the presence of injected optical signal

Previously, the spontaneous emission was described as an incoherent power wave because it distributes itself continuously over a relatively wide band of wavelengths with random phases between adjacent wavelength components. However the signal wave has to be treated coherently since its transmission is affected by resonance effects especially when the reflectivities at the facets distorts the constructive interference within succeeding reflected waves.

The figure below is the simplified drawing of an amplifier of length L and facet reflectivities R_1 and R_2 . The amplitudes denoted with the superscript (+) and (-) represents waves propagating in



(+z) and (-z) directions respectively.

The differential equations describing the variation of the signal wave along the amplifier along (+) and (-) z-directions are given by the following travelling-wave equations.

$$\frac{d}{dz} \mathbf{b}^{(+)}(z) = -i\beta \mathbf{b}^{(+)}(z) + \frac{1}{2} (\mathbf{g}_s(z) - \alpha) \mathbf{b}^{(+)}(z) \quad (26)$$

$$\frac{d}{dz} \mathbf{b}^{(-)}(z) = i\beta \mathbf{b}^{(-)}(z) - \frac{1}{2} (\mathbf{g}_s(z) - \alpha) \mathbf{b}^{(-)}(z) \quad (27)$$

Where β is the effective wavevector described as

$$\beta = 2 \frac{\pi n_{eff}}{\lambda_s} \quad (28)$$

The first term in the right hand side of equations (25) and (26) accounts for the change in phase of the optical signal as it travels along the amplifier. The second terms denote the net amplification of the signal amplitude. Remark that both waves will grow in amplitude in the direction of their superscript if the modal gain is higher than scattering losses.

The solutions of equations (25) and (26) are

$$\mathbf{b}^{(+)}(z) = \mathbf{b}^{(+)}(0) \exp(-i\beta z) \exp \left\{ \frac{1}{2} \int_0^z [\mathbf{g}_s(x) - \alpha] dx \right\} \quad (29)$$

$$\mathbf{b}^{(-)}(z) = \mathbf{b}^{(-)}(L) \exp[-i\beta(L-z)] \exp \left\{ \frac{1}{2} \int_z^L [\mathbf{g}_s(x) - \alpha] dx \right\} \quad (30)$$

The depletion of electron density is now due to the amplification of signal photons rather than spontaneous emission. The corresponding change is reflected into the electron density as

$$N_{el}(z) = \frac{\tau_{sp}}{(dN_w)_e} J - \frac{\tau_{sp} c}{(\Gamma N_w)_g} \mathbf{g}_s(z) \left[|\mathbf{b}^{(+)}(z)|^2 + |\mathbf{b}^{(-)}(z)|^2 \right] \quad (31)$$

Boundary conditions for the Fabry-Perot Laser Amplifier (FPLA)

The appropriate boundary conditions for the FPLA must take into account the reflection and transmission at the facets. At $z=0$, the field reflectance is taken as r_1 and the transmittance as t_1 . At $z=L$, the equivalent quantities are denoted as r_2, t_2 . The relationship between mentioned reflectances and transmittances to the reflectivities R_1, R_2 are established as

$$r_1 = \sqrt{R_1} \quad (32)$$

$$r_2 = \sqrt{R_2} \quad (33)$$

$$t_1 = \sqrt{1 - R_1} \quad (34)$$

$$t_2 = \sqrt{1 - R_2} \quad (35)$$

The boundary conditions at $z=0$ and $z=L$ (see figure) are given by

$$b^{(+)}(0) = t_1 a^{(+)} + r_1 b^{(-)}(0) \quad (36)$$

$$b^{(-)}(L) = r_2 b^{(+)}(L) \quad (37)$$

$$a^{(-)} = r_1 a^{(+)} + t_1 b^{(-)}(0) \quad (38)$$

$$c^{(+)} = t_2 b^{(+)}(L) \quad (39)$$

Using equations (28),(29), (35) and (36), one can calculate the actual value of photon amplitudes at the boundaries as a function of one pass gain G_s , facet reflectivities R_1 and R_2 , input optical amplitude $a^{(+)}$ and the phase shift due to resonance effect as

$$b^{(+)}(0) = \frac{(1 - R_1)^{1/2} a^{(+)}}{1 - (R_1 R_2)^{1/2} G_s \exp(-2i\beta L)} \quad (40)$$

$$b^{(-)}(L) = \frac{[G_s R_2 (1 - R_1)]^{1/2} a^{(+)} \exp(-i\beta L)}{1 - (R_1 R_2)^{1/2} G_s \exp(-2i\beta L)} \quad (41)$$

where the one-pass gain G_s is given by

$$G_s = \int_0^L [g_s(x) - \alpha] dx \quad (42)$$

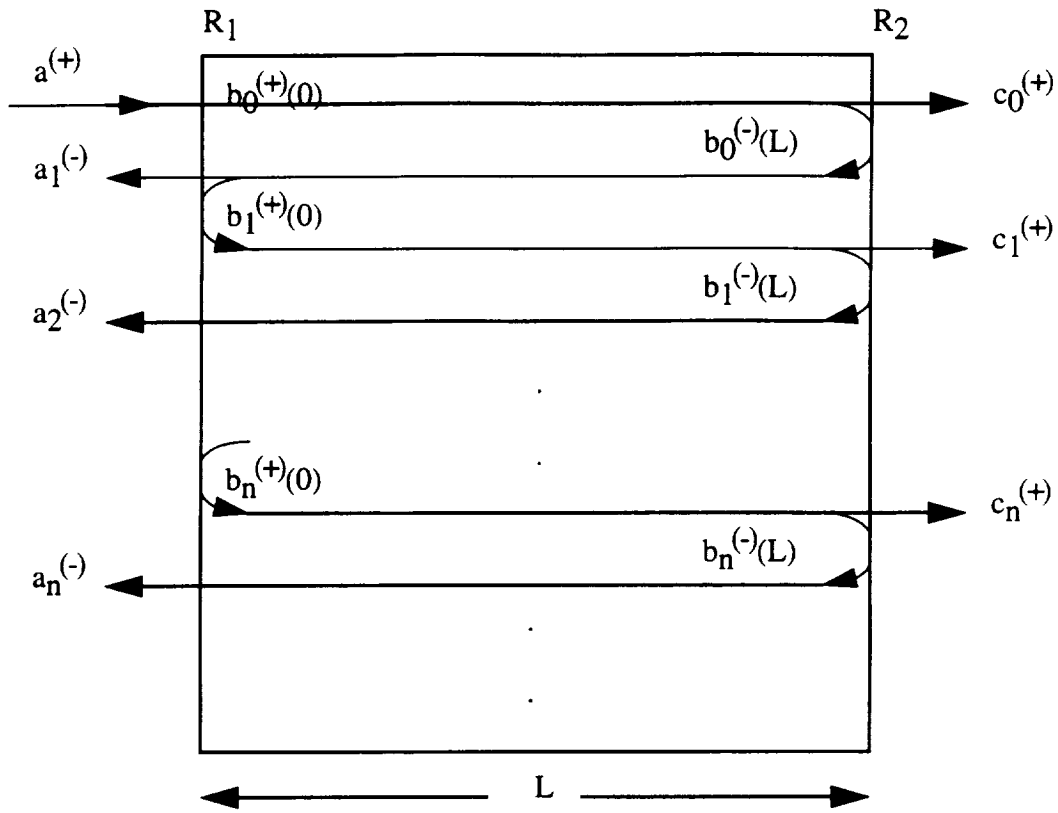
Now, one can calculate the photon densities inside and outside of the amplifier (see figure) by making use of equations (28), (29), (37), and (38). A better understanding of equation (39) and (40) would be established if one obtains them through infinite summations of reflected or transmitted waves at the device boundaries.

The previously mentioned method constructs the steady-state photon amplitudes at $z=0$ and $z=L$ by adding the resulting contribution of each reflection as shown in the figure below where $b_n^{(+)}(0)$, $b_n^{(-)}(L)$, $a_n^{(-)}$ and $c_n^{(+)}$ stand for

$$b_n^{(+)}(0) = t_1 a^{(+)} (r_1 r_2 G_s)^n \exp(-2in\beta L) \quad (43)$$

$$b^{(-)}(L) = t_1 r_2^{(n+1)} r_1^n G_s^{\binom{n+1}{2}} \exp(-(1+2n)i\beta L) \quad (44)$$

$$a_n^{(-)} = \frac{t_1 b_n^{(+)}(0)}{r_1 \exp(-i\beta L)} \quad (45)$$



$$c_n^{(+)} = \frac{t_2 b_n^{(-)}(L)}{r_2 \exp(-i\beta L)} \quad (46)$$

Thus the effective boundary photon densities are given by the previously mentioned summations of individual reflections at the corresponding facet as

$$b^{(+)}(0) = \sum_{n=0}^{\infty} b_n^{(+)}(0) = \left(t_1 a^{(+)} \right) \sum_{n=0}^{\infty} (r_1 r_2 G_s)^n \exp(-2in\beta L) \quad (47)$$

$$c_n^{(+)} = \frac{t_2 b_n^{(+)}(L)}{r_2 \exp(-i\beta L)} \quad (46)$$

Thus the effective boundary photon densities are given by the previously mentioned summations of individual reflections at the corresponding facet as

$$b^{(+)}(0) = \sum_{n=0} b_n^{(+)}(0) = \left(t_1 a^{(+)} \right) \sum_{n=0} (r_1 r_2 G_s)^n \exp(-2in\beta L) \quad (47)$$

$$b^{(-)}(L) = \sum_{n=0} b_n^{(-)}(L) = \left(r_2 \sqrt{G_s} \exp(-i\beta L) \right) b^{(+)}(0) \quad (48)$$

The term in the right hand side of equation (46) is nothing but a summation from zero to infinity of a geometrical series of radius $(r_1 r_2 G_s \exp(-2i\beta L))$. The summation converges eventually to equation (39) when the one pass-gain G_s is smaller than the inverse of the product of reflectances that is when $G_s < \frac{1}{r_1 r_2}$, namely when the amplifier is operating below threshold. Thus equations (39) and (40) are mathematically correct only when the amplifier is not lasing.

The advantage of using the approach of regrouping all the reflected waves at one boundary into one expression is to simplify the problem into one which only deals with two optical densities traveling in opposite direction (see figure) without dealing with the summation of infinite partial summations.

Relation between power and photon densities

The electron and photon densities used in the model equations are implicit model parameters describing the amplifier behaviour at microscopic level. However these parameters are not observable and have to be linked with their corresponding counter parts at macroscopic level. Such a

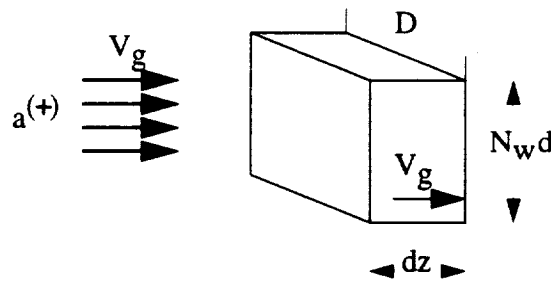
relationship has been established between the electron density and injected current density within the equation (30). A similar approach can be used to relate the injected optical power to the injected photon density and to the photon densities inside the amplifier through equations (28), (29), (39), (40). The mentioned equations are

$$P_{in} = D \frac{d h c^z}{\Gamma n_g \lambda} |a^{(+)}|^2 \quad (49)$$

$$P_{out} = D \frac{d h c^z}{\Gamma n_g \lambda} |c^{(+)}|^2 \quad (50)$$

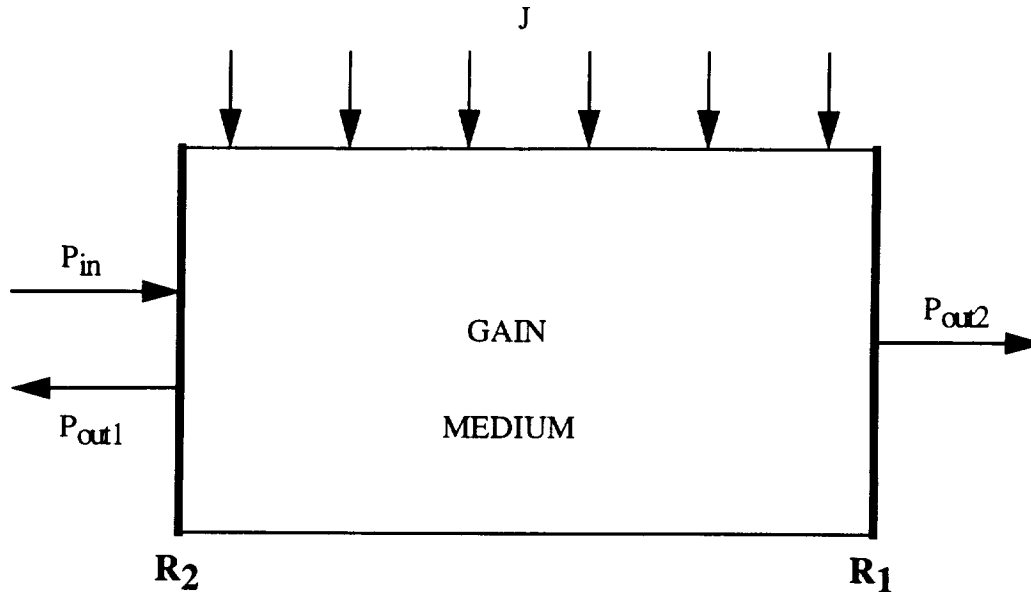
Equations (48) and (49) are easily derived using difference methods. Namely, the differential energy ΔE passing through the aperture to the active region of the amplifier during a differential time Δt assuming %100 coupling efficiency is as it is evident from the figure

$$\Delta E = |a^{(+)}| \frac{(D N_w d)}{N_w \Gamma} (h\nu) v_g \quad (51)$$



where $h\nu$ is the energy of one photon and v_g is the group velocity. Writing the energy of a photon in terms of its wavelength λ , the group velocity in terms of the group index n_g and letting Δt approach to zero, one obtains equation (48).

Calculation of amplifier efficiency



In the model, only one-sided efficiency is considered, that is the extracted power is represented by $(P_{out2} - P_{in})$ or $(P_{out1} - P_{in})$. In the former case, the reflected power P_{out1} is a loss factor decreasing one sided amplifier efficiency. A practical way to minimize the reflected power is to keep facet reflectivities low, that is using the device as a one pass amplifier. Another way of eliminating efficiency loss through reflected power is to use a double pass amplifier with a very high reflectivity at the second facet (≈ 1) and a very low one at the first (≈ 0), the extracted power being $(P_{out1} - P_{in})$.

The two amplifier described above differ in the value of one pass gain, the latter showing lower gain due increased saturation effect. The two different definitions of efficiency are presented below for one pass and double pass amplifiers respectively.

$$\text{Efficiency} = \frac{P_{out2} - P_{in}}{P_{el}} = \frac{P_{out2} - P_{in}}{I(R_s I + V_f)} \quad (52)$$

$$\text{Efficiency} = \frac{P_{out1} - P_{in}}{P_{el}} = \frac{P_{out1} - P_{in}}{I(R_s I + V_f)} \quad (53)$$

The inconvenience with the double pass amplifier is that the threshold of oscillation is reached more easily due to the high reflectivity at the second facet changing the amplifier into an injection locked laser. Also, frequency detuning effects at high pump power which are undesirable for a MOPA array, are more profound compared to travelling amplifier case due to the decrease in band width.

However it has been reported [1] that the use of a double-pass structure results in efficiency improvement in quantum well laser amplifiers.

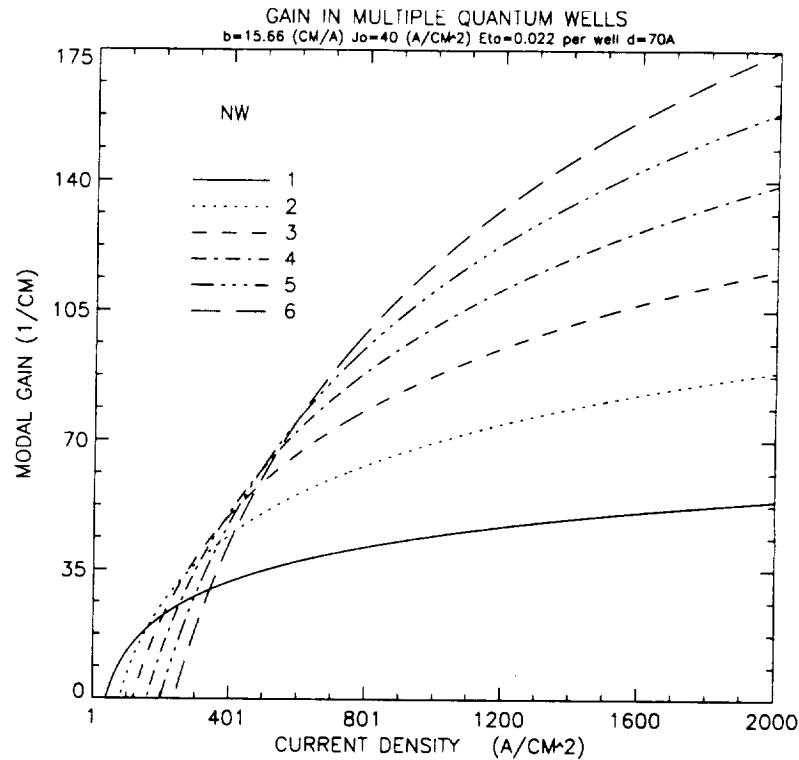
Gain in Multi-Quantum Well Lasers

The exact quantum mechanical calculation of the gain in a quantum well laser is cumbersome and computing wise very expensive. However, it is possible to use simpler expressions like the one given in equation (1) representing the gain-current relationship in a semi-logarithmic way. Another approximation developed by Wilcox [2] et al. reported good agreement between semi-logarithmic and calculated curves (rms error less than 5%).

$$g_s(z) = (\Gamma N_w) j_o b \log \left(\frac{N_{el}(z)}{N_{el}^0(T)} \right) \quad (54)$$

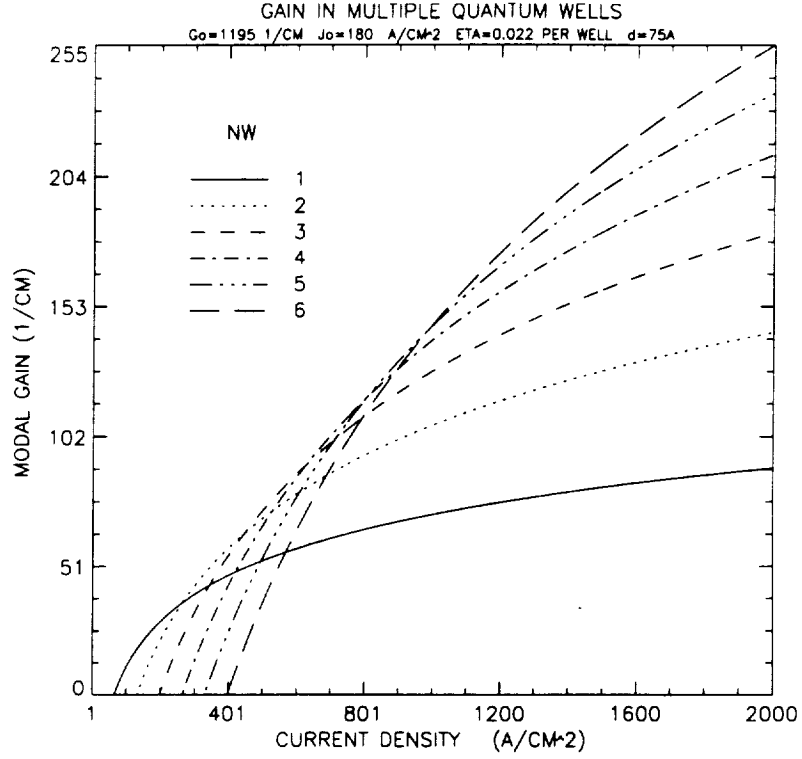
where b and j_o have meanings of gain-current coefficient and current per well at transparency re-

spectively. Corresponding plots illustrating the equations (1) and (20) are given below.



It can be noted that the two graphs resulting from two different approximation schemes have non-negligible differences between them. The main reason of this difference is that the basic assumptions on which quantum mechanical analysis is based are different in both cases as well as some structural parameters such as the aluminum content in and out of the quantum well region. Although such a variation won't have a big impact on the theoretical optimization presented in this report, it may play a very important role in trying to validate the theoretical data with experimental one. Correcting the semi-logarithmic material gain equation with the help of some experiments will be necessary before starting numerical simulations. The numerical analysis presented in this paper makes use of equation (1) only.

It is also important to note the dependence of transparency electron density on temperature in both



(1) and (22). The relationship is eventually modeled as

$$N_{el}^o(T) = N_{el}^o \exp\left(\frac{\Delta T}{T_o}\right) \quad (55)$$

where ΔT is the relative temperature variation defined as

$$\Delta T = R_{Th} P_{av} = R_{Th} (J^2 A^2 R_s + J A V_f) (1 - Eff) \quad (56)$$

The serial and thermal resistances in (4) can be expressed in terms of a bulk component inversely proportional to the area of the diode and a constant term due to metallic contacts as

$$R_s = \frac{R_{so}}{DL} + R_{sc} \quad (57)$$

$$R_{Th} = \frac{R_{Tho}}{DL} + R_{Thc} \quad (58)$$

Equation (4) basically states that the energy not used in the amplification of the optical signal is converted in phonons.

In an actual amplifier many parameters are effected by changes in temperature. However, it is possible to lump the effect in one parameter, namely the transparency current density with the use of a characteristic temperature T_0 . The validity of the approach for accurate modeling will hopefully be evaluated with the results of this thesis. However, since in semiconductors phonon recombination results in a small number of minority carriers (unlike superconductors) the approach is commonly used in the literature.

Numerical implementation of the amplifier model

The system of non-linear equations describing the laser amplifier model can not be solved analytically due to its mathematical complexity. The only solution method resides in numerical analysis. From the physics of the device inherent within the system of equations, one can assume that below threshold, there is a unique solution for each of the unknown variables. Above threshold, the system of equations becomes transcendental, however that mode of operation (lasing) is out of the scope of this thesis.

The aim of the simulation is to obtain signal photon densities along the amplifier length in order to determine the output power, consequently the net gain and efficiency of the amplifier. However, this also necessitates the determination of the variation of electron density and modal gain along the device together with the overall efficiency to take the effect of temperature shift into account. In the discrete setup, the amplifier is divided into a grid of 20 equidistant points (this sampling seemed to be adequate even for amplifiers as long as 0.15 millimeter) and the integrations of the modal gain is achieved through the trapezoidal rule at the corresponding points of the grid.

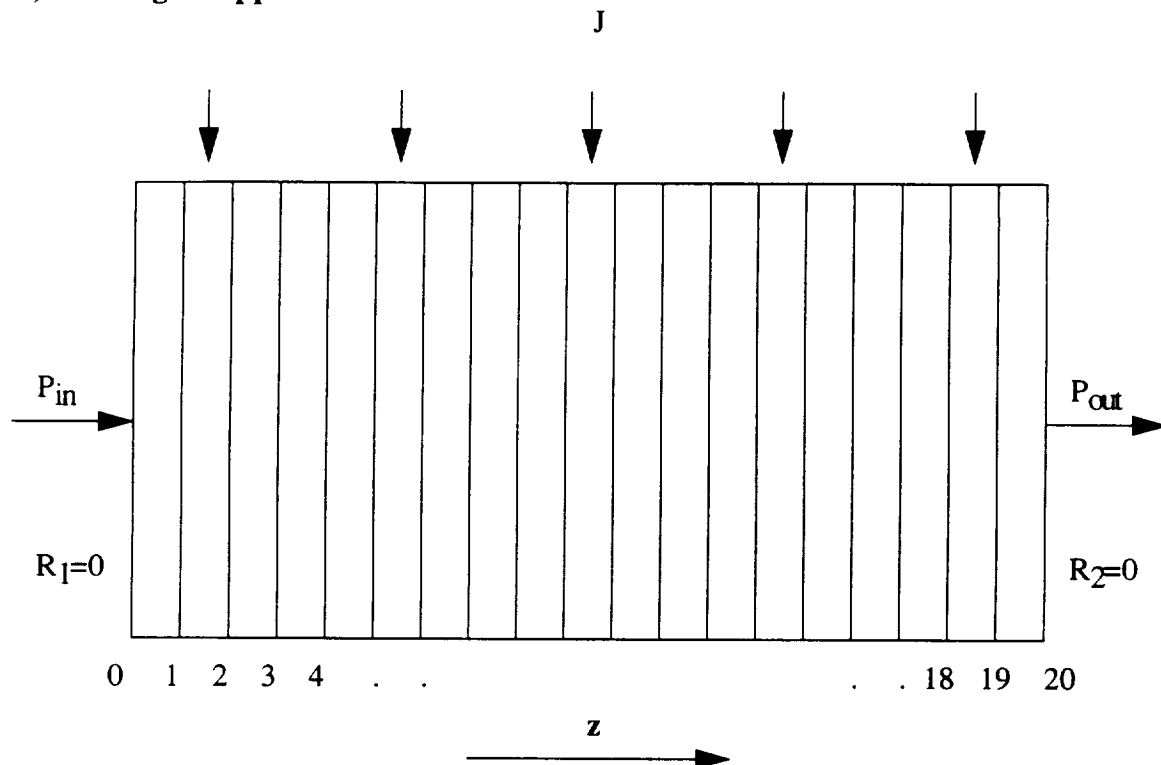
In the most general case, the main variables involved in the analysis are electron density (30), photon densities corresponding to (absolute values) (28) and (29), absolute value of boundary values of signal amplitudes (39) (40), the efficiency of the amplifier defined as in (16) or (17), the temperature shift, and the modal gain of the amplifier (1). Among these variables, the electron and photon densities together with modal gain can be considered as vectors of size equal to the number of grid points (20). Thus, a solution vector to the problem should satisfy self-consistency at every point of the grid.

The numerical analysis established is better understood if it is explained for the simplest amplifier structure (travelling-wave amplifier) first in the absence of effects created by varying tempera-

ture. Then, it is easier to follow the way with which convergence problems arising from temperature shift, high saturation, facet reflectivities and operation near threshold are handled.

Travelling wave type amplifiers

a) Small signal approach



In the case of a travelling wave amplifier, facet reflectivities are equal to zero. Consequently, the incident photon signal suffers no internal or external reflections and is amplified during its unique pass along the device. The boundary photon density values within the amplifier as described in (39) and (40) then becomes

$$|b^{(+)}(z)|^2 = |a^{(+)}|^2 \quad (59)$$

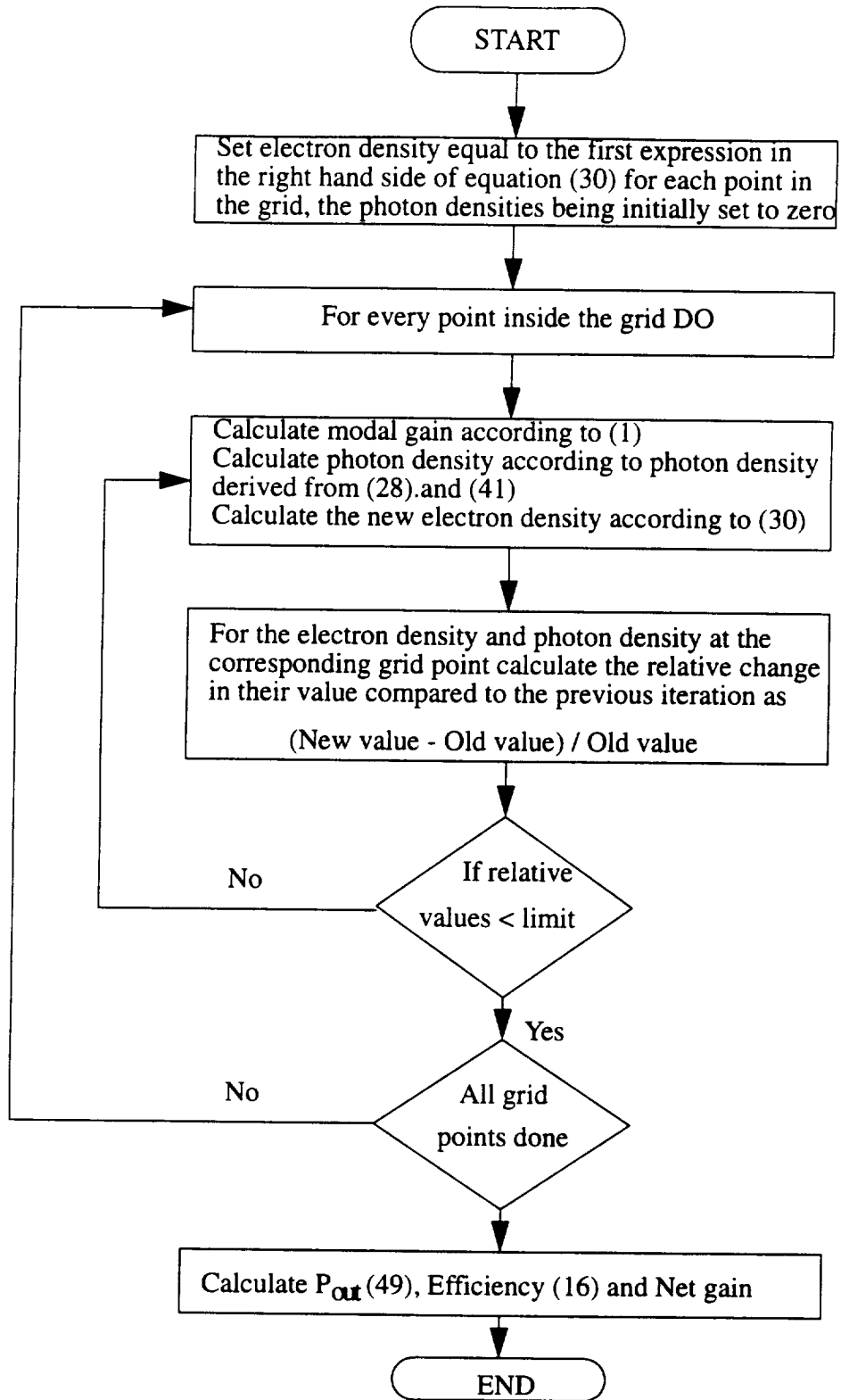
$$|b^{(-)}|^2 = 0 \quad (60)$$

Obviously, in this structure, the total gain is equal to one-pass gain of the amplifier and there is no signal wave propagating in (-z) direction. The inputs to the diode are the current density J and the input signal power P_{in} . The known device parameters are the length L , the width W , the number of quantum wells n_w , the confinement factor per well Γ , the optical loss coefficient α , the signal wavelength λ , the group index n_g , the gain coefficient G_0 , and transparency current density J_0 . The basic unknowns are electron and photon densities at each grid point in the amplifier.

One can easily see in equations (30)(28) and (1) that electron and photon densities within an amplifier are strongly coupled to each other. In the small signal approximation, the unknown electron density vector is close to its unsaturated value, making the modal gain vector close to its actual value as well. Thus, it is possible to force the electron and photon densities to converge to a self-consistent solution by starting from the initial value of the electron density and calculating the modal gain and photon densities iteratively at each point of the grid by plugging one variable in the expression of the other according to (1),(28) and (30). The method of solution is algorithmically described below.

It is important to note that, self-consistency of the solution is based on the relative variation of electron and photon densities with respect to their value in the previous iteration. If the relative variation for each variable at every grid point is smaller than a preset infinitesimal limit (10^{-12}), then convergence is achieved. It is possible to push this limit further down, however the precision of digital calculations and time constraints impose a lower limit.

The described algorithm work very fast because the number of iterations needed is small due to the



method used and to the initial value assigned to the unknowns being close to their actual value. Due to small-signal approximation, the second expression in the right side of equation (30) is smaller than the first one, keeping the electron density positive. However, for a moderately high product of modal gain and photon density at given grid point, the electron density may become negative. This is undesirable because the the logarithm in gain expression described in (1) becomes undefined. To account for this problem, it is necessary to modify the convergence procedure to keep electron density always positive.

b) Large signal approach

A solution to keep electron density positive during iterations is to control its variation instead of letting equation (30) decides on it. The previous approach is used till the value of simulated electron density at any point in the amplifier becomes negative. Then the electron density at that point is reset to its previous non-negative value. A dummy variable will also be set to the same value. At this point, the electron density is decreased (could be as well increased) by some percentage and the new value is put back in the iteration. From the calculated new gain and photon density, the dummy variable is calculated according to (30), the dummy variable playing the role of electron density. Then the value of the electron density is compared to the dummy variable. If the former is larger, than it is decreased by the same percentage. If it is smaller, it is increased by a lower percentage and the loop is repeated again. As the iteration progresses the value of the electron density will approach to its actual value given by (30) without ever becoming negative. The method established for self-consistency is still valid with the new method. That is the electron density is accepted to converge if the percentage change in its value from one step to the other is small enough.

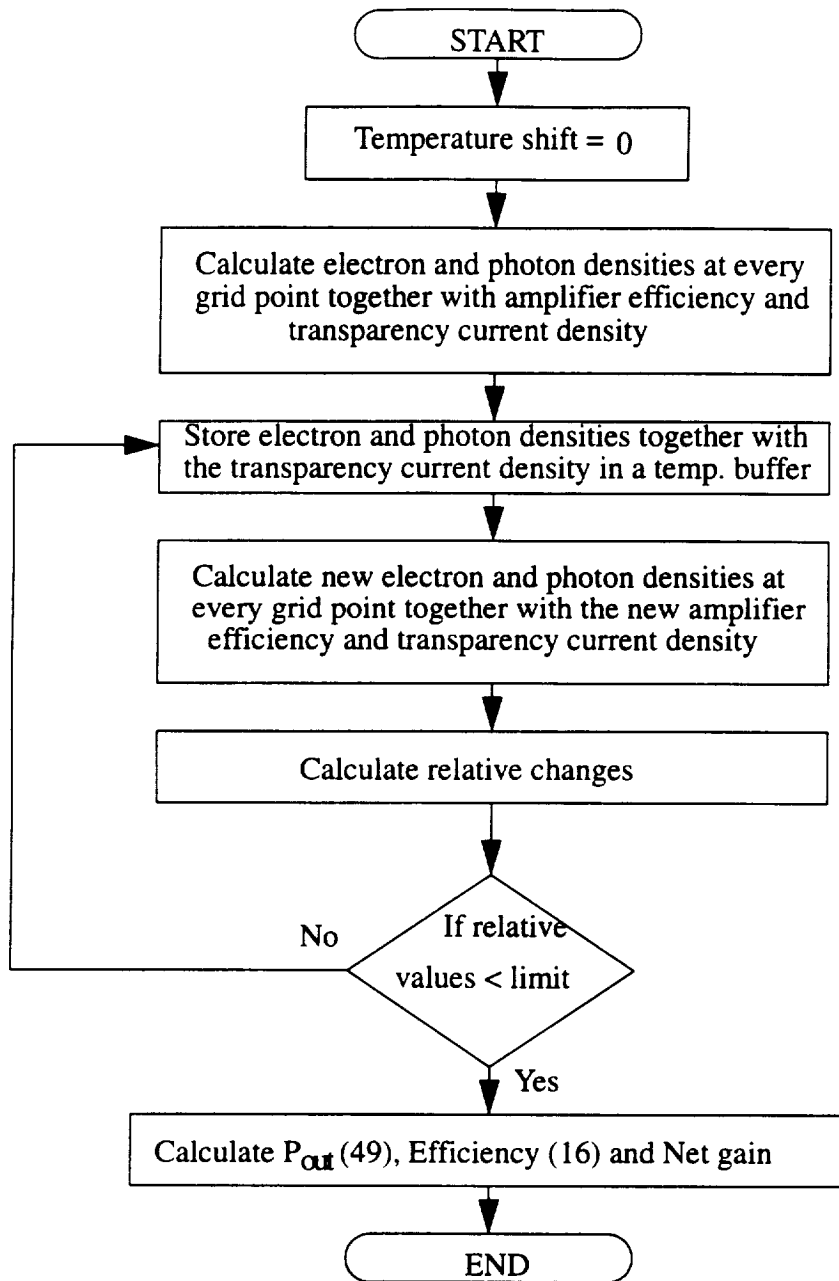
Temperature effects

It has been mentioned before that the temperature effect is lumped into one variable, namely transparency electron density. According to (55), (56) and (1), a decrease in the amplifier efficiency results into an increase in the temperature causing the modal gain at every grid point (overall gain as well) to decrease reducing further the efficiency of the amplifier.

A problem arises while trying to incorporate this variable in the model : the efficiency of the amplifier is not known until the output photon density is known. This however requires the knowledge of the shift in the temperature. The problem is solved iteratively assuming zero temperature shift in the first pass (by pass it is meant the set of model equations converging at every grid point). Then, the intermediate efficiency and transparency electron density of the amplifier is calculated (which is higher than the actual efficiency). The previously obtained electron and photon densities are stored in a buffer to be used as initial grid values for the iterative steps needed to deal with the effect of this new variable.

As seen in the figure, model equations are forced to converge iteratively for this new transparency current density starting from the initial values previously stored in the buffer. A new set of photon and electron density at every grid point together with a new output power and amplifier efficiency are calculated. Relative changes in electron and photon densities at every point and in temperature are calculated. Once again convergence is assumed to be achieved if relative changes are smaller than a predetermined value, that is the electron and photon densities in the amplifier together with the temperature shift don't change significantly from one pass to the other.

To make the model and its numerical analysis clearer, the simulation results for a travelling wave amplifier is plotted in figure () in terms of the variation of electron density, photon density and point modal gain along the amplifier. The amplifier is input an optical signal of 0.15 watts and excited with a current density equal to 2000 amperes per centimeter square. The length and width are taken



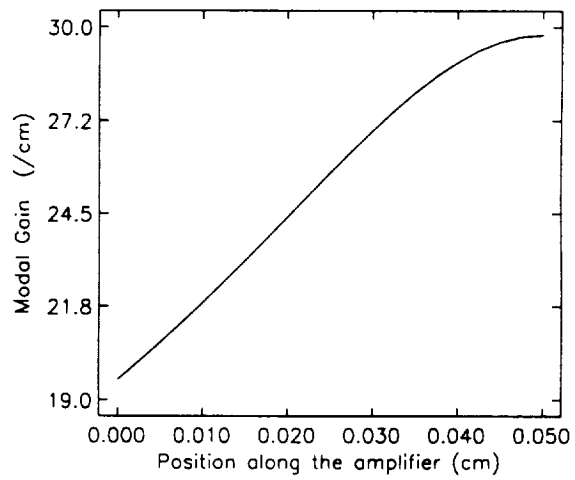
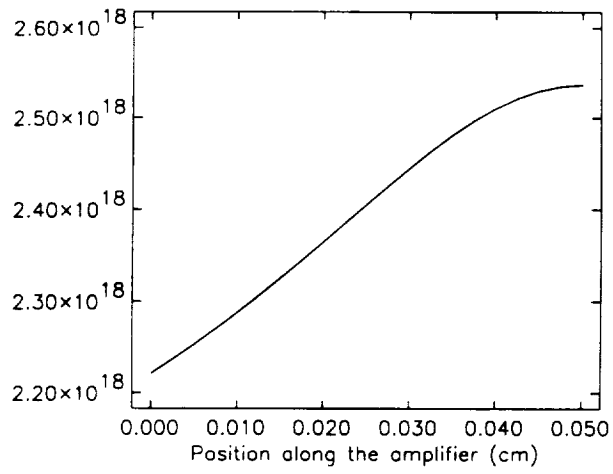
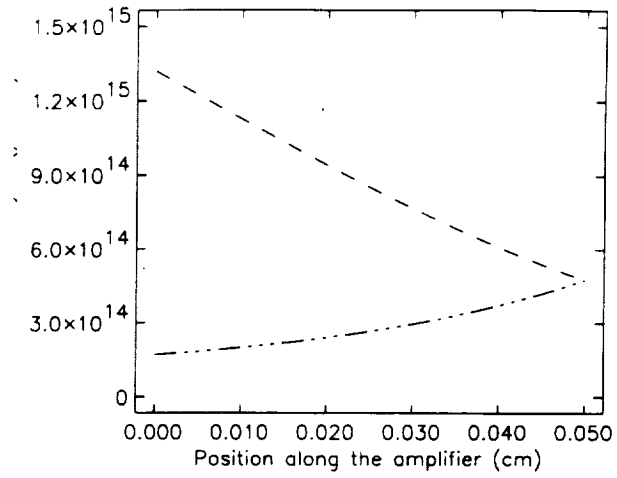
equal to 0.05 and 0.01 centimeters respectively. The number of quantum wells is fixed at 4, the confinement factor at 1.6 percent, the thickness of each quantum well at 75 angstrom and optical loss

coefficient at 5 per centimeter. The expression given in (1) is used for the modal gain with gain coefficient equal to 1195 per centimeter and transparency current density equal to 180 amperes per centimeter square.

Figure ()-i shows that the optical signal intensity grows linearly with distance within the amplifier. This observation is rather contradictory to what one might expect from equation (29) which describes an exponential profile. The linearity can be explained with the help of the second expression in the right hand side of equation (31) accounting for the depletion. That is, for the amplifier simulated, the electron density is depleted to such an extent to reduce the gain and thus the integral in the right hand side of (29) causing the observed linear profile. It can be shown with simple algebra that such linearity requires the modal point gain to vary as $\frac{1}{z}$ as shown in figure ()-iii. The electron density profile follows from the modal gain using (1).

The analysis of the travelling wave amplifier is simplified by the absence of optical reflections due to zero facet reflectivities. However, for Fabry-Perot type amplifiers, the dependence of boundary value signal densities on one-pass gain as described by (40) and (41) makes the analysis and numerical computations rather involved.

Signal wave propagating in the direction



Fabry-Perot type amplifiers

The problems encountered in the numerical analysis of Fabry-Perot type amplifiers are two-fold. The first difficulty is related to the presence of a signal wave travelling in $-z$ direction and to the imprecision in boundary value photon densities. The second difficulty resides in the denominator of (40) and (41) becoming negative during iterations causing convergence problems.

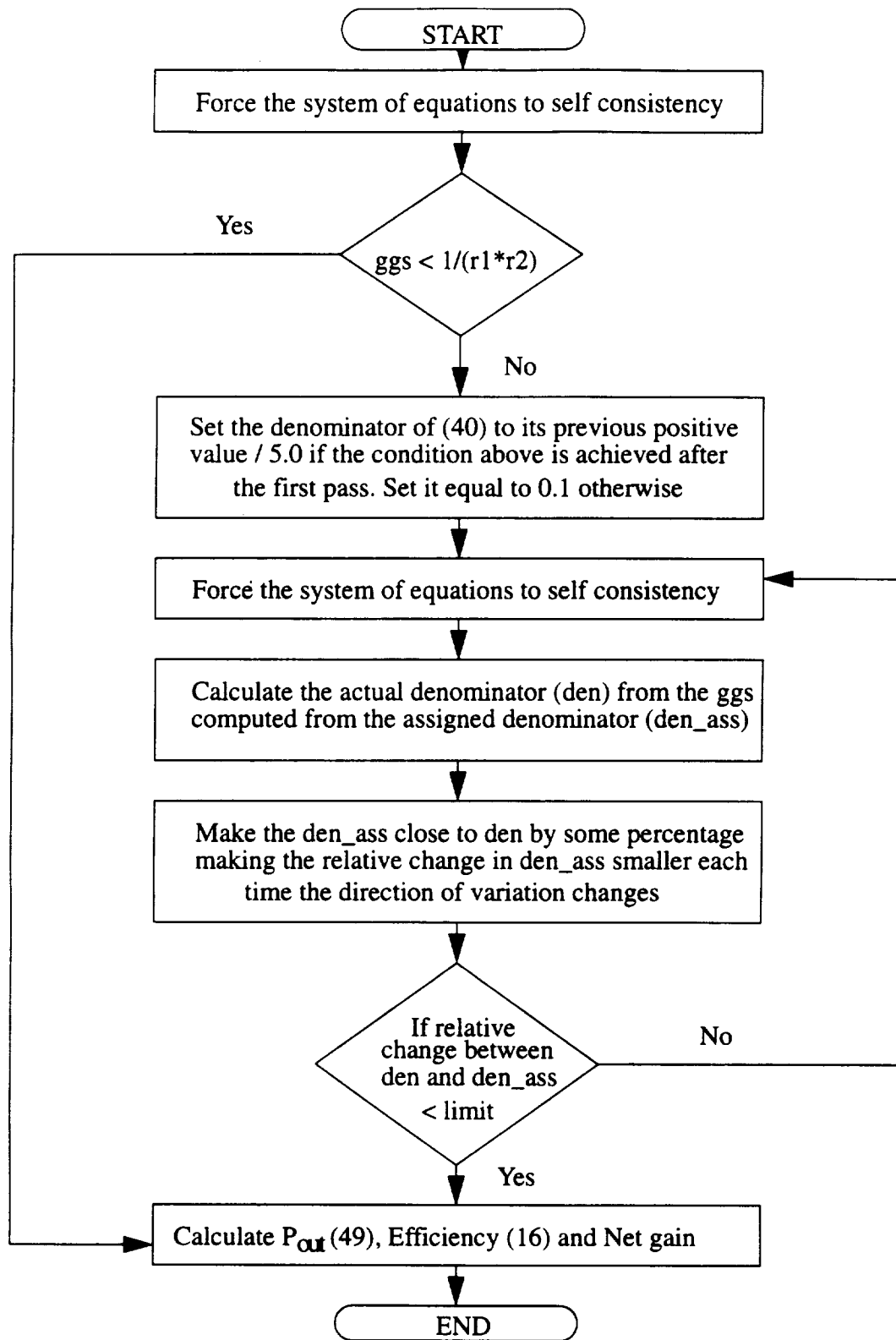
a) Non-zero facet reflectivity effects

To clarify the way in which the effect of reflectivities is included in the model, it is assumed that the calculated amplifier one-pass gain resides below its theoretical threshold of oscillation value during computation. The way this restriction is relaxed, is described in the subsequent section.

The methodology is somehow similar to the one adapted for temperature effects. The one-pass gain will initially be assumed equal to its unsaturated value. The intermediate boundary value photon densities, given by (40) and (41), are then calculated using the intermediate one pass gain. Consequently the value of calculated photon densities within the amplifier are higher than their actual value. In the second pass, the one pass-gain calculated from the previous step is used in (40) and (41). Remark that it is now smaller than its actual value due to excessive saturation. After some sufficient number of passes, self consistency in electron and photon densities (thus one pass gain) and temperature shift is achieved.

b) Computational problems associated with near threshold of oscillation operation

As mentioned earlier, the system of equations describing the operation of a laser amplifier becomes transcendental above the threshold of oscillation. During iterations, the value of one pass gain might be higher than its maximum theoretical value at oscillation resulting in convergence of equations

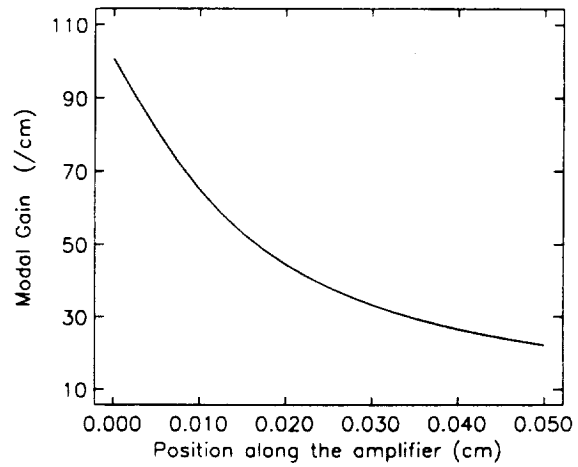
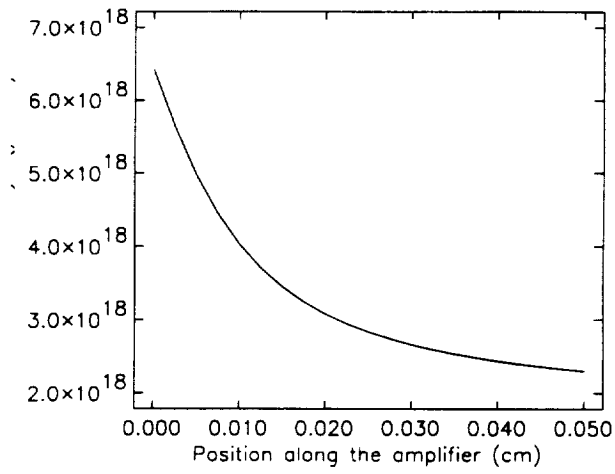
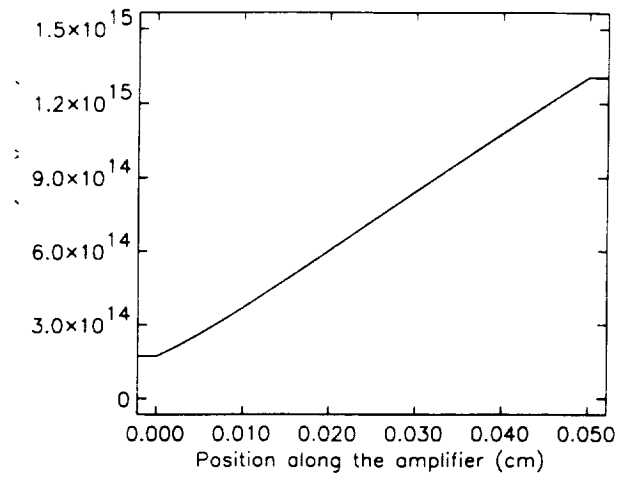


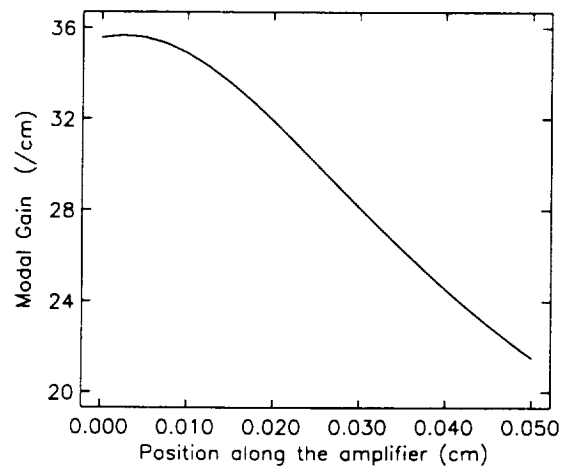
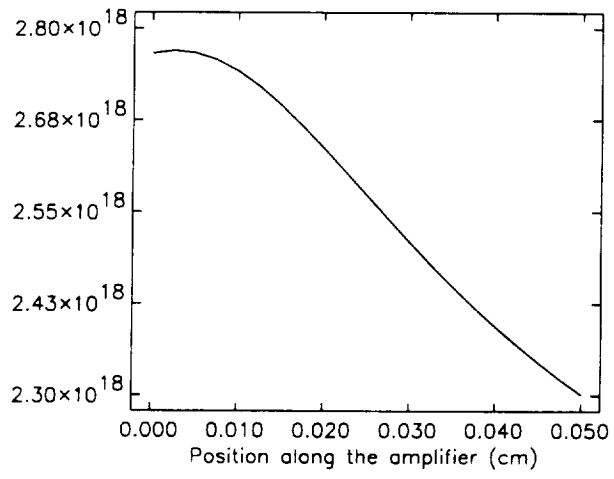
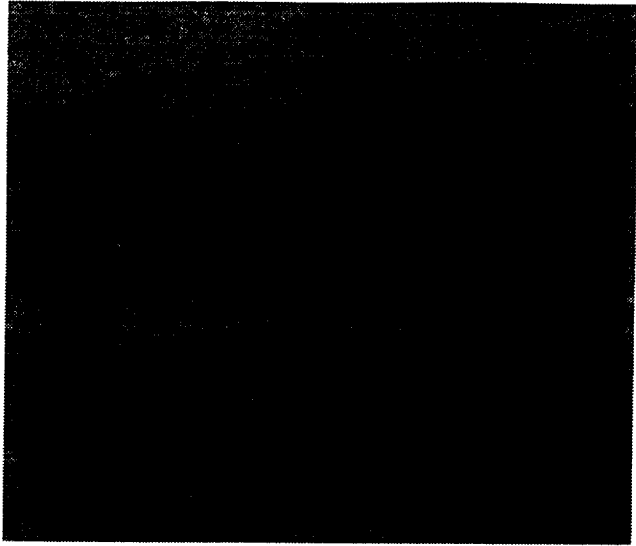
to a wrong set of solutions or not convergence at all. This problem is taken care similarly to the problem associated with negative electron density. For an amplifier for which, the denominator of (40) becomes negative, the variation of the denominator is no more dependent upon the one-pass gain. Rather, it is varied externally till it convergences to the previous denominator expression while remaining positive. The details of the algorithm can be seen in figure () above.

To illustrate the model with non-zero reflectivities, the amplifier used in section () is simulated for two different set of reflectivities. In the first computation R_1 and R_2 are both taken equal to 0.1. In the second one, R_1 is taken as 0 and R_2 as 1 (double-pass amplifier). The electron density, photon density and point modal gain profiles corresponding to these amplifiers are illustrated in figure () and () respectively.

From figure ()-i, It can be seen that the signal photon density is not continuous at $z=0$ (air-semiconductor interface). This is due to the denominator of equation (40) modeling the boost in the signal density inside the resonant cavity due to amplified internal reflections. Another discontinuity is present in signal photon density travelling in $+z$ direction at $z=L$. This is just due to non-unity transmittance of the second facet. The signal wave in $-z$ direction is weaker than the one in $+z$ direction because for the given operational parameters, the one-pass gain of the device is smaller than R_2^{-1} . As a consequence, the electron density is more depleted towards the right hand side of the amplifier as seen in figure ()-ii.

In the case of the double-pass amplifier, the photon density in $+z$ direction reflect from the right facet of the diode (acting as a mirror) and amplified by the same one pass gain before exiting the amplifier from left end. Consequently the total photon density is higher toward the left facet of the diode depleting the electron population deeper in that region.





Analysis of the effect of amplifier parameters on gain and efficiency

The purpose of the modeling is to simulate the behavior of a quantum well laser amplifier as closely as possible in order to optimize amplifier parameters for maximum gain and efficiency and to understand the trade-offs in trying to do so.

The parameters mentioned above are length, width, facet reflectivities, confinement factor per well, number of quantum wells, excitation and pump power levels.

Constraints on parameters involved in optimization

a) Width

To understand the effect of width on efficiency and gain of the amplifier it is necessary to look in equations (12), (13) and (14) more closely. Let's assume that the series resistance of the laser diode is inversely proportional to its area, and R_{s0} is the series resistance in ohms of unit area. Then the series resistance R_s is given by

$$R_s = \frac{R_{s0}}{DL} \quad (18)$$

Putting equation (12),(13),(18) in equation (14) yields

$$Efficiency = \frac{P_{out2} - P_{in}}{I(R_s I + V_f)} = \frac{D\xi(|c^{(+)}|^2 - |a^{(+)}|^2)}{\frac{R_{s0}}{DL}(JDL)^2 + V_f(JDL)} = \frac{\xi(|c^{(+)}|^2 - |a^{(+)}|^2)}{R_{s0}J^2L + V_fJL} \quad (19)$$

where ξ corresponds to

$$\xi = \frac{d h c^2}{\Gamma n_g \lambda} \quad (20)$$

Now, if we assume that the active region of the amplifier receives the same input photon density-independent of the width of the amplifier, that is if the injected power is scaled proportionally to the width so that $|a^{(+)}|^2$ will remain constant, then the output photon density $|c^{(+)}|^2$ will remain unchanged. Consequently the efficiency will remain unaffected by the change in the width of the amplifier. This means that the problem of finding the optimum width and optimum input power can be considered together because the only parameter that is important is the power density injected to the amplifier. Thus, it is reasonable to keep the width constant and big enough to conform with the requirements of a broad area amplifier and try to find the optimum input power. A typical value for the width is 100μ . This value will be used through out the optimization.

In reality, the electrical resistance of the diode is more accurate if a constant serial resistance is added to the right-hand side of (18) accounting for the effect of metallic contacts. This, results in a term in the denominator of equation (19) which is dependent on the width of the amplifier. The implication of such a change in the model is that the efficiency of the amplifier will decrease substantially with increasing width because of the increasing electrical power loss at metallic contacts.

So, the width of the amplifier should conform with the requirements of a broad area amplifier but at the same time it should be kept as small as possible to increase the efficiency.

b) Input Power

High efficiency in a diode amplifier is achieved, if the pumped electrical power is effectively transformed into optical power. This requires operation of the device in a highly saturated regime, implying the use of relatively high excitation levels. However, the reflective facets of the amplifier can only operate up to a maximum value of power density beyond which they are damaged. This limit can be roughly set at $(10 \text{ MW} / \text{cm}^2)$. Let's denote this value by D_{max} which stands for maximum density. The corresponding maximum power limit P_{max} can then be expressed as

$$P_{max} = \frac{D_{max} D d}{\Gamma} \quad (21)$$

In the case of a travelling wave amplifier the power density at the second facet is higher than the one at the first facet. Thus the input power level and the gain of the medium should be arranged in such a way that the output power density shouldn't exceed the facet damage limit.

The model doesn't treat the spontaneous emission, the signal to noise ratio being very high for saturated operation regime below the threshold of oscillation. It has been reported [3] that if the input laser intensity is higher than 10 kW/cm^2 , then regardless of the facet reflectivity, the output laser intensity is less dominated by ASE and less sensitive to the injected current density and input laser frequency. Accordingly, for a diode with a width of $100 \mu\text{m}$, confinement factor of 2% and quantum well thickness of 10 nm, the minimum injected optical power should be 0.005 W in order to neglect the photon density contributed by ASE.

c) Confinement factor per well

When an optical mode of the amplifier is too tightly confined to the active region, the divergence angle of the optical wave at the output facet is quite large resulting in considerable power loss in coupling light into the amplifier. Thus, there should be an upper limit for the confinement factor. Following an empirical approach, this limit is experimentally determined to be 2.2%.

However a small confinement factor is not very desirable either, due to decreasing efficiency resulting from a less saturated electron population. The excitation level can be increased up to some point to keep the input photon density to the amplifier constant, but the modal gain of the amplifier will still be lower compared to the amplifier with higher confinement factor (1).

The effect of other parameters will be explained in subsequent sections.

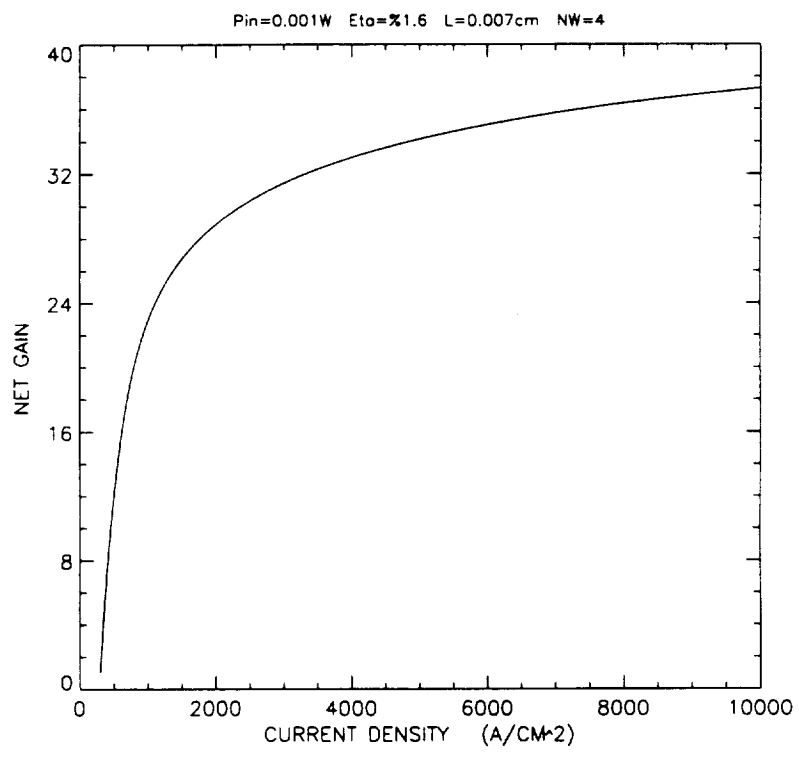
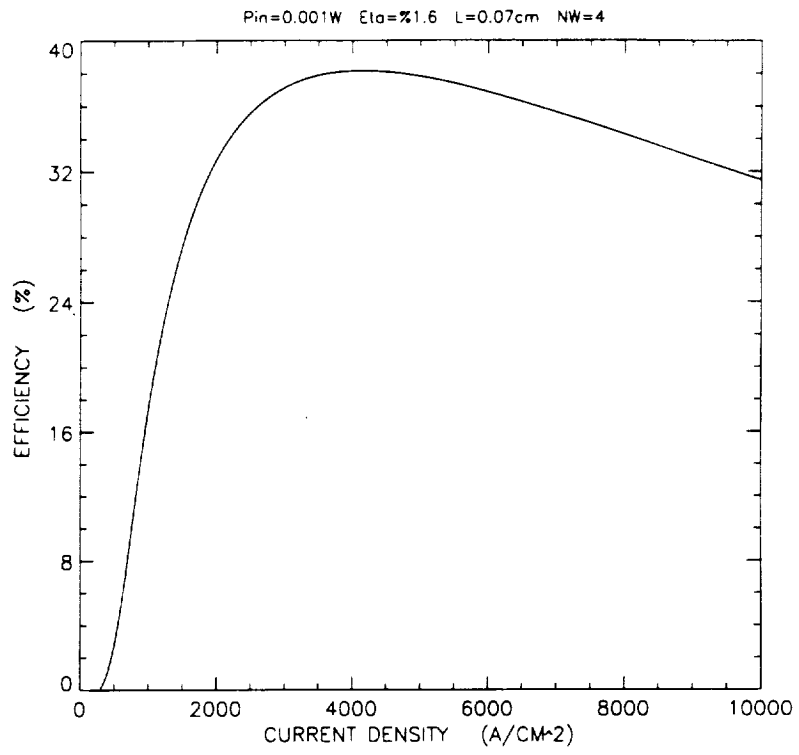
Variation of gain and efficiency with pumped-in current

The understanding of the changes in the performance of the device as a function of the excitation is very important because the understanding of the effect of the remaining variables can then be more easily achieved in this multivariate optimization problem. Also the excitation is continuous in nature and offers experimental ease in its manipulation compared to the injected power level, number of quantum wells etc.

As it can be seen from previous graphs, the quantum-well gain rolls over at a high injected carrier density. This gives the amplifier the ability to operate at a high excitation level without exceeding the oscillation threshold. A positive consequence of this is low small-signal gain and high extractable power.

The thickness of the active region of quantum-well laser amplifier being much thinner than that of a more conventional double heterostructure laser its internal efficiency is also considerably higher, resulting into a higher overall efficiency. A bigger portion of the electrical power being converted into optical power, the amount of heating is less severe, therefore contributing to a higher efficiency. The graphs below illustrates the variation of efficiency and net gain of the amplifier with increasing excitation.

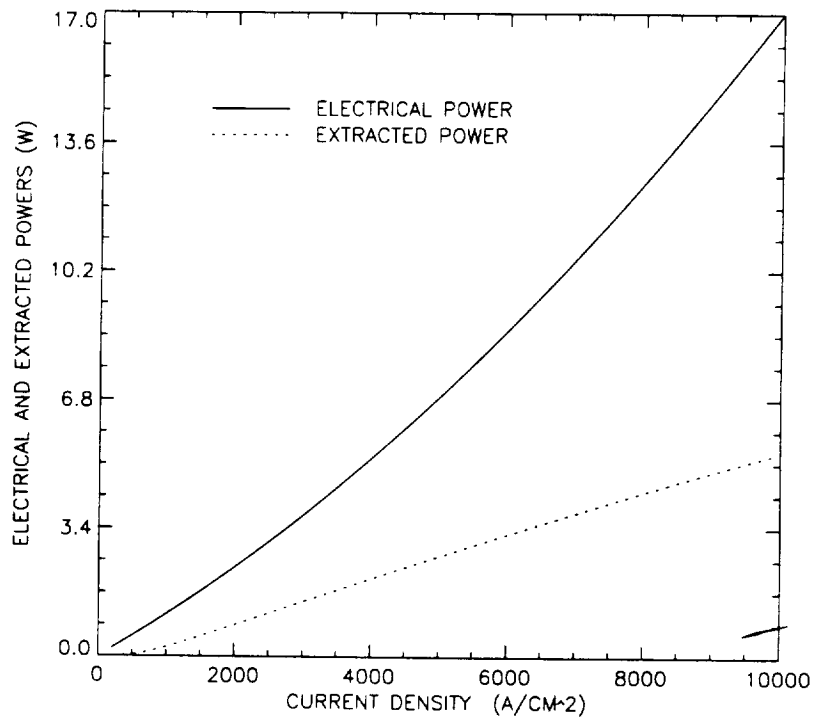
As can be seen from the first graph, amplifier efficiency initially increases with excitation. As the pumped-in electrical power increases, the fraction of input electrical power contributing to amplifier output optical power increases relative to the fraction spent in achieving transparency in the gain medium. Also, at low values of current density, the amplifier gain varies linearly, explaining the initial linear increase of the net gain with excitation in the second figure. The rate of increase of the efficiency decreases gradually with further increase in the current density. As a result,



C-2

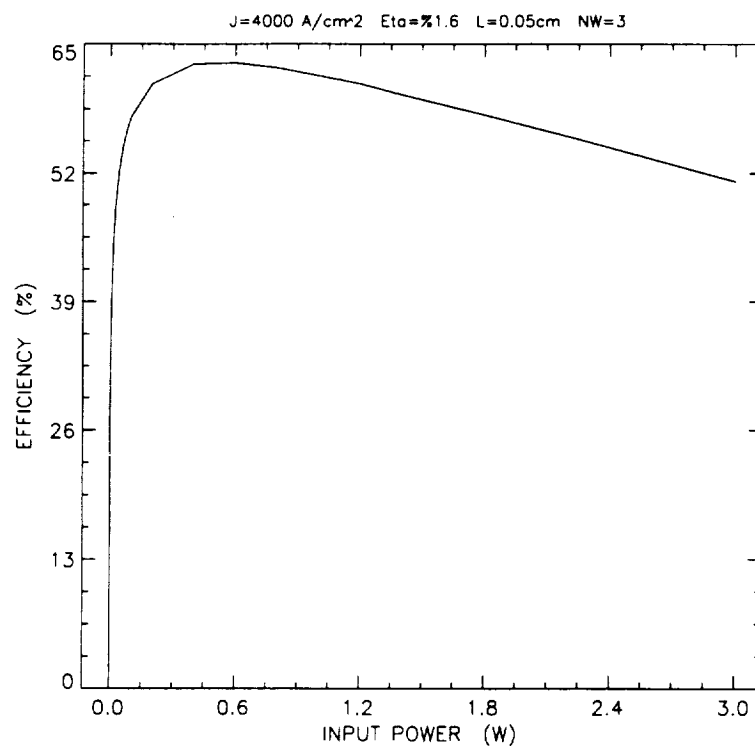
the efficiency goes up to a maximum P_{eff} (Peak efficiency) and then start going down. The main factor responsible from that change is the quadratic dependence of electrical power on current density. With increasing excitation, the denominator of efficiency equation (electrical power) grows more rapidly than the numerator (extracted power). The gain roll-over and the saturation of the material gain makes the rate of increase of the extracted power with respect to current density (almost a constant for relatively high saturation) lower than that of input electrical power (quadratic). The third figure illustrates the variation of the electrical and extracted powers together with respect to current density.

If the net gain at peak efficiency is not big enough, it can be increased by another 5dB at the expense of decreasing efficiency (20%). This trade-off will be a part of our optimization algorithm letting us compare the gain of different amplifiers, their efficiency being decreased with increasing current density down to a minimum desirable efficiency (50%).



Variation of gain and efficiency with injected power

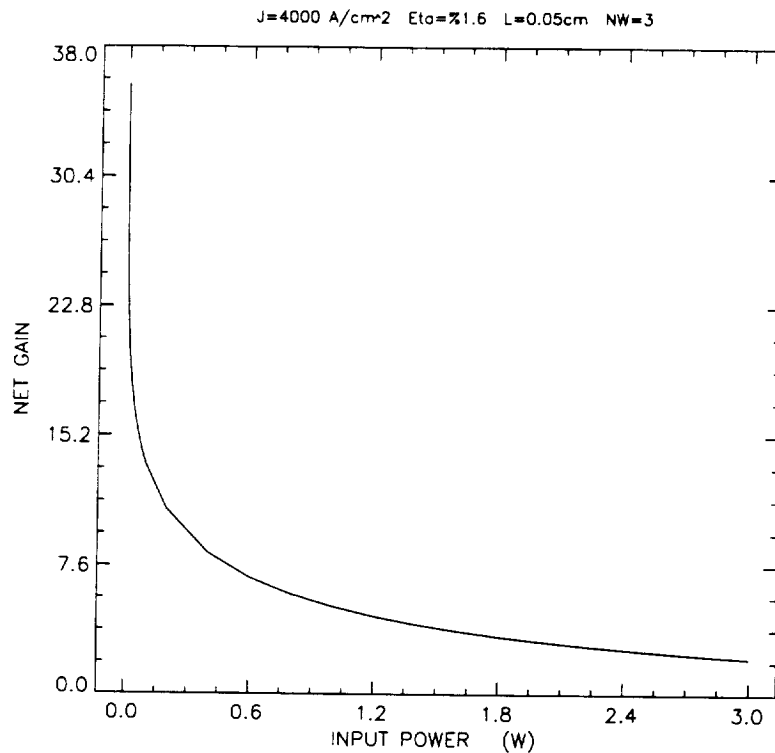
The effect of the saturation in the model can be better understood by looking at the variation of gain and efficiency for an amplifier with changing injection levels. The figures below illustrates the effect of changing input power for an amplifier with relatively high pumping rate.



It can be observed that the efficiency increases very rapidly from 0 to 61 percent when the input power increases from 0.0001 to 0.6 Watts, where it reaches its peak and then starts going down with a relatively lower rate. The gain in the region corresponding to increasing efficiency is marked by an abrupt descent, the rate of decrease gradually going down with increasing injected power levels. It is interesting to note the asymmetry in the rate of variation of efficiency and net gain in the region

of increasing efficiency. Eventually the explanation of that phenomena can be found in the numerator of the efficiency expression (the denominator being constant) by making the assumption that the diode acts like a travelling wave amplifier for reflectivities as low as 10^{-4} (this assumption has been numerically verified). This is to say that the net gain of the amplifier is equal to one-pass gain. Then we can rewrite the efficiency as,

$$Eff = \frac{P_{in} (G_s - 1)}{P_{el}} \quad (23)$$



When the input power is very low, the gain of the system available to the injected photon is very high even in the presence of spontaneous emission due to non-saturated electron density. However, the small-signal gain is the maximum available gain and its value practically remain unchanged up to effectively saturating power levels. For a very small input power ($\leq 10^{-6}$ W), despite the large value of the small-signal gain the product in the numerator of equation (23) is very small resulting

into almost zero efficiency. This practically means that the extracted power is very low compared to provided electrical power although the gain is practically maximum.

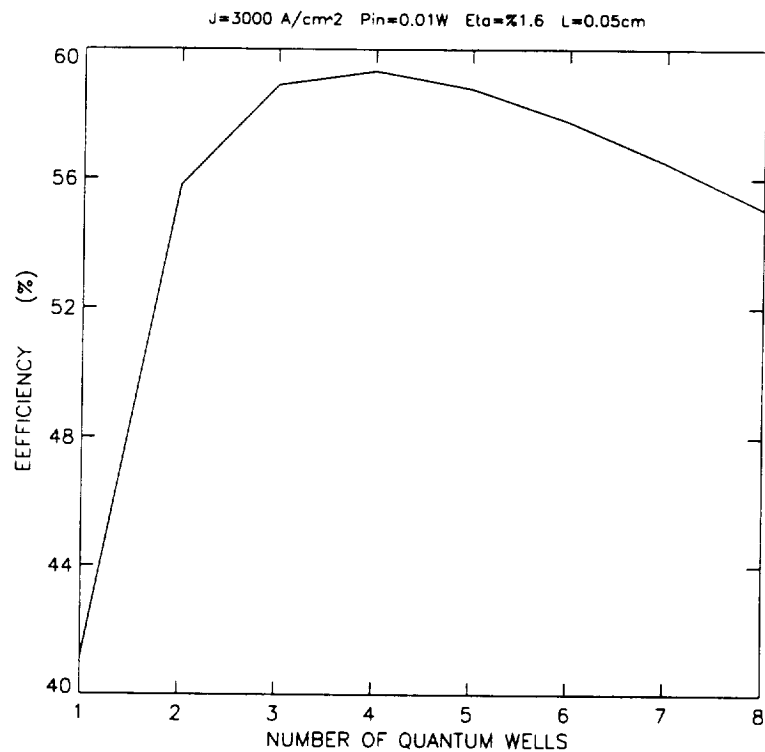
With increasing injected power, the electron population in the amplifier starts depleting according to equation (2), hence resulting into a lower net gain due to the logarithmic dependence of the gain on electron density. However, as far as the extracted power is concerned, the increase in the input power remains more important than the decrease of the net gain till peak efficiency is reached.

Beyond that point, the decrease in the net gain is not overcome by the increase in injected power resulting into a gradual decrease in the efficiency.

It can be observed that the decrease rate of the net gain with increasing injection level goes down. The principal reason is the parallel decrease in the rate of increase of photon population resulting from increasing saturation.

Variation of gain and efficiency with the number of quantum wells

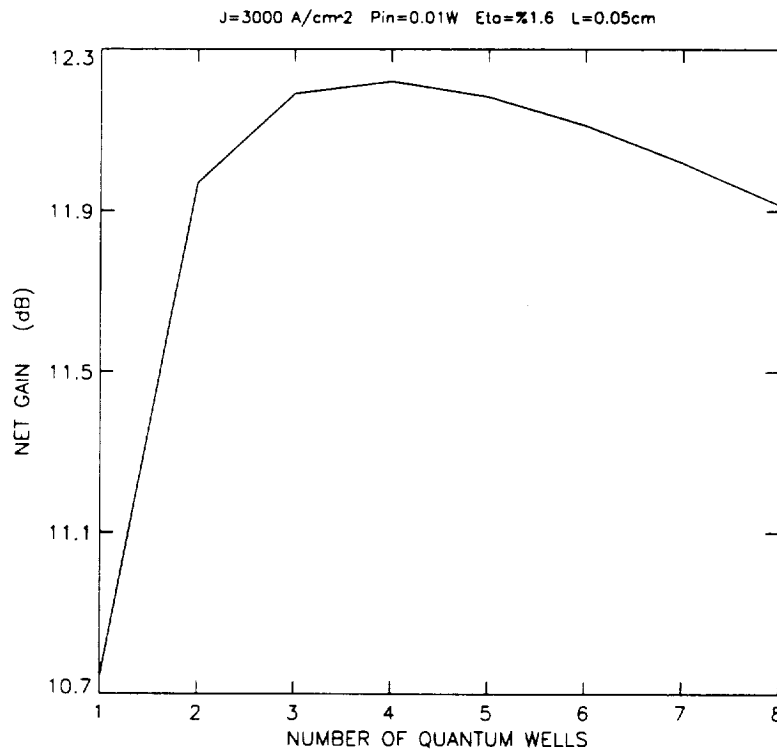
The optimization of the number of quantum wells to be used in the amplifier is one of the main reasons why a numerical simulation of a detailed model was required. An experimental investigation would be money-wise and time-wise very expensive. The numerical results summarized in the graphs below show that other input parameters being constant, there is an optimum number of quantum wells for which gain and efficiency are maximum assuming that the amplifier is moderately saturated.



As it is apparent from the first term in the right hand side of equation (2), increasing the number of quantum well decreases the unsaturated electron density per well. But in computing the total gain,

we multiply the gain from each well by the number of quantum wells. And the effect of this linear multiplier is dominant over the effect of the reduction of electron population per well because the latter appears as a divider in the semilogarithmic gain expression. Thus we can conclude that the overall effect of increasing the number of wells is to increase the unsaturated gain.

However, when the amplifier is operating at moderately saturated regime, as the graphs illustrate, an attempt to increase the gain will also increase the photon population present in the active region of the device, enhancing the saturation effect. Thus for sufficiently high number of quantum wells, the combined effect of the decrease in the first term and the increase in the second term of equation (2) reduces the electron population up to such extent that the linear multiplier (N_{qw}) in the gain expression is no more capable of increasing the net gain of the device.

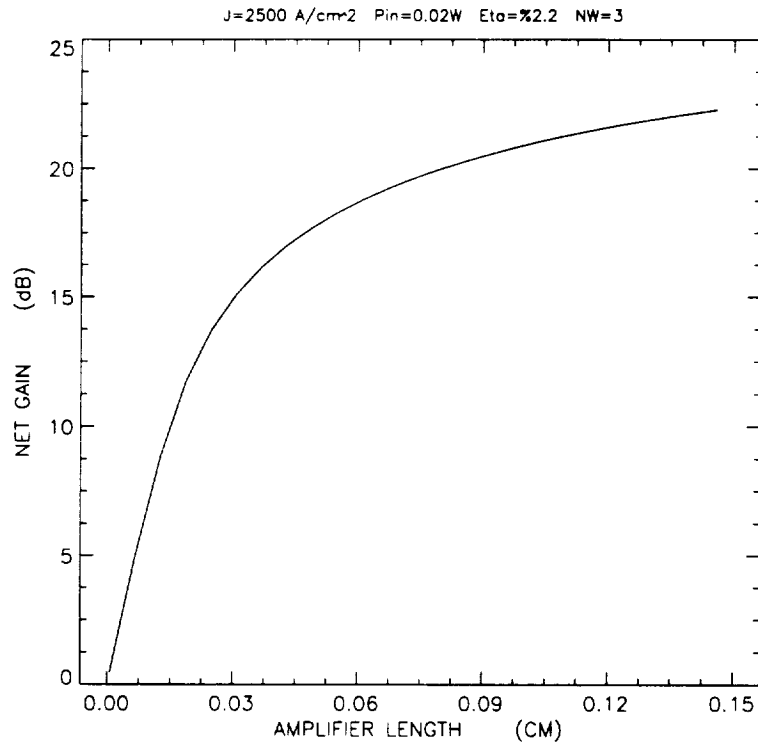


The electrical and optical powers provided to the diodes are the same. The travelling wave amplifier approximation still being valid, equation (23) explains the similarity between the gain and efficiency versus number of quantum well graph.

For an undersaturated amplifier, increasing the number quantum well will result into an increase in both the efficiency and the gain contrary to the over-saturated case where an increase in the number of quantum well will result into a less efficient and lower gain device.

Variation of gain and efficiency with amplifier length

According to equation (10) the one pass gain of the amplifier (net gain in travelling wave amplifier case) is the integral of the of the net local gain along the amplifier. In the small signal case, the net gain of the amplifier increases linearly with respect to the length, the value of the local net gain being the proportionality constant. This simple treatment is no more valid for the large signal case due to the saturation effect.



The figure above illustrates the variation of the net gain of an amplifier with length for a moderately saturating input power and relatively high electron pumping rate. As it can be observed, the increase in the net gain of the amplifier with increasing length results in a higher photon population inside the active region enhancing the effect of saturation. This results in the roll over of the gain

curve instead of the linear behavior predicted for the small signal case. However it is important to note that, beside the depletion of the electron population the net gain keeps increasing with length even for relatively long devices.

To understand the behavior of the efficiency with changing length it is necessary to examine how the electrical and extracted powers are effected. The current density being kept constant, an increment in the length results in an increment in the current provided to the diode. The series resistance of the amplifier however decreases due to the first expression in the right hand side of equation (14).

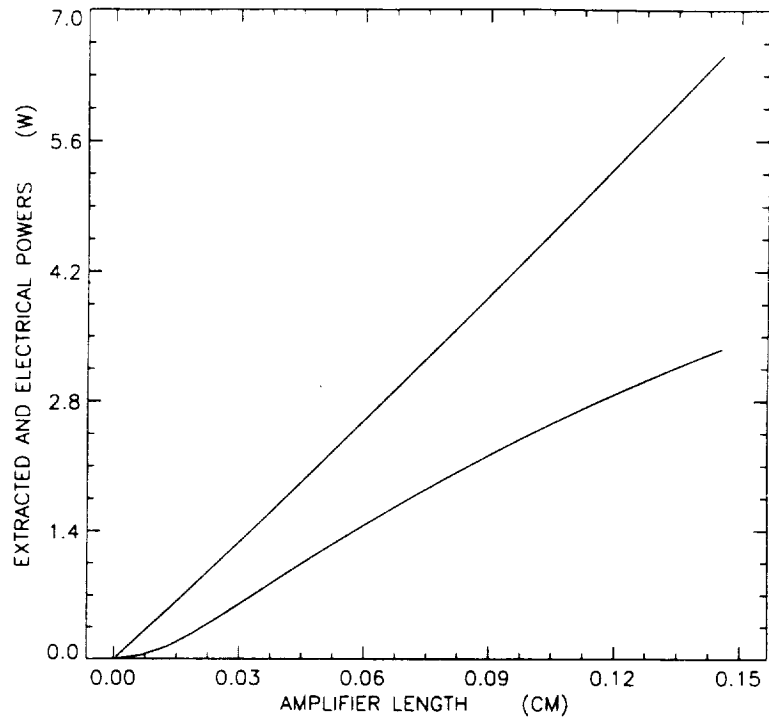
After some simple manipulation the electrical power can be rewritten as

$$P_{el} = [(V_f + R_o J) DJ] L + [R_1 (DJ)^2] L^2 \quad (24)$$

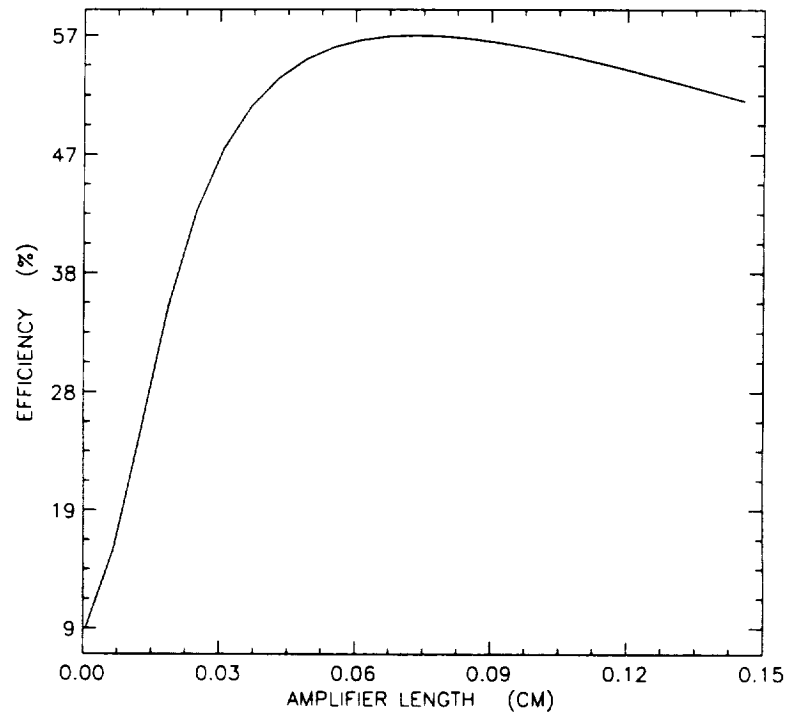
Where R_o and R_1 are the constants in equation (14). In the range of data the simulation is run, the first term in the right hand side of equation (24) is much bigger than the second one. This explains the linear relationship of electrical power with length in the graph illustrated below.

The relationship established between the gain and the extracted power in equation (23), explains the variation of the latter with varying length. The second derivative of the extracted power curve is zero at a length close to 0.08 centimeters. At this point the second derivative is changing sign from positive to negative. The quotient of both powers (as indicated in the equation (15)) defining efficiency, reveals this phenomena producing a maximum at the same point which is nothing but the peak efficiency observed in the graph below. Thus, other parameter remaining constant, an amplifier has an optimum length for which the efficiency is maximum

J=2500 A/cm² Pin=0.02W Eta=%2.2 NW=3

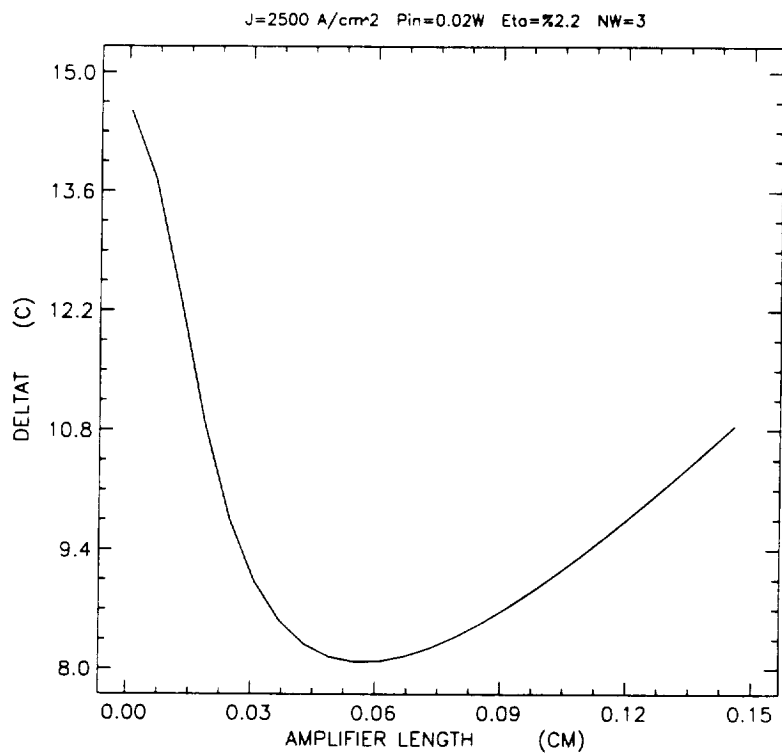


J=2500 A/cm² Pin=0.02W Eta=%2.2 NW=3



It is once again possible to increase the net gain at the expense of efficiency by increasing the length of the amplifier beyond its optimum efficiency value.

The relative temperature variation corresponding to the analysis developed above is illustrated below. The explanation of the shape of the curve is straightforward from equation (4).



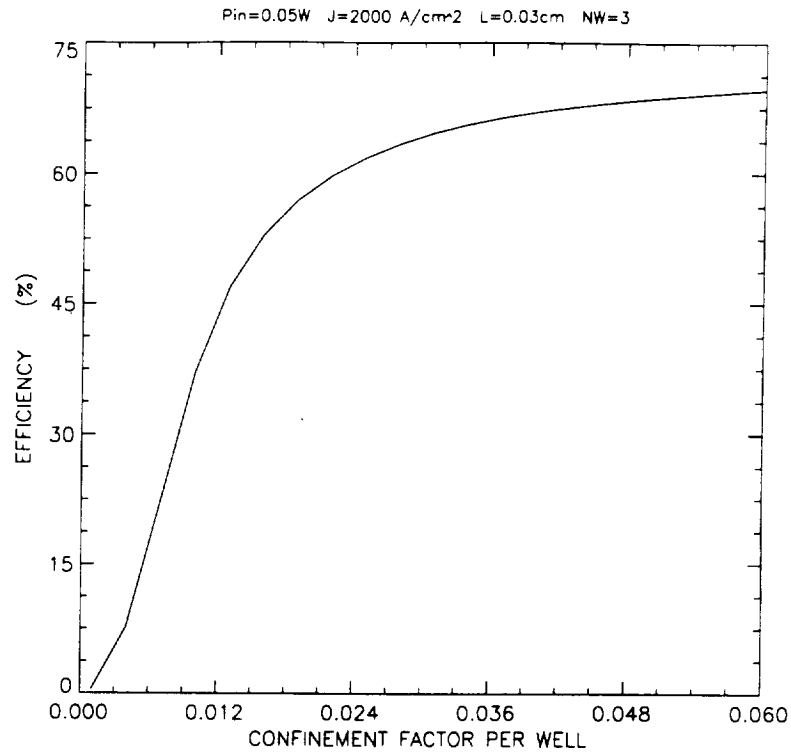
Variation of gain and efficiency with optical confinement factor

The optical confinement factor per well is one of the most important model parameters affecting the incident optical power density and modal gain at the same time. The parameter also appears in equation (2) but it cancels out with the one present in the modal gain expression (1). Eventually, it would be more convenient to use the material gain only to make more physical sense but it is not done so to preserve the notation used in Marcuse's paper.

To go from incident and exiting power levels to corresponding photon densities and vice versa, a classical approach is used relating the two by making use of the energy of a photon, the group velocity, the aperture of the active medium and confinement factor as expressed in equation (12) and (13). The use of confinement factor here accounts for the determination of the fraction of power in the active region of the quantum well structure, where amplified photonic energy will couple into the mode as described by equation (1).

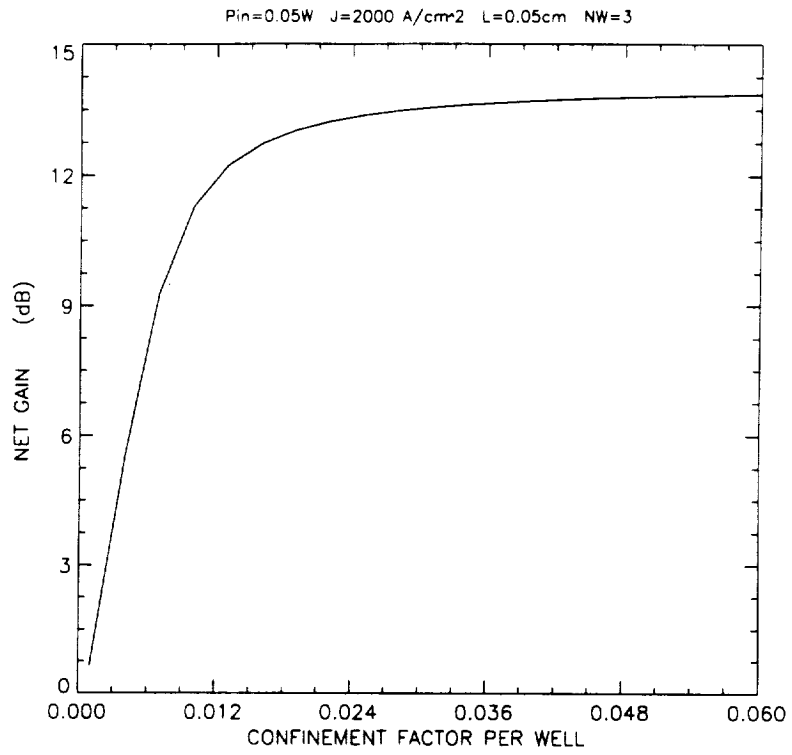
As far as the net gain of the amplifier is concerned the ratio of equation (13) by equation (12) will result in the cancellation out of the confinement factor present in both of the equations. The only parameter directly affected is then the one pass gain described by equation (10) which then modifies the signal photon densities at the diode boundaries as described by (8) and (9).

It is straightforward from the corresponding expressions mentioned previously that increasing the confinement factor will result into an increase in the modal gain which in turn will increase the one pass gain. In the Fabry-Perot case, the signal photon densities at the boundaries of the device will then be higher resulting into a high overall photon population following (5) and (6). However a higher photon density inside the amplifier will tend to deplete the electron population working against the increase of the net gain predicted from the previous analysis. The overall effect of in-



creasing the confinement can be seen from the graph displayed above which illustrates the roll over of the net gain following the saturation effect becoming more dominant over the counter influences mentioned before.

It is interesting to point out that the net gain of the amplifier doesn't increase substantially beyond 2.2% confinement per well which was the limit set experimentally. However it is also important to note that both efficiency and gain can be simultaneously improved by forcing the previously set limit. Especially the gain in efficiency beyond the preset limit is far from being negligible as it is clear from the graph presented below.



The behaviour of the efficiency can easily be understood recalling the travelling wave approximation described by (23).

Amplifier Optimization

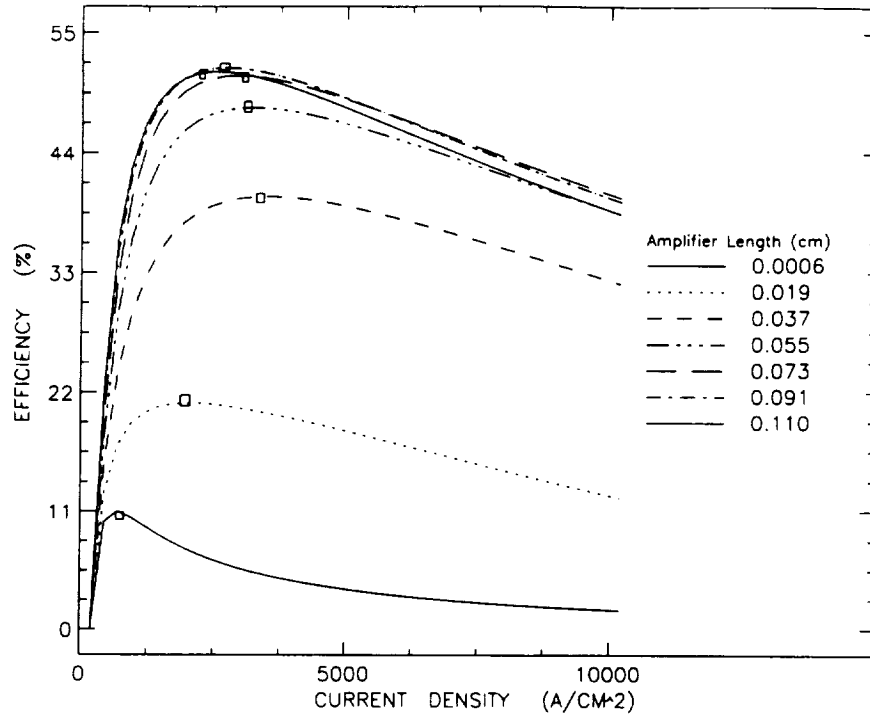
In the preceding sections, the variation of the gain and efficiency of the amplifier is described with respect to device parameters such as length, width, number of quantum wells, facet reflectivities, confinement factor and to operational parameters such as current density and injected power. The effects of the parameters are analyzed one at a time to give an intuitive feeling about the physics hidden behind the model equations. It is suggested that a travelling wave amplifier will perform better than a Fabry-Perot amplifier and that the confinement factor per well has to be as large as possible within the limit imposed by the coupling loss of the optical system. It is also shown that most of the parameters mentioned above has an optimum value maximizing efficiency others remaining constant. Finally, some simple trade-offs in the optimization of efficiency and gain are outlined.

A simple optimization scheme would be to run the numerical simulation everywhere inside the physically significant region of the n dimensional parameter space, n being the number of parameters to optimize. But even the most optimistic prediction of such task in terms of computation time is not less than a year. So an intelligent approach is needed to develop an empirical optimization scheme. One way of approaching the problem is to generate summary graphs which regroup the important information (peak efficiency) contained in a family of graphs. Such a method definitively causes loss of information but the cost of that is not very expensive if enough care is given in the analysis of the generated outputs.

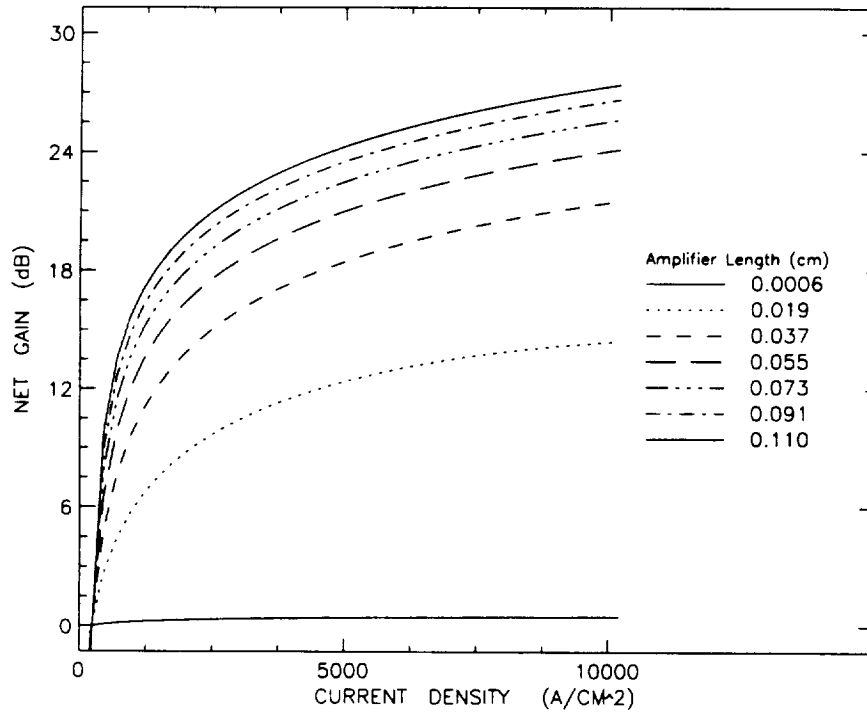
The procedure can be applied to two variables at a time. When the corresponding summary graph is constructed, the procedure can be extended to incorporate a third variable and so on

The graphs below illustrate the variation of efficiency and gain with current density for amplifiers having different lengths. The first graph reveals an initial increase in the peak efficiency with in-

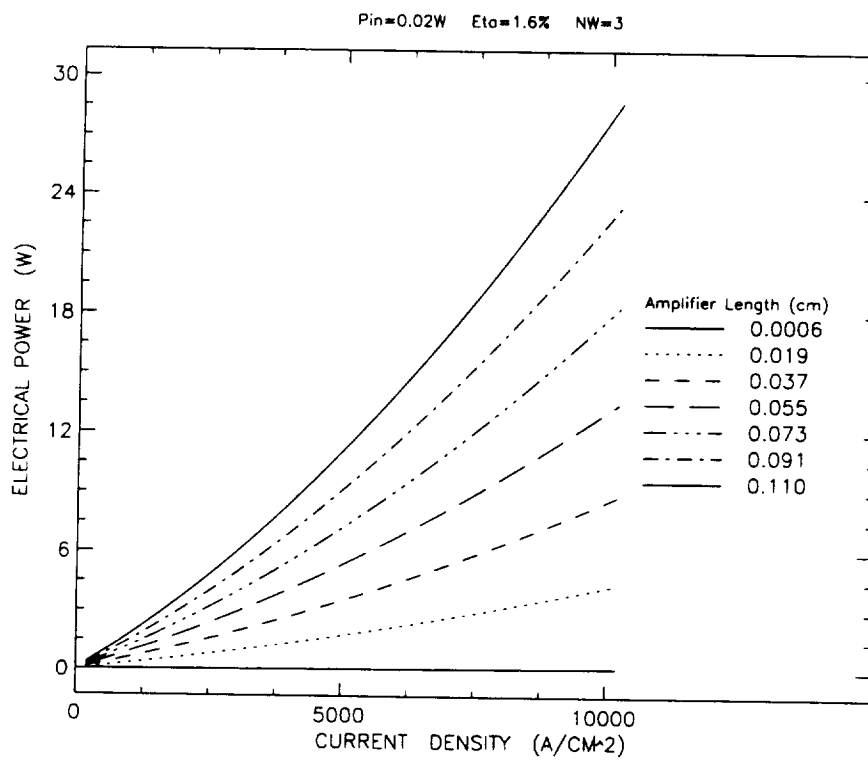
Pin=0.02W Eto=1.6% NW=3



Pin=0.02W Eto=1.6% NW=3



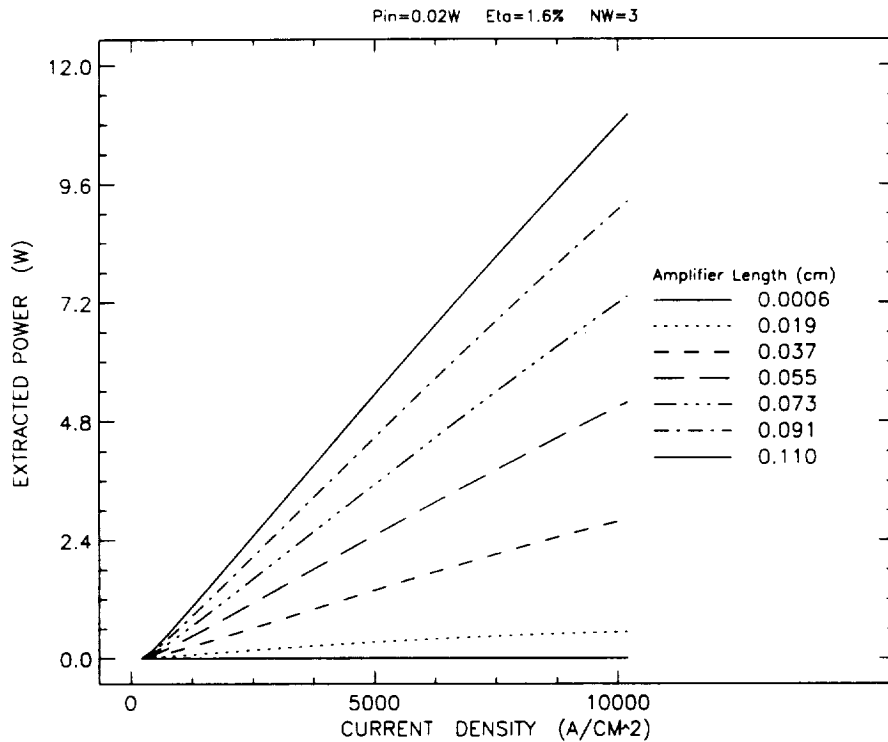
creasing device length followed by a decrease for relatively long amplifiers. The second graph portrays the increase of one pass gain with increasing length. An increase in length results in a higher gain at all current densities. The gain curve seems to shift upward with a decreasing rate. This is as well due to the fact that with increasing length, equal length increments results in proportionally smaller improvements in gain as to the saturation. The understanding of the effect of amplifier length on device performance would be simplified if extracted and electrical powers corresponding to the simulation presented above are analyzed. Previously mentioned graphs are presented below.



The fact that extracted power varies linearly with current density independent of the length (although with different slope) results from the fact that at corresponding injected power level the amplifier is highly saturated and the increase in the photon population reduces an increase of output power down to a linear profile through depletion of electron population as mentioned in the previ-

ous sections. In an amplifier operating in these conditions, an increase in the length will increase the gain of the device but with a decreasing rate as it can be observed from the slopes of extracted power curves. For very short amplifiers the net gain of the device is very small as it is clear from equation (10), no matter how big is the applied electron density in an experimentally reasonable range.

The electrical power applied to the diode varies pseudo-linearly with current density for relatively short amplifiers as predicted by equation (24). It can be seen that the second term in the right hand side of the equation has a quadratic dependence on the length and thus is negligible compared to the first term which only has a linear dependence. Furthermore, the forward voltage is much bigger than the product of the current density and R_0 even at very high current densities, resulting in an overall linear dependence, explaining the previous observation. With increasing

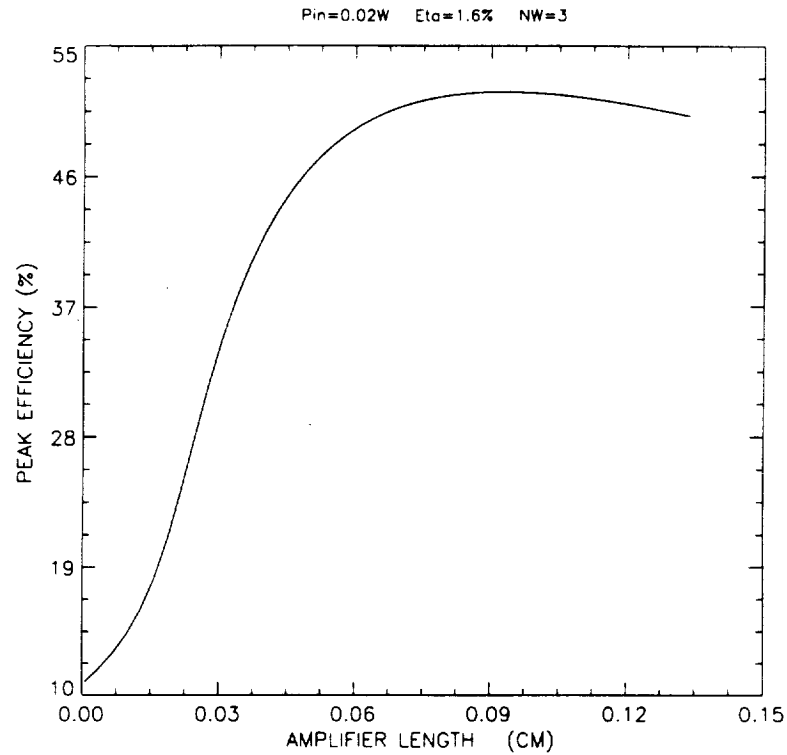


length, the terms quadratic in current density are no more negligible leading to a parabolic variation of applied electrical power with current density.

For relatively short amplifiers, the rate of increase of injected electrical power catches up with that of extracted power at a higher current density, shifting the peak efficiency to the right. But with increasing length of the amplifier, the electrical power dramatically becomes a quadratic function of the current density, and thus forces the peak of the efficiency to smaller current densities. This, simultaneously explains the two-way variation of the peak efficiency in both current density and efficiency axes.

It can be observed that the portions of the graphs corresponding to current densities below peak efficiency contains no useful information for the optimization because both gain and efficiency attain higher values at the remaining part of the simulation. Other portions of the graphs illustrates a previously mentioned trade-off between efficiency and gain. Even that information can be given away to only keep the value of peak efficiencies since a higher peak value will provide more room for a trade-off of efficiency with gain. The choice of quantum well laser amplifier instead of the more conventional double heterostructure laser was made following a similar argument to increase the efficiency giving away a portion of the gain which would have been otherwise higher. Together with the peak efficiencies it is needed to keep track of the current densities and the gain corresponding to these peaks to make sense out of the summarized information. The summary graphs generated are presented below. Remark that the peak efficiencies coincides with the small rectangles on the original efficiency graph. The simulation is run only up to peak efficiency thus saving a important amount of time.

Now, it is possible to generate a family of summary curves varying a third parameter, injected power or the number of quantum wells. As before, it is possible to shrink down the excessive information by only keeping track of the peak efficiency values of the graphs and the corresponding remaining parameters. This procedure can be applied till the effect of all the variables is taken into



account. The summary of summary graphs obtained at the end should dictate many amplifier structures with high gain and efficiency as desired. Note that the confinement factor has to be the last factor to be included since it may not necessarily result into a maximum in the summary graphs thus avoiding further shrinking.

To give an example of the described procedure a sample overall simulation is implemented using the same gain function, width, transparency current density etc as before, but with varying number of quantum wells, confinement factor per well, amplifier length, input optical intensity and injected electrical power.

To shorten the amount of simulation, the current density steps used to implement the first stage of

summary graphs is kept relatively large resulting in plots with discontinuous derivatives at some points. This artifact is due to over or underestimating the current density at which the peak efficiency occurs and should be disregarded.

The first page of figures show the variation of peak efficiency, peak gain, current density at peak efficiency and extracted and electrical powers at peak efficiency with amplifier length for different input optical power levels varying from 0.3W to 1.5W for an amplifier with a confinement factor of 0.011 per well and one quantum well in its active region. The second and third page illustrates the same simulation for devices with three and five number of quantum wells respectively. Following that, the same analysis is repeated for a confinement factor per well of 0.016, this value being previously determined to be an experimental maximum.

The explanation of these graphs is rather involved. Before this though, it is worth recalling that the optimization is aiming at predicting physical variables (length, confinement factor, width, and number of quantum wells) for amplifier structures that will yield optimum efficiency and gain at physically realizable input optical and electrical power levels. All of physical variables except amplifier length requires very precise and irreversible epitaxial growth processes. Consequently, their prediction is more important than the others, for which the only requirement is to be within their physically realisable range.

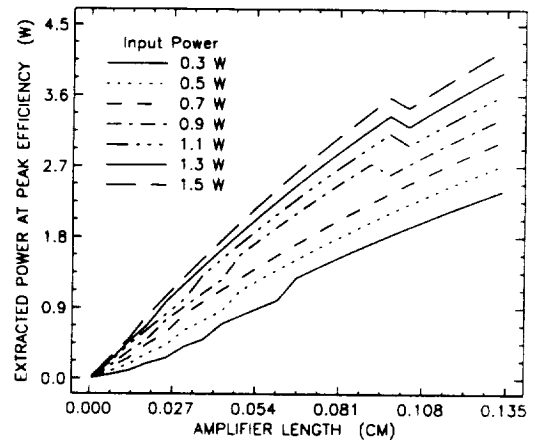
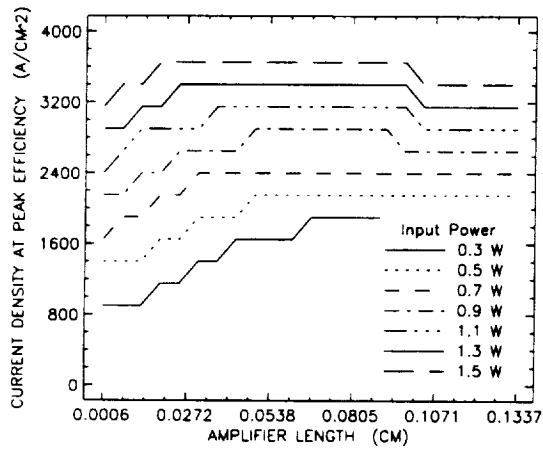
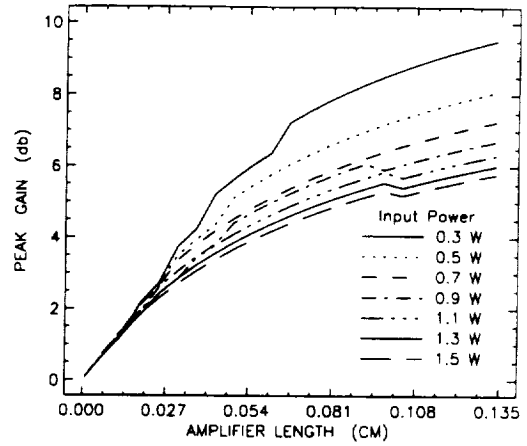
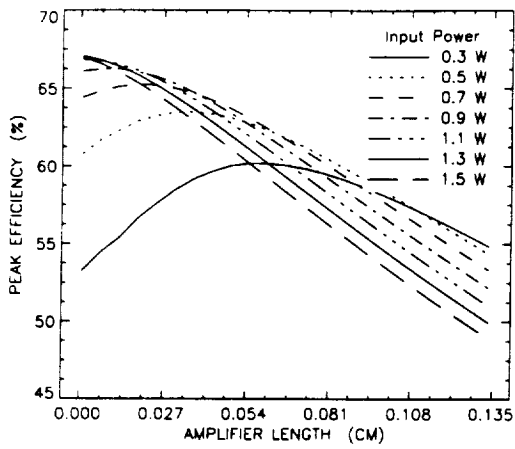
In figure p1f1, it can be seen that increasing injected power increases the peak efficiency while shifting the length at peak efficiency to shorter values. The current density required at peak efficiency has become higher as well, while the peak gain has become lower. If one looks to (description figure), it is clear that increasing the input optical power should require a higher current density to reach peak efficiency to produce the effect in figure p1f1. This is in agreement with the saturation expression in the amplifier gain.

This simulation is eventually more important than it seems. It shows that the most efficient amplifier is eventually very short for a given confinement factor. Increasing the injected power reduces

the gain of the amplifier proportionally. However, together with decreasing device length and increasing current density one can extract more optical power with respect to electrical power spent at the expense of gain. The material gain being very small for such a device and thus the overall gain being almost equal to unity, the photon and electron densities in the active region can be assumed constant along the amplifier. This result makes a lot of sense because it states that for an amplifier of infinitesimal length, there is an optimal set of electron and photon concentrations for which the amplification is maximum. However, such a device is far from being ideal since a gain of at least 10db is required for an array made of these amplifiers to be of practical use due to coupling losses. So one has to increase the gain while keeping efficiency as high as possible. However this is not a very easy task because increasing the length of the amplifier will result into a nonuniform electron and photon distribution along the device making the efficiency at an infinitesimal length element of the diode smaller than its optimum. The best set of parameters for optimum efficiency for a given amplifier length is thus the one that on average makes the electron and photon concentrations along the amplifier deviate the least from their optimum value. Although, this procedure is relatively easy to understand and visualize for a travelling wave amplifier, it is very difficult for a device with non-zero facet reflectivities. The reason for that is the fact that in the latter case the photon and electron densities at a given location in the amplifier become dependent not only on the same quantities at previous locations but also on those in the remainder of the device length. That is the overall gain becomes a feedback factor as described by the Fabry-Perot model (see related equations). It is this complication that necessitated a simulation approach to this problem in order to understand the physics of the device and to optimize its parameters, making an analytical treatment impossible.

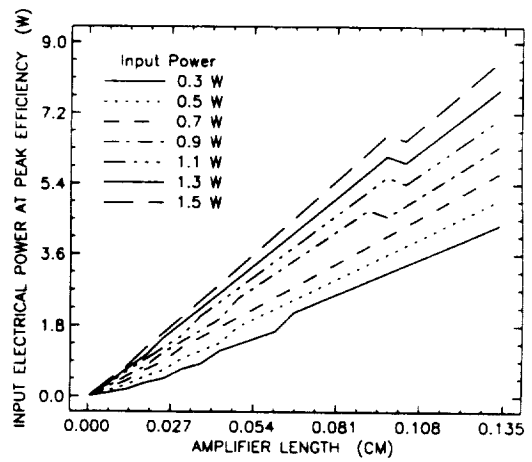
Returning back to optimization, one can now look at the remaining figures by keeping in mind that the purpose is to find amplifier parameters that results into a gain higher than 10db while keeping the electron and photon densities close to their ideal value on the average. Fig1p1 and fig2p1 shows

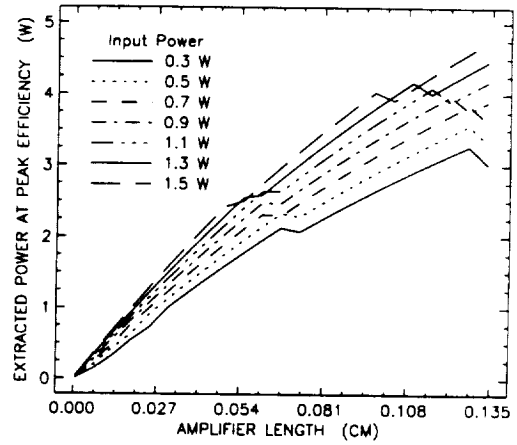
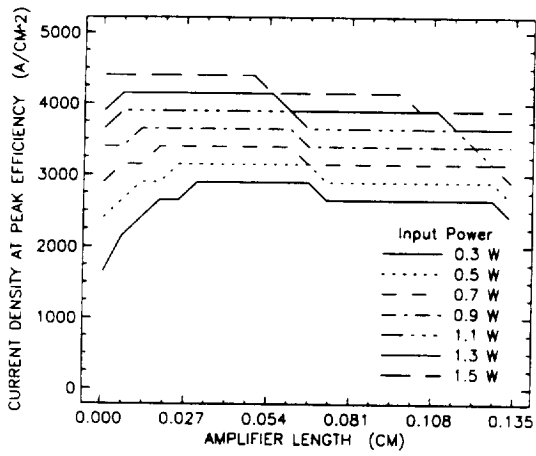
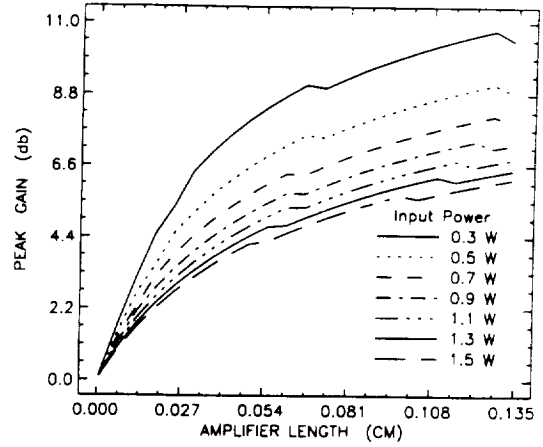
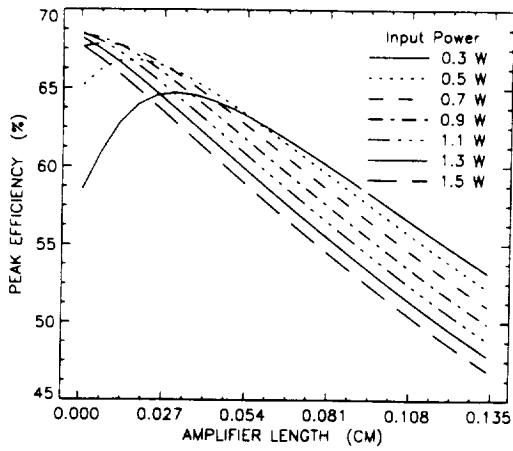
the trade off between gain and efficiency very clearly. One has to remember however that more gain can be achieved by increasing either current density or amplifier length at the expense of efficiency. This is where the choice of number of quantum wells and confinement factor comes in the picture. For a confinement factor per well of 0.011, an amplifier with 5 quantum wells and a length of 0.135 centimetre seems to be an acceptable choice promessing an overall gain of 11.4db at 50% efficiency. This amplifier is predicted to achieve this performance when supplied with a current density of 3200 A/cm^2 and an input optical power of 0.3W. It is interesting to note that the lowest signal power offered the best trade-off between gain and efficiency yielding the highest efficiency at the maximum gain with minimum electrical power. Also, as predicted previously higher confinement factor per well (0.016) yielded better gain and efficiency achieving 11db at 53% efficiency with an input power of 0.3W and excitation of 2500 A/cm^2 . It is clear that better results could be predicted by using lower optical power.



$\eta = 1$

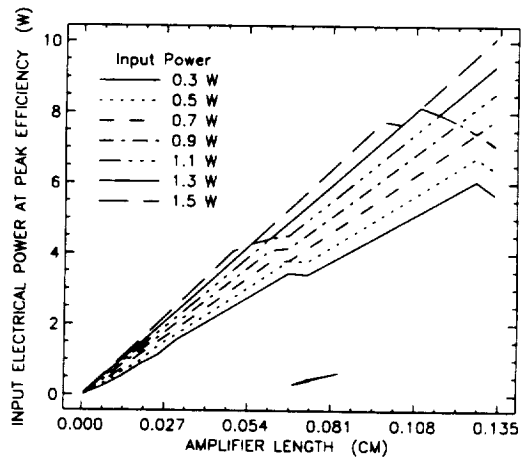
$\eta = 0.01$

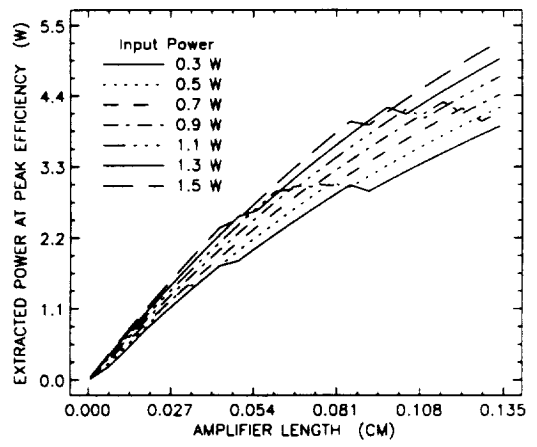
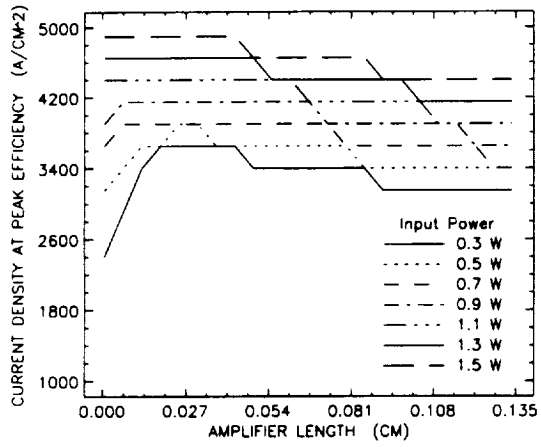
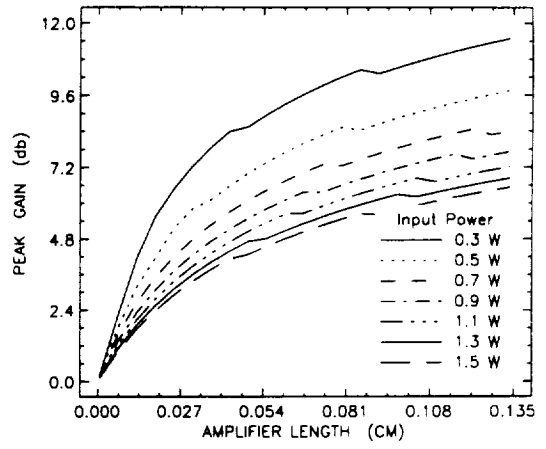
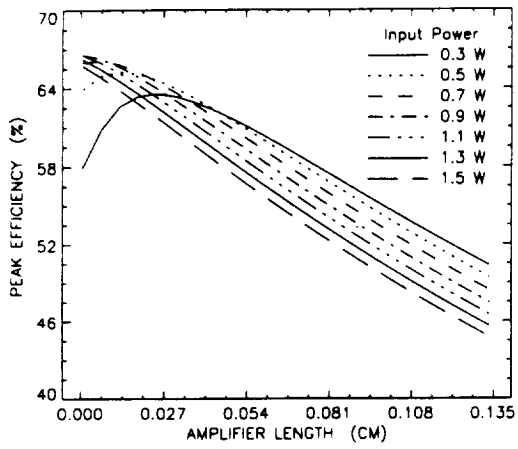




$\eta = 3$

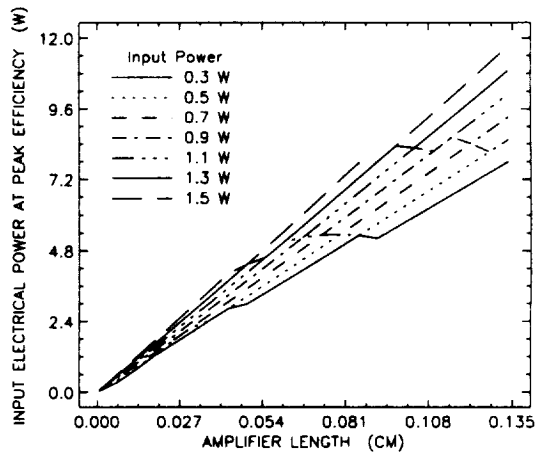
$\eta = 0.011$

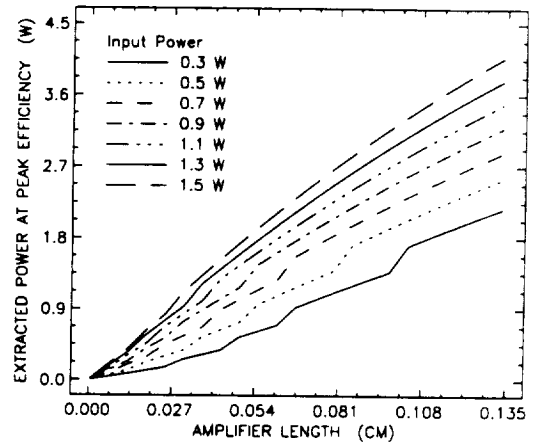
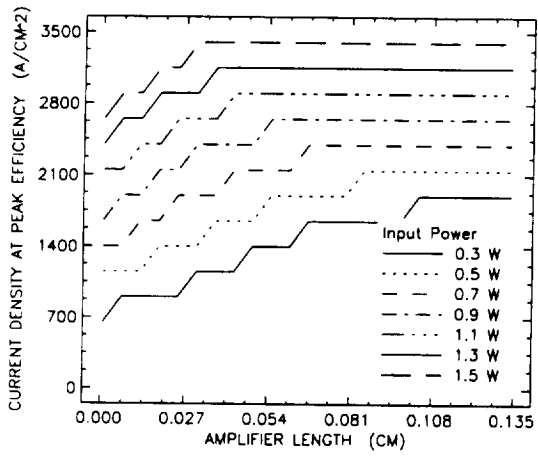
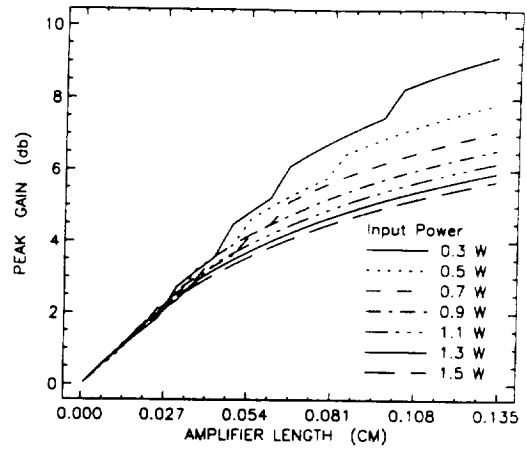
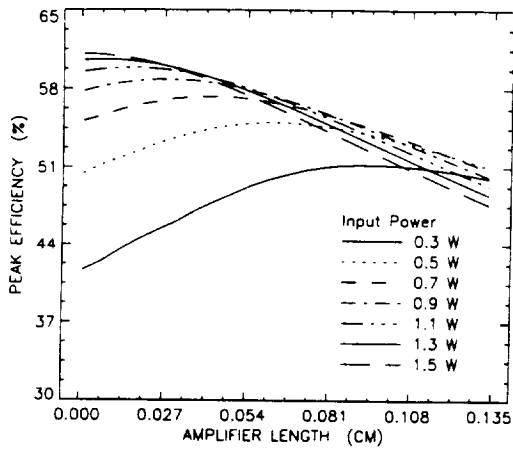




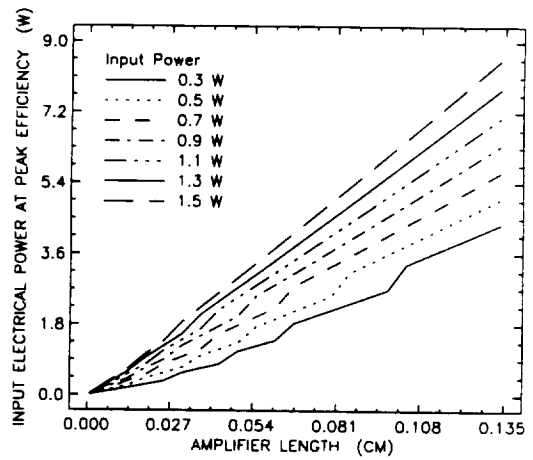
$\mu_{00} = 5$

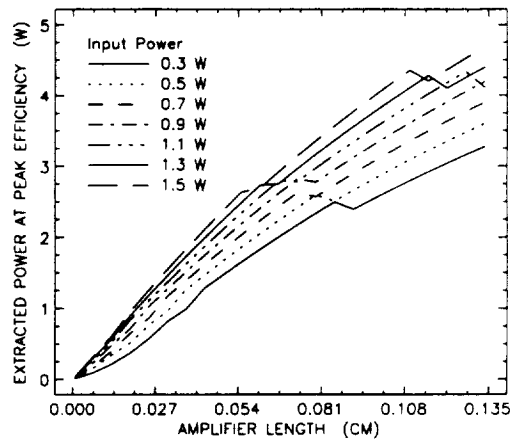
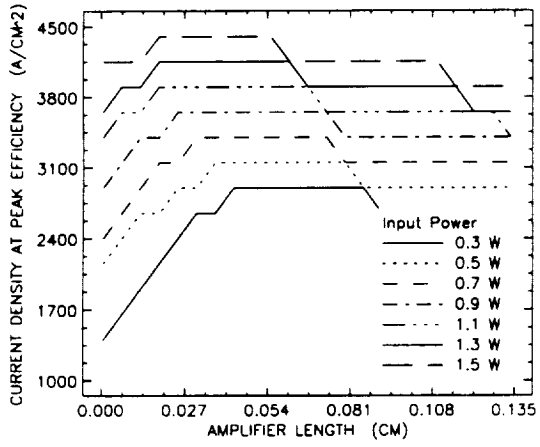
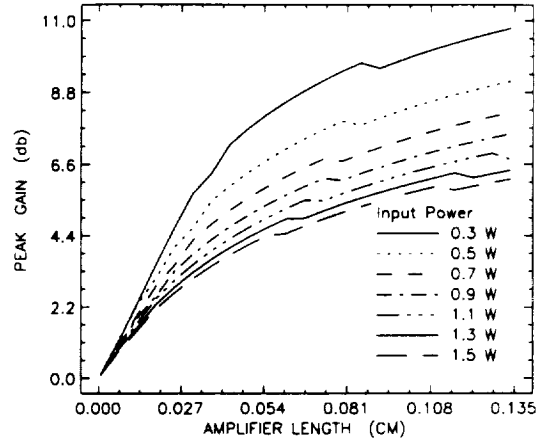
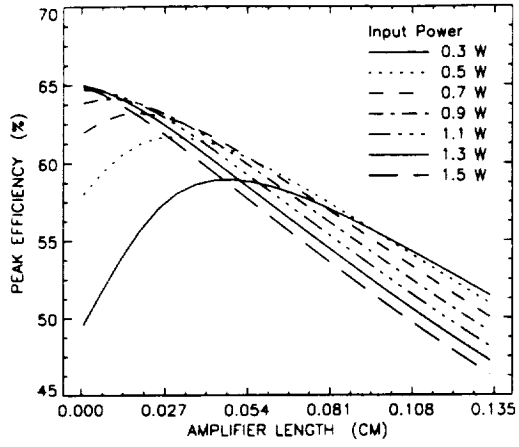
$\mu_{11} = 0.11$



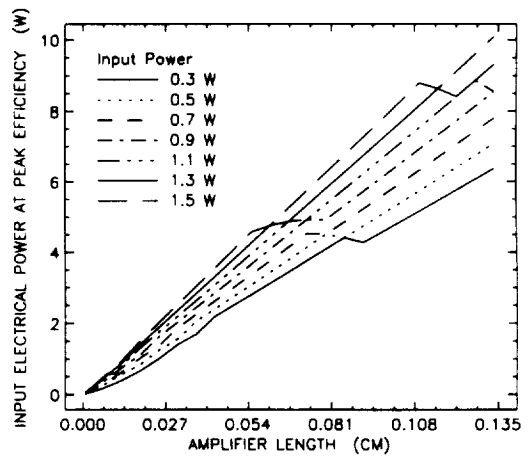


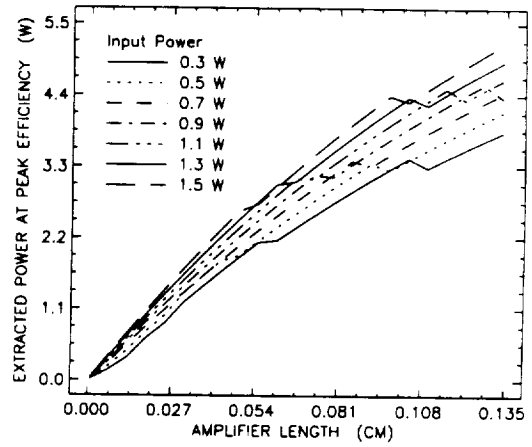
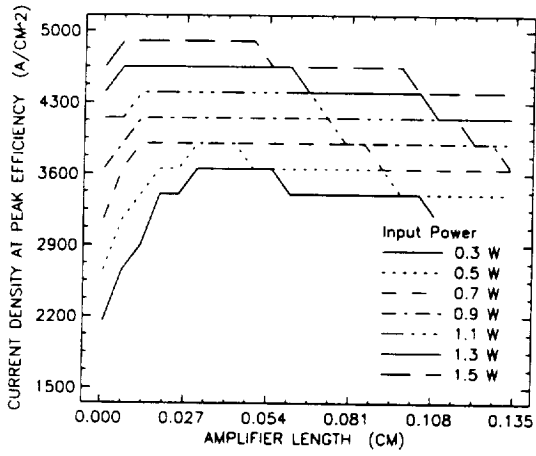
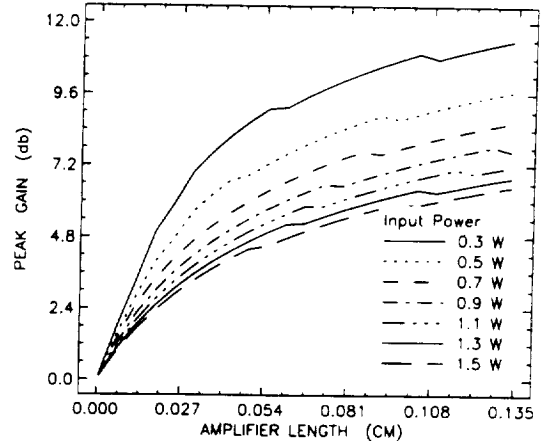
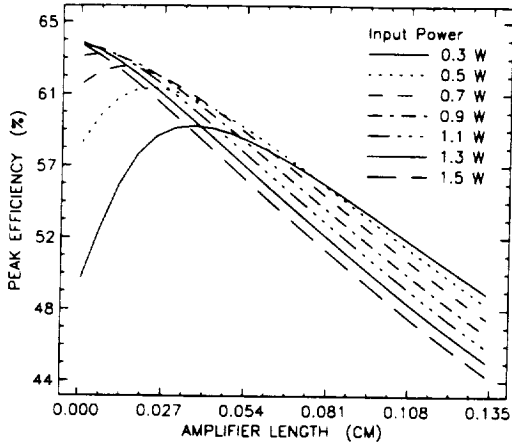
2200 → 1
 0.7 = 0.000



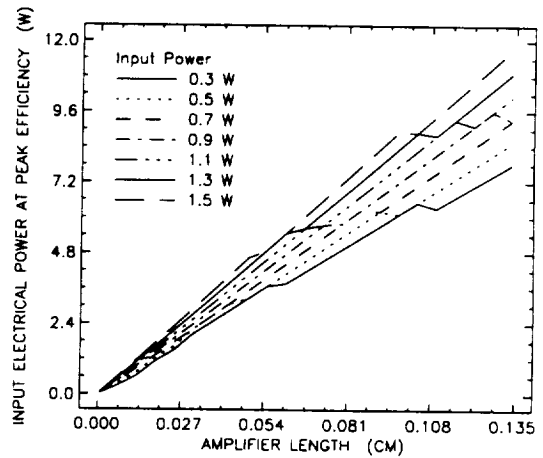


Handwritten notes: 2.2 - 2.6 and 2.2 - 2.6





$\eta = 5$ $\eta = 0.016$



References

B. Johnson , and S. T Eng, “ Solving the Schrodinger equation in arbitrary quantum-well potential profiles using the transfer matrix method,”IEEE journal of quantum electronics.26(11), 2025-2035 (1990).

A.K.Ghatak, K. Thyagarajan, and M.R.Shenoy, “ A novel numerical technique for solving the one dimensional Schroedinger equation using matrix approach-Application to quantum well structures,”IEEE journal of quantum electronics.24(8),1524-1531 (1988).

P.A. Andrekson, N.A. Olsson, T. Tanbun-Ek, R.A. Logan, D.Coblentz, and H. Temkin, “Novel technique for determining internal loss of individual semiconductor lasers,”

G.Eisenstein, N. Tessler, U. Koren, J.M.Wiesenfeld, G.Raybon, and C.A. Burros, “ Length dependence of saturation characteristics in 1.5-um multiple quantum well optical ammplifiers,” Ieee Photonics technology letters. 2 (11), 790-791 (1990).

P.W. A Mc Ilroy, A. Kurobe, and Y. Uematsu, “Analysis and application of theoretical gain curves to the design of multi -quantum-well lasers,” IEEE Journal of quantum electronics.QE 21(12), 1958-1963 (1985).

T. Mukai, and Y. Yamamoto, “ Gain , frequency bandwidth, and saturation output power of Al-GaAs DH amplifiers,” IEEE Journal of quantum electronics.QE 17 (6),1028-1034 (1981).

R.H. Yan, S.W. Corzine, L.A. Coldren, and I. Suemune, "Corrections to the expression for gain in GaAs," IEEE journal of quantum electronics. 26 (2) , 213-216 (1990).

J.Z. Wilcox, G.L. Peterson, S Ou, J.J. Yang, and M. Jansen, "Gain and threshold-current dependence for multiple quantum-well lasers," J. Appl. Phys. 64 (11), 6564-6567 (1988).

J. O. Binder, and G. D. Cormack, "Prediction of the gain versus injection current characteristic of individual semiconductor laser amplifiers", Journal of lightwave technology. 8 (7), 1055-1063 (1990).

D.T.F. Marple, "Refractive index of GaAs", Journal of Applied Physics, 35 (4), 1241-1242 (1964).

D. Welford, and A. Mooradian, "Output power and temperature dependence of the linewidth of single frequency cw (GaAl)As diode lasers", Appl. Phys. Lett. 40(10), 865-867 (1982).

A. Olsson, and C.L. Tang, "Coherent Optical Interference Effects in External-Cavity Semiconductor Lasers", IEEE Journal of Quantum Electronics, QE-17 (8), 1320-1323 (1981).

Nagaatsu Ogasawara, Ryoichi Ito, and Ryuiji Morita, "Linewidth Enhancement Factor in GaAs/AlGaAs Multi-Quantum-Well Lasers", Japanese Journal of Applied Physics, 24 (11) L519-L521 (1985).

S. E. H. Turley, G. H. B. Thompson, D. F. Lovelace, "Effect of Injection Current on the Dielectric Constant of an Inbuilt Waveguide in Twin-Transverse-Junction Stripe Lasers", *Electronics Letters*, 15 (9), 256-257 (1979).

J. H. Manning, and R. Olshansky, "Carrier-Induced Index Change in AlGaAs Double-Heterostructure Lasers", *Electronics Letters*, 17 (14), 506-507 (1981).

K. Stubkjaer, Y. Suematsu, M. Asada, S. Arai, and A.R.Adams, "Measurements of Refractive-Index Variation With Free Carrier Density and Temperature for 1.6 μ m GaInAsP/InP Lasers", *Electronics Letters*, 16 (23), 895-896 (1980).

A. Olsson, and C.L. Tang, "Injected-Carrier induced Refractive-Index change in Semiconductor Laser", *Appl. Phys. Lett.*, 39 (1), 24-26 (1981).

D. Welford and A. Mooradian, "Observation of Linewidth Broadening in (GaAl)As Diode Lasers Due to Electron Number Fluctuations", *Appl. Phys. Lett.*, 40 (7), 560-562 (1982).

M. Cross, and M. J. Adams, "Effects of Doping and Free Carriers on the Refractive Index of Direct-Gap Semiconductors", *Opto-electronics*, 6 , 199-216 (1974).

Joanne Manning, Robert Olshansky, and Chin Bing Su, "The Carrier- Induced Index Change in Al-GaAs and 1.3 μ m InGaAsP Diode Lasers, *IEEE Journal of Quantum Electronics*, QE-19 (10),

1525-1530 (1983).

C. H. Henry, R. A. Logan, and K. A. Berthness, "Spectral Dependence of the Change in Refractive Index Due to Carrier Injection in GaAs Lasers", *J. Appl. Phys.*, 52 (7), 4457-4460 (1981).

J.G. Mendoza-Alvarez, F. D Nunes, and N. B. Patel, "Refractive Index Dependence on Free Carriers for GaAs", *J. Appl. Phys.*, 51 (8), 4365-4367 (1980).

Minoru Ito, and Tatsuya Kimura, "Carrier Density Dependence of Refractive Index in AlGaAs Semiconductor Lasers", *Quantum Electronics Letters*, QE-16 (9), 910-911 (1980).

H. S. Sommers, Jr., "Complete Experimental Evaluation of the Carrier Dependence of the Refractive Index from the Frequency Modulation Spectra of Single Mode Injection Lasers", *Appl. Phys. Lett.*, 42 (11), 928-930 (1983).

A. Olsson, and C.L. Tang, "Coherent Optical Interference Effects in External-Cavity Semiconductor Lasers", *IEEE Journal of Quantum Electronics*, QE-17 (8), 1320-1323 (1981).

Weng W. Chow, "Amplified Spontaneous Emission Effects in Laser Amplifiers", *SPIE Modeling and Simulation of Laser Systems*, 1045, 139-147 (1989).

Weng W. Chow, and Richard R. Craig, "Amplified Spontaneous Emission Effects in Semiconductor Laser Amplifiers", *IEEE Journal of Quantum Electronics*, 26 (8), 1363-1368 (1990).

Jacques Arnaud, Jean Fesquet, Francois Coste, Pierre Sansonetti, "Spontaneous Emission in Semiconductor Laser Amplifiers", *IEEE Journal of Quantum Electronics*, QE21 (6), 603-608 (1985).

Tadoshi Saitoh, Yoshio Suzuki, and Hidenao Tanaka, "Low Noise Characteristics of a GaAs-AlGaAs Multiple-Quantum-Well Semiconductor Laser Amplifier", *IEEE Photonics Technology Letters*, 2 (11), 794-796 (1990).

Daniel T. Cassidy, "Comparison of Rate-Equation and Fabry-Perot Approaches to Modeling a Diode Laser", *Applied Optics*, 22 (21), 3321-3326 (1983).

G. Hugh Song, Karl Hess, Thomas Kerkhoven, and Umberto Ravaioli, "Two Dimensional Simulator for Semiconductor Lasers", *IEEE*, 143-146 (1989).

Takaaki Mukai, Yoshihisa Yamamoto, Tatsuya Kimura, "Optical Amplification by Semiconductor Lasers", *Semiconductors and Semimetals*, 22 (E), 265-318 (1985).

S. R. Chinn, P. S. Zory, and A. R. Reisinger, "Computer Modeling of GRIN-SCH-SQW Diode Lasers", *SPIE Laser Diode Technology and Applications*, 1043, 157-166 (1989).

Jens Buus, and Rob Plastow, "A Theoretical and Experimental Investigation of Fabry-Perot Semiconductor Laser Amplifiers", *IEEE Journal of Quantum Electronics*, QE-21 (6), 614-618 (1985).

Yoshihisa Yamamoto, "Characteristics of AlGaAs Fabry-Perot Cavity Type Laser Amplifiers", *IEEE Journal of Quantum Electronics*, QE-19 (10), 1047-1052 1980.

David K. Wagner, Robert G. Waters, P. L. Tihanyi, Daily S. Hill, Andrew J. Roza, Jr., Hubert J. Vollmer, M.M. Leopold, "Operating Characteristics of Single-Quantum-Well AlGaAs/GaAs High-Power Lasers", *IEEE Journal of Quantum Electronics*, 24 (7), 1258-1265 (1988).

David S. Gao, S. M. Kang, Robert P. Bryan, James J. Coleman, "Modeling of Quantum-Well Lasers for Computer-Aided Analysis of Optoelectronic Integrated Circuits", *IEEE Journal of Quantum Electronics*, 26 (7), 1206-1216 (1990).

J.C. Simon, "Semiconductor Laser Amplifier for Single Mode Optical Fiber Communications", *Journal of Optical Communications*, 4 (2), 51-62 (1983).

M. J. Adams, J.V. Collins, and I.D. Henning, "Analysis of Semiconductor Laser Optical Amplifiers", *IEE Proceedings*, 132 Pt J (1), 58-63 (1985).

Dietrich Marcuse, "Computer Model of an Injection Laser Amplifier", *IEEE Journal of Quantum Electronics*, QE-19 (1), 63-72 (1983).

Y.L. Wong, and J.E. Carroll, "A Travelling-Wave Rate Equation Analysis for Semiconductor Lasers", *Solid State Electronics*, 30 (1), 13-19 (1987).

Weng W. Chow, and Richard R. Craig, "Power Scaling in Quantum-Well Laser Amplifiers", *IEEE Journal of Quantum Electronics*, 27 (10), 2267-2273 (1991).

Peter John Stevens, and Takaaki Mukai, "Predicted Performance of Quantum-Well GaAs-(GaAl)As Optical Amplifiers", *IEEE Journal of Quantum Electronics*, 26 (11), 1910-1917 (1990).

Lars Gillner, Edgar Goobar, Lars Thylen, and Mats Gustavsson, "Semiconductor Laser Amplifier Optimization: An Analytical and Experimental Study", *IEEE Journal of Quantum Electronics*, 25 (8), 1822-1827 (1989).

I.D. Henning, M. J. Adams, and J.V. Collins, "Performance Predictions from a New Optical Amplifier Model", *IEEE Journal of Quantum Electronics*, 21 (6), 609-613 (1985).

P. A. Kirkby, and G. H. B. Thompson, "High Peak Power from (GaAl)As-GaAs Double-Heterostructure Injection Lasers", *Appl. Phys. Lett.*, 22 (12), 638-640 (1973).

Gary Harnagel, David Welch, Peter Cross, and Don Scifres, "Two New Structures in Phase-Coupled Array Technology Produce Diffraction-Limited Output Beams", *Lasers & Applications*, June, 135-138 (1986).

M. Ettenberg, H. S. Sommers, Jr., H. Kressel, and H. F. Lockwood, "Control of Facet Damage in GaAs Laser Diodes", *Appl. Phys. Lett.*, 18 (12), 571-573 (1971).

Osamu Ueda, Kiyohide Wakao, Satoshi Komiya, Akio Yamaguchi, Shoji Isozumi, and Itsuo Umebu, "Catastrophic Degradation of InGaAsP/InGaP Double-Heterostructure Lasers Grown on (001) GaAs Substrates by Liquid-Phase Epitaxy", *J. Appl. Phys.*, 58 (11), 3996-4002 (1985).

P.G. Eliseev, "Degradation of Injection Lasers", *Journal of Luminescence*, 7, 338-356 (1973).

M. Ettenberg, and H. Kressel, "The Reliability of (AlGa)As CW Laser Diodes", *IEEE Journal of Quantum Electronics*, QE-16 (2), 186-200 (1980).

C. H. Henry, P. M. Petroff, R. A. Logan, and F. R. Merritt, "Catastrophic damage of $\text{Al}_x\text{Ga}_{1-x}\text{As}$ Double-Heterostructure Laser Material", *J. Appl. Phys.*, 50 (5), 3721-3732 (1979).

N. Chinone, R. Ito, and O. Nakada, "Limitations of Power Outputs from Continuously Operating GaAs- $\text{Ga}_{1-x}\text{Al}_x\text{As}$ Double-Heterostructure Lasers", *J. Appl. Phys.*, 47 (2), 785-786 (1976).

M. Ikeda, O. Ueda, S. Komiya, and I. Umebu, "Thermal Strain-Induced Degradation Mechanism in the Visible AlGaAs/GaAs Laser", *J. Appl. Phys.*, 58 (7), 2448-2452 (1985).

William J. Fritz, "Gradual Bulk Degradation in (AlGa)As Laser Diodes During -20°C tests due to Arsenic Out-Diffusion", J. Appl. Phys., 66 (6), 2260-2264 (1989).

L. D. Zhu, B. Z. Zheng, Z. Y. Xu, J. Z. Xu, and G. A. B. Feak, "Optical Gain in GaAs/GaAlAs Graded- Index Separate-Confinement Single-Quantum-Well Heterostructures", IEEE Journal of Quantum Electronics, 25 (6), 1171-1178 (1989).

Jinwei Wang, Henning Olesen, and Kristian E. Stubkjaer, "Recombination, Gain and Bandwidth Characteristics of $1.3\text{-}\mu\text{m}$ Semiconductor Laser Amplifiers", Journal of Lightwave Technology, LT-5 (1), 184-189 (1987).

G.Eisentein, U. Koren, G. Raybon, T. L. Koch, J.M.Wiesenfeld, M.Wegener, R.S. Tucker, and B.I.Miller, "Large- and Small-Signal Gain Characteristics of $1.5\ \mu\text{m}$ Multiple Quantum Well Optical Amplifiers", Appl. Phys. Lett., 56 (13), 1201-1203 (1990).

L. D. Zhu, B. Z. Zheng, and A. B. Feak, "Temperature Dependence of Optical Gain, Quantum Efficiency, and Threshold Current in GaAs/GaAlAs Graded-Index Separate-Confinement Heterostructure Single-Quantum-Well Lasers", IEEE Journal of Quantum Electronics, 25 (9), 2007-2012 (1989).

Masayuki Ishikawa, Hideo Shiozawa, Kazuhiko Itaya, Gen-ichi Hatakoshi, and Yutaka Uematsu, "Temperature Dependence of the threshold Current for InGaAlP Visible Laser Diodes", IEEE Jour-

nal of Quantum Electronics , 27 (1), 23-29 (1991).

H. C. Hsieh, "Maximum Heat-Sink Temperature for CW Operation of a Double-Heterostructure Semiconductor Injection Laser", IEEE Journal of Quantum Electronics, 25 (10), 2079-2083 (1989).

D. P. Bour, N. W. Carlson, G. A. Evans, "Characteristic Temperature of GaInP/AlGaInP Single Quantum Well Lasers", Electronics Letters, 25 (18), 1243-1245 (198).

Z. L. Liao, James N. Walpole, Dean Z. Tsang, and Vicky Diaduk, "Characterization of Mass-Transported p-Substrate GaInAsP/InP Buried-Heterostructure Lasers with Analytical Solutions for Electrical and Thermal Resistances", IEEE Journal of Quantum Electronics, QE-24 (1), 36-42 (1988).

L. F. Tiemeijer, P. J. A. Thijis, J. J. M. Binsma, and T. V. Dongen, "Direct Measurement of The Transparency Current and Valence Band Effective Masses in Tensile and Compressively Strained InGaAs/InP Multiple Quantum-Well Laser Amplifiers", Appl. Phys. Lett., (5) 3, 554-556 (1992).

Donald M. Fye, "Practical Limitations on Optical Amplifier Performance", Journal of Lightwave Technology, LT-2 (4), 403-406 (1984).

END